Polyspermy blocks used by the African clawed frog *Xenopus laevis*

By

Katherine Lynn Wozniak

Bachelor of Science, Duquesne University, 2014

Submitted to the Graduate Faculty of

The Dietrich School of Arts and Sciences in partial fulfillment

of the requirements for the degree of

Doctor of Philosophy in Molecular, Cellular, and Developmental Biology

University of Pittsburgh

2019

UNIVERSITY OF PITTSBURGH

DIETRICH SCHOOL OF ARTS AND SCIENCES

This dissertation was presented

by

Katherine Lynn Wozniak

It was defended on

February 25, 2019

and approved by

Dr. Deborah Chapman, Associate Professor, Department of Biological Sciences

Dr. Ossama Kashlan, Assistant Professor, Department of Medicine

Dr. Kirill Kiselyov, Associate Professor, Department of Biological Sciences

Dr. Miler Lee, Assistant Professor, Department of Biological Sciences

Dissertation Advisor: Dr. Anne Carlson, Assistant Professor, Department of Biological Sciences

Polyspermy blocks used by the African clawed frog *Xenopus laevis*

Katherine Lynn Wozniak, PhD

University of Pittsburgh, 2019

Preventing polyspermy, the fertilization of an egg by multiple sperm, is essential for the normal embryonic development of most sexually reproducing species. Eggs therefore have multiple mechanisms to prevent the entry of sperm into an already fertilized egg. The two most common polyspermy prevention mechanisms are known as the fast and slow polyspermy blocks. As these names imply, the fast block occurs within seconds of fertilization to create an electrical barrier to inhibit entry of additional sperm. The fast block has only been observed in externally fertilizing organisms, such as frogs and sea urchins, where the sperm-to-egg ratio is elevated at the moment of fertilization. The pathway by which sperm-egg contact culminates in membrane depolarization was not known for any species. I studied the fast polyspermy block in the African clawed frog, *Xenopus laevis*. Using electrophysiology, developmental biology, and bioinformatics techniques, I uncovered that the Ca^{2+}-activated Cl^- channel, TMEM16A, conducts the depolarizing current of the fast block, and that fertilization opens this channel in a signaling pathway requiring phospholipase C and inositol triphosphate. In a separate line of experimentation, I studied the slow polyspermy block in *X. laevis*; a pathway that occurs ubiquitously in sexual reproducers within minutes of fertilization. In this pathway, eggs exocytose cortical granules to release compounds that transform the extracellular matrix that surrounds eggs into a protective barrier impenetrable by sperm. The mechanisms enabling the creation of this barrier were largely-unknown. Using confocal microscopy and fluorometry, I determined that fertilization induces the release of Zn^{2+} from cortical granules in frogs and fish eggs, similar to mammalian eggs. Furthermore, exposing

frog and sea urchin eggs to extracellular Zn^{2+} hindered fertilization in a concentration-dependent manner. Taken together, these results suggesting that fertilization-induced Zn^{2+} release is a conserved process that may contribute to the slow polyspermy block. Overall, my work aims to broaden our understanding of the diverse pathways that block polyspermy.

Table of Contents

List of Tables

List of Figures

Abbreviations

2-APB: 2-Aminoethoxydiphenyl Borate

Ani9: 2-(4-chloro-2-methylphenoxy)-N-[(2-methoxyphenyl)methylideneamino]-acetamide

ANOVA: Analysis of variation

ASW: Artificial sea water

BEST2A: Bestrophin 2A

BME: β-mercaptoethanol

CaCC: Ca^{2+}-activated Cl^- channel

$CaCC_{inh}$-A01: 6-(1,1-Dimethylethyl)-2-[(2-furanylcarbonyl)amino]-4,5,6,7-tetrahydrobenzo[b] thiophene-3-carboxylic acid

Caged-IP_3: Myo-inositol 1,4,5-trisphosphate, P4(5)-1-(2-nitrophenyl) ethyl ester

DIDS: 4,4′-Diisothiocyanatostilbene-2,2′-disulfonic acid disodium salt hydrate

DMSO: Dimethyl sulfoxide

ECM: Extracellular matrix

ER: Endoplasmic reticulum

GO: Gene Ontology

IC_{50}: Half-maximal inhibitory concentration

IP_3: Inositol 1,4,5-triphosphate

IP_3R: Inositol 1,4,5-triphosphate receptor

MemE: Membrane anchored eGFP

MR: Modified Ringers solution

MONNA: N-((4-methoxy)-2-naphthyl)-5-nitroanthranilic acid

N.S.: Not significant

PIP_2: Phosphatidylinositol 4,5-bisphosphate

PLC: Phospholipase C

SEM: Standard error of the means

$T16A_{inh}$-A01: 2-[(5-Ethyl-1,6-dihydro-4-methyl-6-oxo-2-pyrimidinyl)thio]-N-[4-(4-methoxyphenyl)-2-thiazolyl]-acetamide

TEVC: Two electrode voltage clamp

TMEM16A: Transmembrane protein 16A

TPM: Transcripts per million

TRPV4: Transient receptor potential cation channel, subfamily V, member 4

RNA-seq: RNA-sequencing

xBEST2A: *Xenopus laevis* bestrophin 2A

Xesto: Xestospongin C

xTMEM16A: *Xenopus laevis* transmembrane protein 16A

ZP: Zona pellucida

ZP2: Zona pellucida glycoprotein 2

Preface

I would like to dedicate my dissertation to the strong women that came before me: Betty Remy and Gertrude Wozniak.

Acknowledgements:

First and foremost, I would like to thank the Carlson Lab for creating a welcoming environment to learn and share ideas. To my mentor, Dr. Anne Carlson, thank you for your enthusiastic guidance and support these last five years. Not only have you taught me how to be a rigorous biophysicist and developmental biologist, but you have also led by example on how to be an empowered woman in science. To my lab mates, Wase Tembo and Rachel Bainbridge, thank you for your willingness to pause your work at any moment to help me troubleshoot problems. I truly appreciate our commitment to helping each other succeed. To our undergraduate researchers, thank you all for your dedication. Specifically, on the zinc project, I have had the pleasure of mentoring: Monica Sauer, Ben Wisner, Meli Linderman, Maddy Czekalski, Meghan Hanson, and Kavya Pasumarthy. Lastly, thank you to our technician, Zane Crowell, for diligently caring for our animals and lab space.

The Department of Biological Sciences has provided a diverse support network that is always willing to help. I specifically want to thank my committee members, Dr. Debbie Chapman, Dr. Ossama Kashlan, Dr. Kirill Kiselyov, and Dr. Miler Lee, for their insights into my project, as well as their support for my academic and career choices. I would also like to thank Cathy Barr, our graduate administrator, for always going above and beyond to solve any clerical problems that

I have experienced. Additionally, I would like to thank Tom Harper for his assistance in the Microscopy Suite.

The University of Pittsburgh is a thriving research hub that I am humbled to be a part of. I would like to thank our collaborators at Pitt: Wesley Phelps, Dr. Miler Lee, Dr. Matthew Nicotra, and Dr. Steve Sanders. I am also thankful for the guidance I received participating in journal clubs in the Renal-Electrolyte Division of Pitt Medical School and at the Magee Women's Research Institute. I would also like to thank our collaborators at Carnegie Mellon University: Dr. Kate Buckley and Dr. Veronica Hinman.

Many thanks to my friends and family for their continued love and support. To my parents, John and Diane Wozniak, thank you for pushing me to pursue excellence. You never confined my path in life; rather, you always did whatever you could to help me fulfill my dreams. Additionally, I would like to thank my sister, Laura Wozniak, for challenging me to be the best role model I could be. Most days she teaches me more about compassion and kindness than I teach her about how to be an adult. To my childhood best friend, Stephanie Mitana, thank you for always reminding me where I came from and where I want to go. Additionally, I would like to thank my undergrad and grad school friends, Kelsey, Vasilii, Beth, Gina, Sarah, Stephanie, Lisa, and Melissa, for keeping me sane during this arduous journey.

Finally, I would like to thank my partner, Max Seel, for staying by my side for the last nine years. Words cannot describe how fortunate I am to have a loving partner that shows up to my lowest moments with chocolate and a smile and accompanies my best days adventuring near and far.

1.0 Introduction

Fertilization is one of the most important processes that must occur correctly in order for sexual reproducing species to proliferate. However, fertilization of an egg by more than one sperm, a condition known as polyspermy, is lethal to a developing embryo. When multiple sperm enter a single egg, there is an excess of centrioles that create multipolar spindles and disrupt mitotic divisions (*1*). Additionally, the zygote inherits an unviable amount of DNA (*2*). Accordingly, polyspermic eggs have no potential for producing a viable embryo in most sexually reproducing species.

1.1 Polyspermy prevention mechanisms

While a few physiologically polyspermic species exist, including various reptiles and birds (*3, 4*), generally polyspermy prevention is necessary to ensure proper embryonic development. Accordingly, eggs have various mechanisms to prevent entry of more than one sperm; the two most common are known as the fast and slow blocks (*5, 6*). The fast polyspermy block is an electrical barrier to sperm entry and is created by a fertilization-induced depolarization of the egg membrane within seconds of gamete unification (*7*). To date, the fast block has only been documented in eggs from oviparous organisms with external fertilization, where the sperm-to-egg ratio is elevated at the time of fertilization (*7-14*). This fertilization-induced depolarization protects

the nascent zygote prior to enactment of the slow block, which occurs tens of seconds to minutes after fertilization (*5, 6*). The slow block occurs ubiquitously in sexual reproducers; it encompasses numerous processes that transform the extracellular matrix (ECM) and plasma membrane of the egg to be impenetrable by sperm (*5, 6, 15, 16*).

Remarkably, both polyspermy blocks were first proposed by Ernest Just 100 years ago based on his own sand dollar fertilization experiments (*17*). Specifically, Just observed the lifting of the egg envelope in response to cortical granule exocytosis 30 seconds after insemination, and he noted that additional sperm were not capable of fertilizing an egg with a raised envelope – a process that would come to be known as the slow polyspermy block (*17*). Because numerous sperm reached the egg before the envelope raised, Just predicted that a more immediate barrier would be necessary to inhibit polyspermy – thereby suggesting the fast polyspermy block (*17*). The study of polyspermy prevention mechanisms has expanded over the past century with hopes of understanding how supernumerary sperm are repelled by fertilized eggs.

1.1.1 The slow polyspermy block

The slow polyspermy block broadly contains two post-fertilization events that physically prevent supernumerary sperm from entering an already fertilized egg. This includes an ECM block and a membrane fusion block (*2, 5*).

Before a sperm reaches an egg, it must traverse the egg ECM that physically surrounds the plasma membrane. This extracellular coating is proximal to the egg membrane is denoted as the zona pellucida (ZP) in mammals, vitelline envelope in amphibians, vitelline layer in sea urchins,

and chorion in fish. This matrix is made of glycoproteins, often referred to as ZP proteins, in most animal eggs (*5, 18-20*). Currently there are six known subfamilies of ZP proteins, which are conserved in vertebrates and invertebrates (*20*). The ZP proteins organize into a non-covalently bonded network that deters overwhelming numbers of sperm from reaching the egg membrane at once (*2, 5*). Sperm must bind to and penetrate the ZP meshwork to reach the egg. Once at the membrane, receptors on the egg are available for sperm to bind to, and gamete fusion occurs. These initial sperm-egg interactions stimulate egg activation, which reawakens the quiescent egg to resume the cell cycle and initiate polyspermy blocks.

In all sexually reproducing species studied thus far, including invertebrates, vertebrates, and flowering plants, egg activation involves an increase of cytosolic Ca^{2+} (*5, 21, 22*). Amplification of this second messenger is crucial for signal transduction in the egg. Increased cytosolic Ca^{2+} stimulates the exocytosis of cortical granules docked at the inner periphery of the egg membrane, which then hardens the egg's ECM (*5, 21, 22*).

The contents of cortical granules transform the extracellular matrix surrounding fertilized eggs into a barrier impenetrable to additional sperm (*23*). Part of this transformation involves enzymatic cleavage of proteins in the ECM to prevent sperm binding. In mammals, sperm bind directly to zona pellucida glycoprotein 2 (ZP2) (*16, 24*). The exocytosis of cortical granules from mammalian eggs includes release of the metalloendopeptidase ovastacin, which cleaves ZP2 and inhibits sperm binding (*16, 24*). Similarly, an astacin-family metalloendopeptidase, alveolin, has been identified in cortical granules of the teleost fish medaka, and the exocytosis of alveolin contributes to chorion hardening (*25, 26*). Though not yet identified, proteases are suspected to be

released from the cortical granules of other animals as well (*5, 6, 27, 28*). In addition to proteases, it has been speculated that other cortical granule components also alter the ECM to inhibit sperm penetration (*5*). The divalent cation zinc (Zn^{2+}) has recently been found to accumulate in mammalian cortical granules (*29-31*). Additionally, it has been suggested that Zn^{2+} released upon cortical granule exocytosis may contribute to the hardening of the ZP (*32*).

In addition to changes in the ECM surrounding the nascent zygote, transformations of the plasma membrane after fertilization also prevent the entry of additional sperm. Unlike fertilization-evoked changes to the eggs' ECM which have been studied in diverse organisms, the membrane fusion block has mainly been studied in mammals (*33*). Sperm-egg contact at the mammalian membrane is mediated by the sperm surface protein Izumo1 binding to the egg receptor Juno (*2, 15*). Following fertilization, Juno is shed from the egg plasma membrane in vesicles, thereby inhibiting sperm recognition and fusion with the egg (*2, 15*). Intriguingly, Juno shedding only occurs following fertilization, not parthenogenic activation or intracytoplasmic sperm injection, thereby suggesting that sperm-egg fusion somehow stimulates the mammalian membrane polyspermy block (*15, 33*). Though a membrane fusion block has been suggested in other animals (*5*), the identity of their sperm-egg receptor complexes is unknown.

1.1.2 The fast polyspermy block

The fast polyspermy block is a fertilization-evoked depolarization of the egg membrane that electrically inhibits the entry of additional sperm into an already fertilized egg. This polyspermy block is needed in externally fertilizing organisms, where the sperm-to-egg ratio is elevated at the moment of fertilization (*7-14*).

In the 1950s, several independent groups laid the groundwork for uncovering the fast polyspermy block by making electrical recordings from various types of eggs during fertilization or artificial activation, including starfish (*34*), toads (*35*), and sea urchins (*36*). Although this fertilization-associated depolarization of the egg seemed to be a shared feature in eggs from externally fertilizing species, it would be another 20 years before scientists would uncover its physiological significance. Elucidating the role of these depolarizations required that scientists be able to control the membrane potential of the egg rather than simply make passive recordings. Creation of the voltage clamp (*37-39*) would ultimately enable the discovery of the fast block. In 1976, Laurinda Jaffe voltage clamped sea urchin eggs and demonstrated that the polarization of sea urchin membranes dictated whether sperm could enter (*7*). Following this initial characterization of the fast block in sea urchins, similar studies expanded the list of known organisms that use the fast polyspermy block to include many, but not all, echinoderms (*14, 40*), ascidians (*13*), anurans (*9, 41*), algae (*11*), and marine worms (*12*).

Diversity amongst the species that employ the fast block and environmental conditions at the site and time of fertilization has given rise to differing fast block signaling pathways. While the molecular mechanisms signaling the fast block differ between species, three characteristics are shared between eggs that undergo the fast block (*42*). First, fertilization induces a depolarization of the egg plasma membrane, referred to as the fertilization potential, which persists for at least one minute (*7, 43*). Second, sperm can bind, but not enter, eggs that are clamped at their fertilization potential voltage (*7, 14, 44*). Lastly, eggs clamped at their resting potential can be penetrated by multiple sperm (*7, 14*).

1.2 Using *Xenopus laevis* to study polyspermy prevention mechanisms

1.2.1 Strengths of *X. laevis* as a model for fertilization

Xenopus laevis, the African clawed frog, is a classic model organism used by biophysicists and developmental biologists alike. The diverse utility of this system has allowed for the creation of a wide-array of well-established experimental tools.

Biophysicists, for example, exogenously express ion channels in *X. laevis* immature, prophase I arrested oocytes for functional studies of these channels (Fig. 1-1) (*45-47*). Thousands of oocytes can be obtained at once by surgically removing ovarian sacs from the frog abdomen. Because *X. laevis* oocytes are large, 1.2-1.3 mm in diameter (*48*), researchers can easily inject cRNA into them to exogenously express their channel of interest. Moreover, by using oocytes as an expression system, we have gained a wealth of knowledge regarding the endogenous channels in the *X. laevis* oocyte (*49-51*).

Developmental biologists use *X. laevis* to study events ranging from fertilization to embryogenesis (*52*). *X. laevis* are external fertilizers that can be induced to ovulate thousands of eggs in a day, which can be synchronously fertilized *in vitro*. Females lay fertilization-competent, metaphase II arrested eggs that are 1.4 mm in diameter, even larger than their oocytes (Fig. 1-1) (*53*). *X. laevis* eggs are amenable to electrophysiological recordings, as well as injection of cRNA and proteins. As *X. laevis* and humans diverged only 360 million years ago (*54*), many facets of their developmental processes are conserved.

1.2.2 The slow polyspermy block in *X. laevis*

As in all species studied thus far, the slow polyspermy block in *X. laevis* is triggered by an increase of cytosolic Ca^{2+} *(6, 21, 55)*. Ca^{2+} initially rises in the egg at the site of sperm contact and travels across the egg as a wave (*22, 55, 56*). A requirement for increased Ca^{2+} in the slow block was demonstrated by fertilizing *X. laevis* eggs loaded with the Ca^{2+} chelator BAPTA (*57*). These eggs did not exocytose their cortical granules and were highly polyspermic (*57*). Four lines of evidence demonstrate that the Ca^{2+} needed for the slow block originates from the endoplasmic reticulum (ER) in an inositol 1,4,5-trisphosphate (IP_3)-dependent pathway. First, the total amount of IP_3 increases in *X. laevis* eggs upon fertilization (*58-60*). Second, injection of IP_3 into *X. laevis* eggs stimulates a global Ca^{2+} increase, as well as cortical granule exocytosis (*61*). Finally, when *X. laevis* eggs were loaded with the Ca^{2+} indicator fura-2 and fluorescently imaged during fertilization in the presence of heparin, an IP_3 receptor (IP_3R) inhibitor, or an IP_3R antibody, the fertilization-induced Ca^{2+} increase was blocked (*62, 63*).

Fertilization signals a *de novo* production of IP_3 by the enzymatic cleavage of phosphatidylinositol 4,5-bisphosphate (PIP_2) by phospholipase C (PLC) (*22*). To test whether PLC activity was necessary for the slow polyspermy block in *X. laevis*, eggs were fertilized in the presence of the general PLC inhibitor U73122 (*58*). These eggs failed to produce a Ca^{2+} wave and had an increased incidence of polyspermy (*58*). Although these results demonstrate that fertilization activates a PLC in *X. laevis* eggs, the molecular identity of this PLC and the signaling pathway that activates this enzyme remain controversial. *X. laevis* eggs contain two PLC isoforms, β and γ, each of which is activated by a different transmembrane receptor stimulus (*64, 65*). Experiments seeking to uncover the PLC that signals the slow block used photometry to monitor

intracellular Ca^{2+} during *X. laevis* fertilization; they demonstrated that neither SH2 domain-mediated activation of PLCγ nor G_q-mediated activation of PLCβ were required (*66*). Another group used the tyrosine kinase inhibitors lavendustin A and PP1 to prevent PLCγ activation and reported that these treatments inhibited the fertilization-induced Ca^{2+} wave (*58, 67*). Due to these contradictory findings, the exact mechanism that stimulates the slow polyspermy block in *X. laevis* has yet to be resolved.

1.2.3 The fast polyspermy block in *X. laevis*

In frogs, as well as other amphibians with a fast block, a fertilization-activated efflux of Cl^- from the egg carries the depolarizing current (*41, 68*). Cl^- currents are often responsible for hyperpolarizing excitable cells. However, amphibians fertilize in freshwater, which is more dilute than the intracellular milieu. Thus, when fertilization signals the opening of Cl^- permeant channels, anions leave the egg to thereby make the membrane potential more positive.

A prominent role of a Cl^- efflux in the fast block was discovered by recording from *X. laevis* eggs during fertilization in differing concentrations of extracellular Cl^-. Normally, fertilization signals a depolarization of the egg from around -20 mV to +5 mV (*9, 43*). Fertilizations in solutions with limited extracellular Cl^- led to larger than normal depolarizations due to a larger driving force; whereas fertilizations in higher extracellular Cl^- resulted in smaller depolarizations (*43*). Additional experiments replaced extracellular Cl^- with other halides to further substantiate that a Cl^- current mediates the fast polyspermy block in *X. laevis*. Typically, Cl^- conducting ion channels can pass other halide anions (*69*). Because halides such as I^- and Br^- are not present in the egg, enriching the extracellular solution with these anions creates a chemical gradient that

supports their influx into the cell. Compared to depolarizations recorded in typical solutions where the dominant extracellular anion was Cl^-, fertilization did not change the membrane potential of eggs inseminated in Br^- containing solutions and induced hyperpolarizations in eggs inseminated in I^- containing solutions (*43*). Fertilization in the presence of I^- or Br^- also lead to an increased incidence of polyspermy (*43*). Together these data reveal that fertilization opens a Cl^- channel in *X. laevis* eggs to mediate the fast block.

In addition to a Cl^- efflux, an increase in intracellular Ca^{2+} is required for fertilization to depolarize *X. laevis* eggs. The necessity for increased cytosolic Ca^{2+} was demonstrated with experiments recording the membrane potential during fertilization of *X. laevis* eggs loaded with the Ca^{2+} chelator BAPTA (*57*); BAPTA binds Ca^{2+} with high affinity and thereby quenches an elevation of this cation (*70*). In these BAPTA-loaded eggs, fertilization failed to evoke a depolarization and caused an increased incidence of polyspermy (*57*). Additional experiments demonstrated that application of a Ca^{2+} ionophore, a lipid-soluble compound that transports Ca^{2+} across the plasma membrane, to eggs increased intracellular Ca^{2+} and evoked a depolarization in the absence of sperm (*43*). Together these results demonstrate that an increase in intracellular Ca^{2+} is required for, and sufficient to, evoke the fast block in *X. laevis* eggs. Overall, these findings gave rise to the hypothesis that a Ca^{2+}-activated Cl^- channel (CaCC) mediates the fertilization-evoked depolarization in *X. laevis* eggs (*71*).

1.3 Dissertation aims

Although the fast polyspermy block was first hypothesized 100 years ago and recorded nearly 40 years ago (*7, 17*), we still do not know the molecular details that signal this pathway in any species. Two aims of my dissertation were to elucidate the intricate cellular mechanisms mediating the fast block to polyspermy in the *X. laevis*, including: 1) the identity of the Cl^- channel responsible for the depolarization, and 2) the source for increased intracellular Ca^{2+}. This work was published in two companion manuscripts in the Journal of General Physiology (*72, 73*), which are featured as chapters 3 and 4 in this document.

The third aim of my dissertation was to investigate a role for extracellular Zn^{2+} exocytosed during the slow polyspermy block from non-mammalian eggs. It has previously been established that Zn^{2+} is released upon fertilization of eggs from multiple mammalian species (*29-31*), and this increased extracellular Zn^{2+} is speculated to contribute to a polyspermy block (*24, 32*). However, a causal relationship between increased extracellular Zn^{2+} and polyspermy prevention has yet to be investigated. Furthermore, the conservation of fertilization-induced Zn^{2+} release has not been examined in non-mammals. I sought to investigate the role of Zn^{2+} in fertilization using *X. laevis*, the zebrafish *Danio rerio*, the sea urchin S*trongylocentrotus purpuratus*, the cnidarian *Hydractinia symbiolongicarpus*, and the axolotl *Ambystoma mexicanum*, which can be found in chapter 5 of this document.

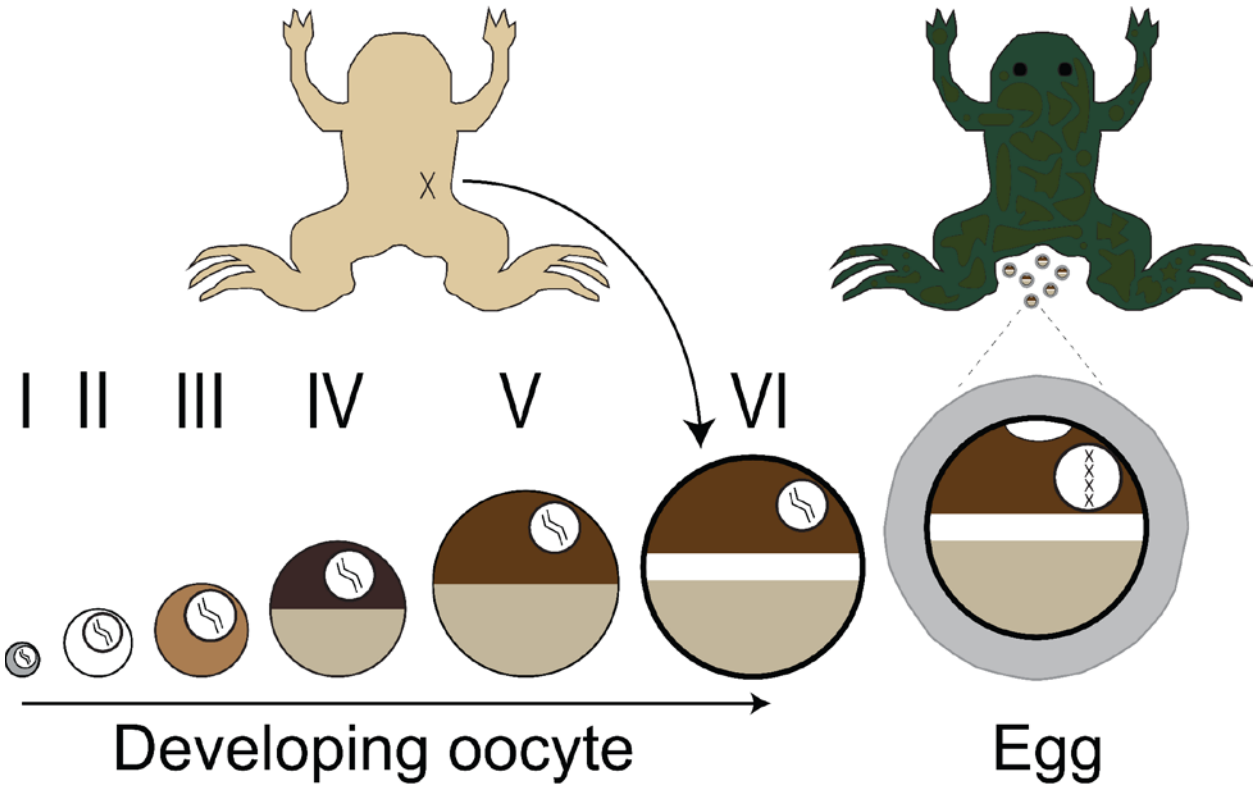

Figure 1-1. Schematic depiction of gamete development in female *X. laevis*

Immature oocytes, ranging from the youngest (stage I) to the most developed (stage VI), are located within the ovaries. These oocytes can be surgically removed from the abdomen of the frog (shown in ventral view at top left) and are commonly used by biophysicists. Upon hormonal induction, stage VI oocytes mature into fertilization-competent eggs, which are laid by the frog (shown in dorsal view at top right). Oocytes and eggs differ with respect to membrane-localized proteins as well as the structure of the cytoskeleton. *This figure was previously published in (72).*

2.0 Methods

2.1 Reagents

Xestospongin C (Xesto), $GdCl_3$, U-73343, and 2-aminoethoxydiphenyl borate (2-APB) were sourced from Tocris (Bristol, UK). U-73122 hydrate, 1 M $MgSO_4$ solution, 0.1 M $ZnCl_2$ solution, 2-[(5-Ethyl-1,6-dihydro-4-methyl-6-oxo-2-pyrimidinyl)thio]-N-[4-(4-methoxyphenyl)-2-thiazolyl]-acetamide ($T16A_{inh}$-A01), and 6-(1,1-Dimethylethyl)-2-[(2-furanylcarbonyl)amino]-4,5,6,7-tetrahydrobenzo[*b*]thiophene-3-carboxylic acid ($CaCC_{inh}$-A01) were purchased from Sigma-Aldrich (St. Louis, MO). N-((4-methoxy)-2-naphthyl)-5-nitroanthranilic acid (MONNA) was sourced from Sigma-Aldrich and Tocris. 2-(4-chloro-2-methylphenoxy)-N-[(2-methoxyphenyl)methylideneamino]-acetamide (Ani9) from ChemDiv (San Diego, CA). SK&F-96365 was sourced from Cayman Chemical (Ann Arbor, MI). Human chorionic gonadotropin (hCG) was purchased from Henry Schien (Melville, NY). All other materials, unless noted, were purchased from Thermo Fisher Scientific (Waltham, MA).

2.2 Animals

All animal procedures were conducted using accepted standards of humane animal care and were approved by the Animal Care and Use Committee at the University of Pittsburgh.

2.2.1 *Xenopus laevis*

X. laevis (frog) adults were obtained commercially (NASCO, Fort Atkinson, WI) and housed at 18 °C with a 12/12-hour light/dark cycle.

2.2.2 *Ambystoma mexicanum*

A. mexicanum (axolotl) adults were obtained commercially (Ambystoma Genetic Stock Center, Lexington, KY) and housed at 18 °C with a 12/12-hour light/dark cycle.

2.2.3 *Danio rerio*

D. rerio (zebrafish) were used in collaboration with Dr. Miler Lee at the University of Pittsburgh. *D. rerio* adults (5-17 months), lab bred TU-AB strain, were housed at 27 °C with a 14/10-hour light/dark cycle.

2.2.4 S*trongylocentrotus purpuratus*

S. purpuratus (sea urchin) were used in collaboration with Dr. Veronica Hinman and Dr. Katherine Buckley at Carnegie Mellon University. Adult *S. purpuratus* were obtained commercially (Monterey Abalone Company, Monterey, CA) and housed at 15 °C with a 12/12-hour light/dark cycle.

2.2.5 *Hydractinia symbiolongicarpus*

H. symbiolongicarpus were used in collaboration with Dr. Matthew Nicotra and Dr. Steven Sanders at the University of Pittsburgh. For these experiments we used sexually mature, lab bred colonies (MN291-10 and MN295-8, male and female, respectively) grown on glass microscope slides and housed at 22-23°C with an 8/16-hour light/dark cycle.

2.3 Experimental methods

2.3.1 Proteomic and RNA sequencing (RNA-seq) analysis

Paired-end raw RNA-seq reads from (*74*) were downloaded from the NCBI Sequence Read Archive (SRA) (https://www.ncbi.nlm.nih.gov/sra) (accession numbers SRX1287719, SRX1287720, SRX1287721, and SRX1287707). Reads were aligned using HISAT2 (*75*) in paired-end mode with default parameters to the *X. laevis* v9.1 genome, obtained from Xenbase (http://www.xenbase.org), then assigned to genes using featureCounts (*76*) on Xenbase primary gene models v1.8.3.2 in unstranded, paired-end mode using the gene_ID attribute and allowing multi-mappers (-p -s 0 -M). Raw counts were then normalized to transcripts per million. Expression values for L and S versions of each gene were summed.

To identify Ca^{2+}-permeant channels, we extracted all genes annotated with gene ontology (GO) molecular function terms that contained the keywords “calcium” and “channel” (Fig. 2-1, for complete dataset see reference (*73*)) using Xenbase GO term annotations. Due to incomplete

annotation of the *X. laevis* genome, GO terms associated with *X. tropicalis* genes were transferred to their *X. laevis* orthologs.

To identify Ca^{2+}-activated Cl^- channels expressed in *X. laevis* eggs, we first identified all channel genes by assembling 25 relevant GO terms that distinguished the following classes of channels: Cl^-, Ca^{2+}, Na^+, and K^+ (Fig. 2-2, for complete dataset see reference (*72*)). To account for possible gaps in GO term annotation, all family members of any gene annotated into the Ca^{2+}-activated Cl^- channel category were also included in further analysis; for example, all TMEM16 family members regardless of their GO annotation were included in this analysis.

For all datasets, heatmaps were generated in R Studio-1.1.383 using the heatmap.2 command from the gplots package. *Proteomic and RNA-seq analyses were conducted in collaboration with Wesley Phelps and Miler Lee.*

To estimate the number of TMEM16A, BEST2A, and IP3R channels in the egg, we combined the protein concentrations with the stoichiometry of the functional channel: two subunits for TMEM16A channels (*77*), five for BEST2 (*78, 79*), and four for IP3R1 (*80, 81*). We then assumed that *X. laevis* eggs are spherical, and calculated their volume based on their measured diameter of 1.4 mm (*53*).

2.3.2 Solutions

2.3.2.1 *X. laevis* fertilization solutions

Variations of Modified Ringers (MR) solution were used for all *X. laevis* fertilization experiments. MR contains (in mM): 100 NaCl, 1.8 KCl, 2.0 $CaCl_2$, 1.0 $MgCl_2$, and 5.0 HEPES, pH 7.8, and is filtered using a sterile, 0.2 µm polystyrene filter (*82*).

Control fertilization recordings were made in our standard solution of 20% MR diluted in DDH_2O (also referred to as MR/5). Various inhibitors were added to MR/5 and used during fertilization recordings. These experimental conditions were made by diluting concentrated stocks of each inhibitor that were each made in water or dimethyl sulfoxide (DMSO). All recordings were made in solutions that contained a final DMSO concentration of <0.5%, except for those made in 500 nM Xesto. The 500 nM Xesto in MR/5 solution contained 2% DMSO; because we have found that fertilization in ≥2% DMSO alone can alter embryonic development (Table 3-2) the control for the Xesto treatment was MR/5 with 2% DMSO.

Development assays were performed in 33% MR diluted in DDH_2O (MR/3). Various inhibitors were added to MR/3, which contained final DMSO concentrations of <0.5%, except for the 500 nM Xesto trials. As described above, the 500 nM Xesto treatment solution contained 2% DMSO; we included MR/3 with 2% DMSO as a control solution for this trial.

2.3.2.2 *X. laevis* and *A. mexicanum* oocyte solution

Oocyte Ringers 2 (OR2) was used to rinse oocytes after collagenase treatment. OR2 is comprised of (in mM): 82.5 NaCl, 2.5 KCl, 1 $MgCl_2$, and 5 mM HEPES, pH 7.6, and is filtered using a sterile, 0.2 µm polystyrene filter (*83*).

2.3.2.3 Two-electrode voltage clamp solution

ND96 was used for two-electrode voltage clamp (TEVC) recordings. ND96 is comprised of (in mM): 96 NaCl, 2 KCl, 1 $MgCl_2$, 10 HEPES, pH 7.6 and is filtered with a sterile, 0.2 µm polystyrene filter (*84*). Various inhibitors were added to ND96, that contained <0.5% DMSO, for TEVC recordings.

2.3.2.4 *D. rerio* activation solution

D. rerio eggs were parthenogenically activated by hydrating dry eggs in DDH_2O (*85*).

2.3.2.5 *S. purpuratus* fertilization solution

Lab-made artificial sea water (spASW) was used for *S. purpuratus* development assays. The spASW is comprised of (in mM): 470 NaCl, 10 KCl, 11 $CaCl_2$, 29 $MgSO_4$, 27 $MgCl_2$, and 2.5 $NaHCO_3$, pH 8, and is filtered using a sterile, 0.2 µm polystyrene filter (*86*).

2.3.2.6 *H. symbiolongicarpus* fertilization solution

Commercial artificial sea water (hsASW) was used for *H. symbiolongicarpus* development assays. The hsASW is comprised of solubilized Instant Ocean Reef Crystals (Instant Ocean Spectrum Brands) at 28 parts per trillion.

2.3.3 *X. laevis* and *A. mexicanum* collection of oocytes

Oocytes were collected from ovarian sacs obtained from *X. laevis* females anesthetized with a 30-minute immersion in 1.0 g/L tricaine-S (MS-222) at pH 7.4, or from *A. mexicanum* females euthanized by a 30-minute immersion in 3.6 g/L tricaine-S at pH 7.4 (*84*). For both types of oocytes, excised ovarian sacs were manually pulled apart, then dispersed by a 90 minutes incubation in 1 mg/ml collagenase in ND96 supplemented with 5 mM sodium pyruvate and 10 mg/L of gentamycin. Collagenase was removed by repeated washes with OR2, and healthy oocytes were sorted and stored at 14 °C in ND96 with sodium pyruvate and gentamycin.

2.3.4 *X. laevis* collection of gametes, fertilization, and development assays

Eggs were collected from sexually mature female *X. laevis*. Female frogs were injected 1,000 IU of hCG into their dorsal lymph sac and housed overnight for 12-16 hours at 14-16 °C. Typically, females began laying eggs within 2 hours of moving to room temperature. Eggs were collected on dry petri dishes and used within 10 minutes of being laid.

In some experiments, eggs were dejellied prior to fertilization (*53, 82*). To remove the jelly coat, eggs were agitated in 45 mM 2-mercaptoethanol in MR/3 (pH 8.5) for 2-3 minutes. Once removal of the jelly coat was confirmed by visual observation, eggs were neutralized in MR/3 (pH 6.5), followed by three washes in MR/3 (pH 7.8).

To determine the effects of Zn^{2+} on dejellying, *X. laevis* eggs were incubated in 1 mM $ZnSO_4$ or MR/3 for 3 minutes. All eggs were washed in MR/3 three times, prior to undergoing the

dejelly protocol. To aid in visualization, all eggs were returned to 1 mM $ZnSO_4$ for imaging. *Kavya Pasumarthy and Meghan Hanson helped with these experiments.*

Sperm were obtained from testes harvested from sexually mature *X. laevis* males (*53, 72, 73*). Following euthanasia by a 30-minute immersion in 3.6 g/L tricaine-S (pH 7.4), testes were dissected and cleaned by manual removal of fat and remaining vasculature. Cleaned testes were stored at 4 °C in MR for usage on the day of dissection or in L-15 medium for use up to one week later.

To create a sperm suspension for whole cell recordings, approximately 1/10 of a testis was minced in 200-300 µL of MR/5; sperm were added to the recording chamber in 25 µL increments. If not used immediately, this solution was stored on ice and used for up to one hour. No more than three sperm additions were added to a given egg during whole cell recordings, and the total volume of sperm suspension added never exceeded 7.5% of the total fertilization solution. Eggs inseminated during whole cell recordings were transferred to MR/3 for up to 47 hours after insemination to monitor development. Development was assessed based on the appearance of cleavage furrows (*53, 72, 73*). *Wase Tembo helped with control and 2-APB recordings.*

Developmental assays were performed by incubating approximately 20-40 eggs per treatment in MR/3 with or without indicated inhibitors for 10 minutes. 1/10 testis was then minced in 200-500 µL of MR, and 20-90 µL of the sperm suspension was used to fertilize eggs depending on the size of the fertilization dish. For the majority of development assays performed, eggs and sperm were incubated in these solutions until approximately 90-120 minutes after insemination

when the initiation of embryonic development was assessed based on the appearance of cleavage furrows (Fig. 2-3). For development assays in ionomycin, eggs were placed in 10 µM ionomycin for 7 minutes, washed in MR/3 three times, and incubated in MR/3 for 120-150 minutes before developmental assessment. *Monica Sauer, Ben Wisner, Meli Linderman, Meghan Hanson, and Kavya Pasumarthy helped with these experiments.*

We found that prolonged incubation of eggs in TMEM16a inhibitors interfered with development. Therefore, eggs in development assays using TMEM16a inhibitors were washed in MR/3 30 minutes after insemination and maintained in MR/3 for an additional 60-90 minutes. Furthermore, to increase the sperm-to-egg ratio during this shorted incubation (*43*), we inseminated eggs with 1/3 of a testis that was then minced in MR and added to each treatment.

Transfer assays were performed by incubating eggs in an initial experimental condition, removing the eggs from this condition, washing three times in the transfer solution, and then maintaining eggs in the transfer solution for the duration of the experiment. Two types of transfer assays were conducted: transfer before insemination and transfer after insemination. When transferred before fertilization, eggs were incubated in the starting solution for 15 minutes and inseminated in the transfer solution. When transferred after insemination, eggs and sperm were incubated together in the starting solution for 30 minutes, then transferred. *Transfer assays were performed by Monica Sauer, Ben Wisner, Meli Linderman, Meghan Hanson, and Kavya Pasumarthy.*

In all development and transfer assays, development was assessed at 90-120 minutes post-insemination based on the presence or absence of cleavage furrows. Developed embryos were considered monospermic or polyspermic based on cleavage furrow symmetry (*43, 87*): embryos with a symmetrical pattern were denoted monospermic and those with an asymmetric and incomplete furrows were deemed polyspermic (*43*) (Fig. 2-3). Each assay was repeated at least three times with different females and on different experiment days.

2.3.5 *D. rerio* collection of gametes

D. rerio gametes were a generous gift from Dr. Miler Lee (University of Pittsburgh, Pittsburgh PA). Selection of mating pairs was random. To stimulate spawning, mating pairs were housed together overnight with a divider separating them (*85, 88*). In the morning, the females were anesthetized in 0.25 mg/mL MS-222 (pH 7.2), rinsed in DDH2O, and patted dry. Eggs were retrieved from anesthetized females by applying pressure to their abdomens (*85*). Dry eggs were collected using a 200 µL pipette tip and placed onto a dry imaging slide. Parthenogenic egg activation was induced by hydrating the eggs with DDH20 (*85*). Successful egg activation was assayed based on the appearance of a blastodisc with cleavage furrows (Fig. 2-3). *Maddy Czekalski and Wesley Phelps helped with these experiments.*

2.3.6 *S. purpuratus* collection of gametes, fertilization, and development assays

Sea urchin gametes were a generous gift from Dr. Veronica Hinman and Dr. Katherine Buckley (Carnegie Mellon University, Pittsburgh PA). Spawning was induced by manually agitating sea urchins or injecting them with 200 – 500 µL of 0.5 M KCl and then agitating (*86*).

Sperm were collected directly from the animal using a 200 µL pipette and placed into a tube. Eggs were released into a beaker of spASW, then rinsed through a 100 µm filter.

For development assays, sperm were activated by diluting concentrated sperm 5:1000 into spASW. 20 µL of activated sperm was used to fertilize eggs in 5 mL spASW with varying concentration of $ZnSO_4$. Successful fertilization was noted within 2 minutes of sperm addition by the raising of the fertilization envelope (Fig. 2-3). Development was assayed 90-120 minutes post-fertilization based on the appearance of cleavage furrows (Fig. 2-3). *Rachel Bainbridge helped with these experiments.*

2.3.7 *H. symbiolongicarpus* collection of gametes, fertilization, and development assays

H. symbioloongicarpus gametes were a generous gift from Dr. Matthew Nicotra and Dr. Steven Sanders (University of Pittsburgh, Pittsburgh PA). Upon the first light exposure for the day, spawning was induced by placing male and female colonies in separate bins (*89*). Gametes were released within 60-90 minutes of light exposure. Eggs were collected from the spawning tank, filtered through a 20 µm cell strainer, and maintained in hsASW. Sperm were collected from the male tank using a 1 mL pipette and maintained in hsASW.

For development assays, equal volumes of sperm and egg solutions were mixed together with varying concentrations of $ZnSO_4$. Development was assayed at 60 minutes post-fertilization based on the appearance of cleavage furrows (Fig. 2-3). *Rachel Bainbridge helped with these experiments.*

2.3.8 Electrophysiology

Electrophysiology recordings were made using TEV-200A amplifiers (Dagan Co.) and digitized by Axon Digidata 1550A (Molecular Devices). Data were acquired with pClamp Software (Molecular Devices) at a rate of 5 kHz.

2.3.8.1 Whole cell recording

Fertilization-evoked depolarizations were recorded in the whole cell configuration. Pipettes made from borosilicate glass were 5-20 MΩ resistance and filled with 1 M KCl. Resting and fertilization potentials were quantified approximately 10 seconds before and after the depolarization, respectively. Depolarization rates for each recording were quantified by determining the maximum velocity of the quickest 1 mV shift in the membrane potential.

2.3.8.2 Two electrode voltage clamp (TEVC)

IP_3-evoked currents were recorded in the TEVC configuration, from *X. laevis* or *A. mexicanum* oocytes held at -80 mV. Recordings were made from wild-type oocytes not expressing any exogenous channel, or from oocytes exogenously expressing xTMEM16A or xBest2A. The cDNA encoding the xTMEM16A channel in the GEMHE vector was provided by L. Jan (University of California San Francisco, San Francisco CA) (*84*). The cDNA encoding the xBEST2A channel was purchased from DNASU (*90*) and was engineered into the GEMHE vector with a carboxy-terminal Ruby tag (*91*) using overlapping PCR and Gibson assembly methods. The sequences for all constructs were verified by automated Sanger sequencing (Gene Wiz). The xTMEM16A and xBEST2A cRNAs were transcribed using the T7 mMessage mMachine Ultra kit (Ambion), and MemE with the SP6 mMessage mMachine kit (Ambion). Defolliculated *A.*

mexicanum oocytes were injected with 5 ng of cRNA for xTMEM16A or xBEST2A (*84*). Prior to recording, injected oocytes were incubated at 14 °C for 24 hours, followed by incubation at 18 °C for 2-5 days.

Both *A. mexicanum* and *X. laevis* oocytes were injected with the photolabile IP_3 analog: *myo*-inositol 1,4,5-trisphosphate, *P*4(5)-1-(2-nitrophenyl) ethyl ester (caged-IP_3). Each oocyte was injected with a 200 µM caged-IP_3 stock made in DDH_2O to reach a final concentration of 5 µM within the oocyte (*84*), and incubated in the dark at 18 °C for 1-5 hours before recording. Pipettes of 1-8 MΩ resistance were pulled from borosilicate glass and filled with 1 M KCl. The nitrophenyl cage on IP_3 was released by flash photolysis with a 250 ms exposure to light derived from the Ultra High Power White LED Illuminator (380-603 nm, Prizmatix) and guided by a liquid light source to the top of oocytes in our recording chambers (RC-26G, Warner Instruments). The bath solution was changed with the gravity fed, pinch valve VC-8 solution changer (Warner Instruments). Background-subtracted peak currents were quantified from two consecutive recordings: one before and one with application of the tested inhibitors. It is not possible to directly compare current amplitudes generated in different oocytes due to the innate variability of the experimental set-up (*i.e*. positioning of the UV light, exact amount of caged-IP_3 in each oocyte, etc.). The proportional difference between peak currents before and with inhibitor application for each oocyte was used to quantify the percent inhibition for each treatment.

2.3.9 Fluorometry

The Zn^{2+} released with fertilization or parthenogenic activation was measured for *X. laevis* by fluorometry with the fluorescent Zn^{2+} indicator FluoZin-3. For *X. laevis*, batches of 30-100

freshly ovulated eggs were dejellied, then inseminated with sperm or activated with 10 µM ionomycin. The MR/3 solution surrounding the eggs was collected 30 minutes after the addition of ionomycin and 45 minutes after sperm addition. Insemination solutions were spun at 3000 rpm for 5 minutes to pellet sperm, and the supernatant was transferred to a new tube. The Zn^{2+} content of each MR/3 sample was quantified using FluoZin-3 photometry.

FluoZin-3 tetrapotassium salt was dispensed from a 1 mM stock in water for a final concentration of 60 nM in each MR/3 aliquot. Fluorescence intensity measurements were recorded in a 1 mm quartz cuvette, in a Fluorolog3 spectrophotometer with FluoEssence software (both from HORIBA, Jobin Yovon). FluoZin-3 containing samples were excited with 492 nm light, and emission was recorded at 514 nm with 3 nm slit widths. The raw photometric signals were corrected for by subtracting the FluoZin-3 free background, collected prior to adding FluoZin-3 to each sample. The ratio of the corrected signal was calibrated (*53, 92, 93*) with equation 1 to determine the concentration of Zn^{2+} in each sample:

$$\text{Equation 1: } [Zn^{2+}] = K^* \times \frac{R - R_{min}}{R_{max} - R}$$

where the constants R_{min} (560393 counts, 1 nM), R_{max} (1808940, 100 nM), and K* (14 nM) were obtained from MR/3 supplemented with known amounts of $ZnSO_4$ ranging from 10 pM to 30 µM fitted to a Hill equation (*53, 92*).

To determine the number of Zn^{2+} ions released with fertilization or parthenogenic activation, the total Zn^{2+} content measured by FluoZin-3 photometry was multiple by the dilution

factor for that sample and Avogadro's number, and divided by the volume of solution collected from each trial and the number of eggs per trial.

2.3.10 Imaging

2.3.10.1 Fluorescent imaging

A. mexicanum oocytes were imaged using a TCS SP5 confocal microscope (Leica Microsystems, Wetzlar, Germany) equipped with a Leica 506224 5X objective. As a membrane control, oocytes were injected with cRNA for a membrane anchored eGFP (*94*). EGFP was excited with a 488 nm visible laser, whereas Ruby was excited with a 561 nm laser. Using a galvo scanner with unidirectional (600 Hz) scanning, sequential frames were captured with 2x line averaging. Images were analyzed using LAS AF (version 3.0.0 build 834) software and ImageJ (*95*).

2.3.10.2 Time-lapse imaging of *X. laevis* and *D. rerio* eggs and *A. mexicanum* oocytes during fertilization and parthenogenic activation

X. laevis and *D. rerio* eggs and *A. mexicanum* oocytes were imaged using a TCS SP5 confocal microscope (Leica Microsystems, Wetzlar, Germany) equipped with a Leica 506224 5X objective. FluoZin-3 was excited with a 488 nm visible laser. Using a galvo scanner with unidirectional (600 Hz) scanning, FluoZin-3 and bright field images were taken every 3-5 seconds for up to 25 minutes. Images were analyzed using LAS AF (version 3.0.0 build 834) software and ImageJ (*95*).

X. laevis egg and sperm were collected and prepared as described above. Dejellied eggs were placed on a microscope slide with 50 µM FluoZin-3 in MR/3. For fertilization experiments,

sperm, prepared in MR/3, was added to the eggs, 1 minute after imaging began. For activation experiments, ionomycin in MR/3 was added to the eggs to reach a final concentration of 10 µM, 1 minute after imaging began. *Maddy Czekalski and Monica Sauer helped with these experiments.*

D. rerio eggs were collected as described above. Dry eggs were placed on a microscope slide. One minute after imaging began, 50 µM FluoZin-3 in DDH_2O was added to the eggs to activate them. *Maddy Czekalski and Wesley Phelps helped with these experiments.*

A. mexicanum oocytes were collected as described above. Oocytes were placed on a microscope slide with 50 µM FluoZin-3 in MR/3. To activate the oocytes, ionomycin in MR/3 was added to the eggs to reach a final concentration of 300 µM, 1 minute after imaging began.

2.3.10.3 Stereoscope images

X. laevis eggs and embryos were imaged using a stereoscope (Leica Microsystems, Wetzlar, Germany) equipped with a Leica 10447157 1X objective and DFC310 FX camera. Images were analyzed using LAS (version 3.6.0 build 488) software and Photoshop (Adobe). For the dejelling assay, *X. laevis* eggs were imaged using an Edmund Optics stereomicroscope with a 10x objective, fitted with a pixiLINK digital camera and the µScope Essential 64x software pixiLINK, Canada). The diameter of the egg and the surrounding jelly coat were determined in Adobe Illistrator (San Jose, CA).

D. rerio eggs were imaged using a Zeiss Stemi 508 stereoscope and Axiocam ERc 5s camera (Carl Zeiss Microscopy, Jena, Germany). Images were analyzed using Photoshop (Adobe). *Wesley Phelps helped capture these images.*

S. purpuratus eggs and embryos were imaged using an inverted Olympus IX73 stereoscope equipped with an Olympus UPlanFL N 10X objective, Olympus TL4 light source, and Olympus U-LS30-3 camera. Images were analyzed using Photoshop (Adobe).

H. symbiolongicarpus eggs and embryos were imaged using Leica M80 Stereoscope equipped with a Leica IC80 HD camera and Zeiss KL1500 LCD light source. Images were analyzed using Photoshop (Adobe).

2.4 Quantification and statistical analysis

Igor (WaveMetrics) and Excel (Microsoft) were used for analysis of electrophysiological recordings, as well as computation of development assays.

2.4.1 Development assays

Analysis of variation (ANOVA) followed by post-hoc Holm-Bonferroni tests were used to compare each inhibitor treatment to the control for developmental assays for chapters 3 and 4, unless otherwise noted.

2.4.2 Whole cell recordings

Data for each experimental condition are displayed in Tukey box plot distributions, where the box contains the data between 25-75%, and the whiskers span 10-90%. Additionally, averaged values ± standard error of the means (SEM), are reported for each experimental condition (Tables S1 & S2). All conditions contain trails that were conducted on multiple days with gametes from multiple females. T-tests (one-tailed for depolarization rates and two-tailed for resting and fertilization potentials) were used to determine differences between inhibitor treatments. Depolarization rates were $\log_{10}$ transformed before statistical analysis.

2.4.3 TEVC

Two-tailed T-tests were used to determine differences between inhibitor treatments for comparisons of relative amplitudes of IP_3-evoked currents. ANOVAs followed by post-hoc honestly significant difference (HSD) Tukey tests were used to compare different currents recorded with the same inhibitors for uncaging experiments.

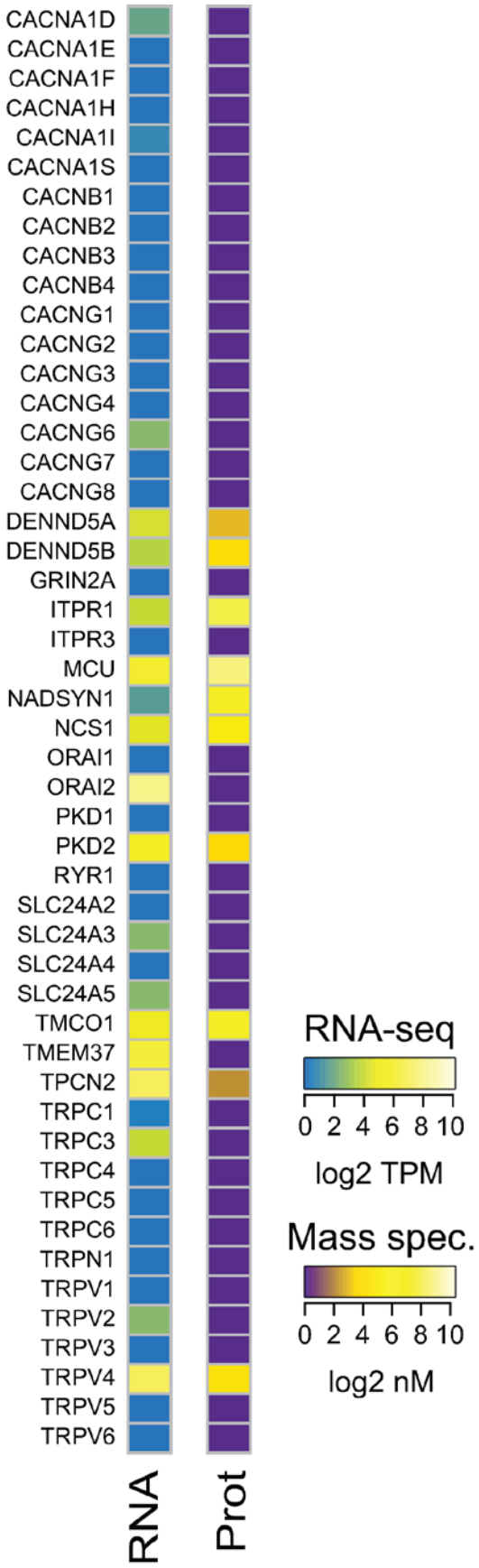
CACNA1D
CACNA1E
CACNA1F
CACNA1H
CACNA1I
CACNA1S
CACNB1
CACNB2
CACNB3
CACNB4
CACNG1
CACNG2
CACNG3
CACNG4
CACNG6
CACNG7
CACNG8
DENND5A
DENND5B
GRIN2A
ITPR1
ITPR3
MCU
NADSYN1
NCS1
ORAI1
ORAI2
PKD1
PKD2
RYR1
SLC24A2
SLC24A3
SLC24A4
SLC24A5
TMCO1
TMEM37
TPCN2
TRPC1
TRPC3
TRPC4
TRPC5
TRPC6
TRPN1
TRPV1
TRPV2
TRPV3
TRPV4
TRPV5
TRPV6
RNA
Prot
RNA-seq
0 2 4 6 8 10
log2 TPM
Mass spec.
0 2 4 6 8 10
log2 nM

Figure 2-1. Ca^{2+}channel expression in *X. laevis* eggs

Heatmaps showing (left) RNA expression levels (based on RNA-seq from (*74*)), as log_2 transcripts per million (TPM), and (right) protein concentrations (based on mass spectrometry from (*64*)) in log_2 nanomolar. Transcripts and proteins are alphabetically organized. *This data was collected in collaboration with Wesley Phelps and Miler Lee. and published in (73).*

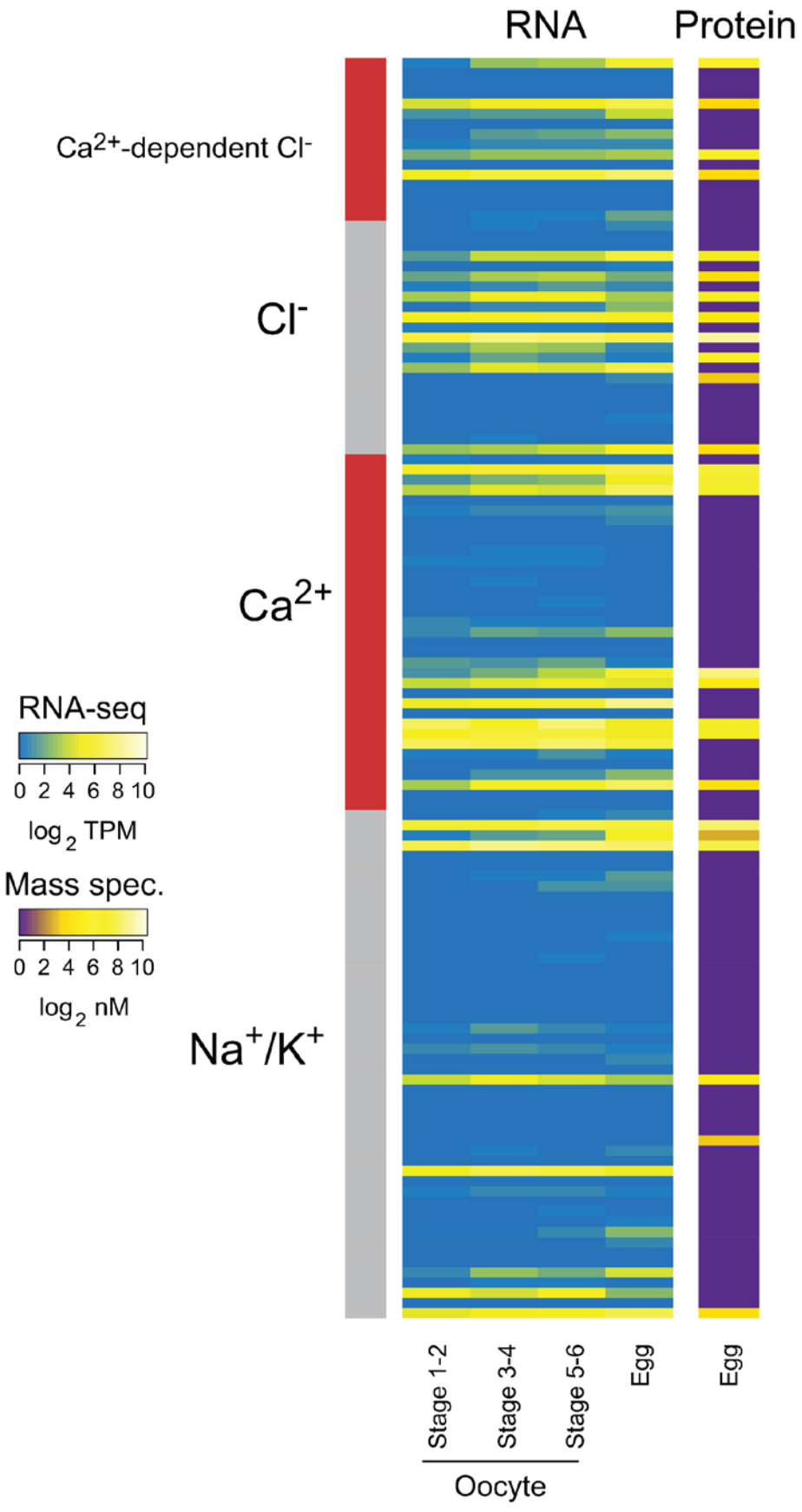
RNA
Protein
Ca2+-dependent Cl-
Cl-
Ca2+
Na+/K+
RNA-seq
0 2 4 6 8 10
log2 TPM
Mass spec.
0 2 4 6 8 10
log2 nM
Stage 1-2
Stage 3-4
Stage 5-6
Egg
Egg
Oocyte

Figure 2-2. Ion channel expression in *X. laevis* eggs

Heatmaps showing (left) RNA expression levels (based on RNA-seq from (*74*)), as $\log_2$ transcripts per million (TPM), and (right) protein concentrations (based on mass spectrometry from (*64*)) in $\log_2$ nanomolar. Transcripts and proteins are grouped by channel type. *This data was collected in collaboration with Wesley Phelps and Miler Lee and published in (72)*

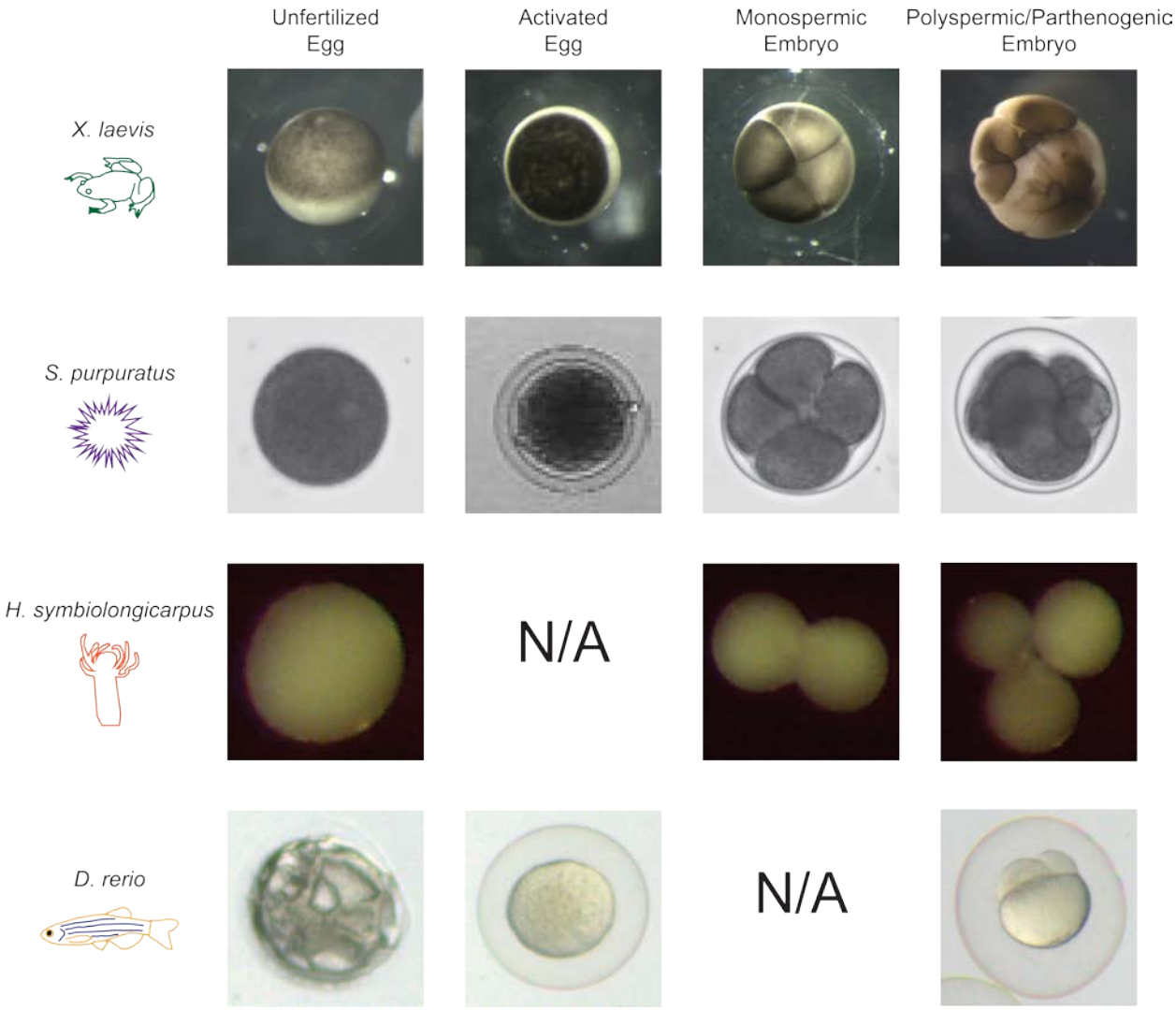

Figure 2-3. Developmental stages of *X. laevis, D. rerio, S. purpuratus*, and *H. symbiolongicarpus* eggs and embryos

Representative images of *X. laevis*, *D. rerio*, *S. purpuratus*, and *H. symbiolongicarpus* unfertilized eggs, activated eggs (either by sperm or parthenogenesis) that show signs of development resuming, monospermic embryos denoted by symmetric cleavages, and polyspermic embryos (or the long-term result of parthenogenic activation) denoted by asymmetric cleavages. Both polyspermic and parthenogenic embryos undergo similar abortive cleavages. N/A represents that

these developmental stages are either not noticeable (*H. symbiolongicarpus* egg activation) or applicable to these studies (*D. rerio* monospermic embryo).

3.0 Fast polyspermy block is signaled by IP_3-evoked Ca^{2+} release in *Xenopus laevis* eggs

3.1 Introduction

Embryonic development is a tightly regulated series of events that begins with the fertilization of an egg by a single sperm. This remarkable process of gamete unification is surprisingly error-prone. For example, the fertilization of an egg by more than one sperm, a condition known as polyspermy, is a significant barrier to successful reproduction (*5*). Polyspermy causes chromosomal abnormalities that are embryonic lethal in nearly all sexually reproducing species. To avoid polyspermy-induced lethality, eggs have developed multiple mechanisms to prevent sperm entry into an already-fertilized egg (*5, 21*). One common polyspermy prevention mechanism utilized by external fertilizers, such as frogs and sea urchins, is the fast polyspermy block. The fast block involves depolarization of the egg within seconds of fertilization to create an electrical barrier that inhibits additional sperm from entering a fertilized egg (*7*). For most species, the molecular pathways driving the fertilization-evoked depolarizations of the fast block are still poorly understood.

In frogs, elevated cytosolic Ca^{2+} is required for the fast polyspermy block (*43, 57*). A prominent role for elevated intracellular Ca^{2+} as a trigger for the fast block has previously been demonstrated by two independent experiments. First, fertilization failed to evoke a depolarization in *X. laevis* eggs loaded with the Ca^{2+}-chelator BAPTA (*57*), demonstrating that increased cytosolic Ca^{2+} is necessary for the fast block. Second, treating *X. laevis* eggs with a Ca^{2+} ionophore, a lipid soluble compound that transports Ca^{2+} across the plasma membrane and increases the intracellular Ca^{2+} concentration, evoked a depolarization in the absence of fertilization (*43*). The ionophore signaled depolarization demonstrated that increased intracellular Ca^{2+} is sufficient to trigger the fast block. Additionally, a Cl^- current is known to depolarize the egg membrane at fertilization to mediate the fast polyspermy block in *X. laevis* (*9, 43, 96, 97*). We have recently demonstrated that the Ca^{2+}-activated Cl^- channel, TMEM16A, conducts this current in eggs from the African clawed frog *Xenopus laevis* (*72*) (*see chapter 4*). Although it is known that increased intracellular Ca^{2+} is required to open TMEM16A channels (*84, 98, 99*), until recently, how fertilization signals changes in Ca^{2+} concentration within the frog egg was unknown.

Here we sought to uncover the mechanisms by which fertilization signals increased intracellular Ca^{2+} in the *X. laevis* egg to activate the fast block. We reasoned that fertilization could signal the opening of Ca^{2+} permeant channels to allow Ca^{2+} entry into the egg; or that Ca^{2+} could be released from an intracellular store. To distinguish between these two possibilities, we interrogated existing proteomics and RNA-sequencing (RNA-seq) data and found that two Ca^{2+}-permeant channels, TRPV4 and PKD2, are expressed in *X. laevis* eggs (*64, 74*). However, insemination in the presence of broad spectrum Ca^{2+} channel inhibitors, at concentrations known to block the candidate channels, did not alter the fertilization-signaled depolarization. In contrast,

inhibition of phospholipase C (PLC) and inositol 1,4,5-trisphosphate (IP_3) receptors (IP_3Rs) on the endoplasmic reticulum (ER) successfully abolished any fertilization-signaled depolarization and increased the incidence of polyspermic fertilizations. Together these results indicate that fertilization activates PLC to release Ca^{2+} from the ER and signal the fast block in *X. laevis* eggs.

3.2 Results

3.2.1 Fertilization signals a depolarization in *X. laevis* eggs

To characterize the fast block to polyspermy, we made whole cell recordings from *X. laevis* eggs during fertilization in the control condition (MR/5 solution). Eggs with stable resting potentials were inseminated by pipetting sperm directly on top, and their membrane potentials were recorded for up to 40 minutes (Fig. 3-1 A) or until the cortex contracted (Fig. 2-3), an early indicator of successful fertilization. Fig. 3-1 A depicts a typical fertilization-evoked depolarization. An average of 5.2 ± 0.5 min (N=31) passed between sperm addition and the recorded depolarization of the fast block, which likely represents the time required for the sperm to penetrate the viscous jelly coat of the egg (*96*). Under control conditions, the average egg resting potential was -17.9 ± 0.9 mV, and the fertilization potential was -2.6 ± 1.1 mV (N=31) (Fig. 3-1 B and Table 3-1). The average rate of depolarization for eggs fertilized under the control conditions was 3.9 ± 0.8 mV/ms (N=31) (Fig. 1 C).

3.2.2 Ca^{2+} entry into the egg is not required for the fast block in *X. laevis*

To identify the source of Ca^{2+} that signals the fast block, we first explored the hypothesis that fertilization may evoke Ca^{2+} entry from the extracellular environment through plasma membrane-traversing Ca^{2+} channels. We interrogated existing proteomics and RNA-seq datasets and identified ten proteins associated with Ca^{2+} transport that are expressed in the *X. laevis* egg (Fig. 3-2) (*64*, *74*). Of these, four were intracellular: the IP_3R found in the ER (ITPR1), the mitochondrial Ca^{2+} uniporter (MCU), the ER localized Ca^{2+} load-activated channel (TMCO1), and the two pore channel located in acidic vesicles (TPCN2) (*100-108*). We also found several proteins that were annotated as Ca^{2+} channels but cannot directly transport ions across the membrane, although they are capable of regulating Ca^{2+}-channel activity: the soluble Ca^{2+} binding protein called frequinin (encoded by NCS1) (*109*, *110*); two guanine nucleotide exchange factors (DENND5A & DENND5B); and the NAD synthase 1 (NADSYN1). The final two proteins were the transient receptor potential subfamily V, member 4 (TRPV4) channel, and polycystin-2 (PKD2). These were the only candidates that have cation-permeant pores that could facilitate Ca^{2+} entry from the extracellular environment into the egg. The proteomics and RNA-seq data reveal that fertilization *could* open a plasma membrane Ca^{2+} channel, either TRPV4 or PKD2, to increase intracellular Ca^{2+} and signal the fast block.

Next, we determined whether Ca^{2+} entry is required for the fast block by recording from *X. laevis* eggs inseminated in the presence of broad spectrum, Ca^{2+}-channel inhibitors. Although we chose inhibitors known to inhibit most Ca^{2+}-permeant channels, we used concentrations demonstrated to block TRPV4 and PKD2: Gd^{3+} (*111*, *112*) or SK&F-96365 (*113*, *114*). There were no significant differences between depolarizations recorded under control conditions (Fig. 3-1)

and in solutions supplemented with 10 μM $GdCl_3$ or 20 μM SK&F-96365 (Figs. 3-3 A&B, $P > 0.05$, T-test). Like eggs fertilized under control conditions, the average resting potential of eggs in Gd^{3+} was -17.0 ± 2.3 mV, and the fertilization potential was -2.6 ± 0.7 mV (N=8, Figs. 3-3 C&D). The depolarization rate for eggs inseminated in Gd^{3+} was 10.6 ± 7.9 mV/ms (N=8, Fig. 3-3 E), compared to 3.9 ± 0.8 mV/ms in control conditions (N=31, Fig. 3-1 B). Eggs recorded in SK&F-96365 had average resting potentials of -13.6 ± 2.0 mV and depolarized to -6.4 ± 1.9 mV (N=6, Figs. 3-3 C&D). The rate of depolarization of these eggs was 6.1 ± 3.7 mV/ms (Fig. 3-3 E).

In addition to determining whether Ca^{2+} entry is required for fertilization to activate a depolarization in *X. laevis* eggs, we also quantified the incidence of polyspermy in eggs inseminated in Gd^{3+} and SK&F-96365. Polyspermic fertilization results in incomplete and asymmetric furrows during the first few cleavage events; whereas, monospermy leads to symmetric furrows (Fig. 2-3) (*43*). We found that blocking extracellular Ca^{2+} from entering eggs had no effect on polyspermy rates (Table 3-2, Fig. 3-2 F, $P > 0.05$, ANOVA). Persistence of normal fertilization-evoked depolarizations and normal cleavage furrow formation in eggs inseminated with Ca^{2+}-channel blockers demonstrates that that Ca^{2+} entry from the extracellular environment is not required for the fast block.

3.2.3 The fast block requires IP_3-evoked Ca^{2+} release from the ER

To explore whether Ca^{2+} release from an intracellular store activates the fast block, we first interrogated an IP_3 mediated pathway. We reasoned that several minutes after fertilization an increase of IP_3 in the egg is known to induce the slow block by signaling Ca^{2+}-release from the ER to initiate cortical granule exocytosis (*55*). Additionally, injecting *X. laevis* eggs with an IP_3R

antibody inhibits this Ca^{2+} wave of the slow block and ceases embryonic development (*66*). Together, these studies indicate that IP_3 is necessary for early signaling events in *X. laevis* eggs. Furthermore, our own bioinformatics substantiates the presence of the IP_3R (encoded by the ITPR1 gene) in *X. laevis* eggs (Fig. 3-2). Based on protein concentrations, we estimate that the *X. laevis* egg contains ~5.3 x 10^{10} IP_3Rs. Although IP_3Rs are abundant in the *X. laevis* eggs, it was unclear whether fertilization could evoke a fast-enough elevation of IP_3 to trigger the fast block. We therefore determined whether blocking IP_3Rs altered the fertilization-signaled depolarization.

In the presence of the potent IP_3R inhibitor, Xestospongin C (Xesto) (*115, 116*), fertilization failed to evoke any depolarization in five independent trials (Fig. 3-4 A), yet all five of these embryos developed cleavage furrows. The resting potential of eggs in 500 nM Xesto was elevated compared to the control (-11.0 ± 1.4 mV in Xesto (N=5) vs -21.5 ± 4.2 mV in MR/5 with 2% DMSO, Fig. 3-4 B, $P < 0.05$, T-test). Importantly, others have shown that most *X. laevis* eggs held at -11 mV are capable of fertilization and the initiation of embryonic development (*96*). Because our Xesto treatment contained 2% DMSO, we controlled for these experiments by inseminating eggs in vehicle alone (2% DMSO in MR/5, Fig. 3-4 C). We found that the biophysical properties of the fast block recorded from eggs inseminated in vehicle alone were not different from control recordings made without DMSO, including the average depolarization rate of eggs inseminated in 2% DMSO (5.8 ± 3.9 mV/ms, N=5), which was statistically indistinguishable from control depolarizations ($P > 0.05$, T-test, Figs. 3-4 B, D-E). Inhibition of the fertilization-signaled depolarization by Xesto thereby demonstrates that IP_3Rs mediate the depolarization of *X. laevis* eggs.

In the presence of less-potent IP_3R inhibitor, 2-APB (*117*), fertilization evoked slower depolarizations compared to controls (Figs. 3-4 E&F). Specifically, fertilization of eggs inseminated in 100 μM 2-APB depolarized at a rate of 0.6 ± 0.3 mV/ms (N=8) compared to 3.9 ± 0.8 mV/ms (N=31) in MR/5 ($P < 0.05$, T-test). Because the depolarization rate is directly proportional to the number of TMEM16A channels opened by fertilization (*72*), a slower depolarization rate in *X. laevis* eggs inseminated in 2-APB reflects an attenuated Ca^{2+} release from the ER to ultimately open fewer TMEM16A channels. Based on rates measured in the presence and absence of 2-APB, we estimate that fertilization opened 6.5-fold fewer TMEM16A channels in the presence of the drug.

Blocking IP_3Rs led to a significant increase in the incidence of polyspermy compared to their control fertilization (Fig. 3-4 G). For example, insemination in the presence of 500 nM Xesto led to 34 ± 6% polyspermy compared to 13 ± 4% in 2% DMSO (Fig. 3 G, T-test, $P < 0.01$). Overall, blockade of the IP_3R with either Xesto or 2-APB diminished the fast block and increased the incidence of polyspermy. Together, these data demonstrate that an IP_3-evoked Ca^{2+} release from the ER is essential for the fast block.

3.2.4 The fast block requires PLC

IP_3 is generated *de novo* by the enzymatic activity of PLC, whereby the membrane phospholipid phosphatidylinositol 4,5-bisphosphate (PIP_2) is cleaved into IP_3 and diacylglycerol (DAG). To determine whether fertilization activates the synthesis of IP_3, we inseminated eggs in the presence of the PLC inhibitor U73122, or its inactive analog U73343 (*118, 119*). The structures of U73122 and U73343 are nearly identical and differ only by a double bond present in the active

site of U73122, which is a single bond is U73343. In seven separate trials, fertilization failed to evoke any depolarization in eggs inseminated in 1 μM U73122 (Fig. 3-5 A). Normal depolarizations, however, were recorded in the presence of comparable amounts of the inactive analog U73343 (N=8, Fig. 3-5 B). Neither the resting potentials nor the fertilization potentials recorded in U73122 and U73343 were different from those recorded in the MR/5 solution ($P > 0.05$, T-test, Figs. 3-5 C&D). Unexpectedly, eggs inseminated in the inactive analog depolarized more quickly relative to control fertilizations at a rate of 14.9 ± 6.6 mV/ms ($P < 0.05$, T-test, Fig. 3-5 E), thereby suggesting possible off-target effects by the inactive analog which have not been previously reported.

We found that eggs inseminated in U73122 had a significantly higher incidence of polyspermy than control (Fig. 3-5 F), where 60 ± 11% (N=3) polyspermy was induced with U73122 versus 11 ± 7% (N=3) in control conditions ($P < 0.01$, ANOVA). By contrast, the incidence of polyspermy in U73343 was the same as control ($P > 0.05$, ANOVA). Together these data suggest that the enzymatic activity of PLC, which generates IP_3, is required to initiate the fast block.

3.3 Discussion

The signaling pathways that underlie these fertilization-evoked depolarizations have remained elusive, despite their widespread use by evolutionarily divergent species. Here we sought to uncover the source of Ca^{2+} that initiates the fast polyspermy block in *X. laevis*. Our data demonstrates that the fast block is signaled by activation of PLC, to increase IP_3 which then

activates the ER-localized IP_3R (Fig. 3-6). Release of Ca^{2+} from the ER then opens TMEM16A channels that depolarizes the egg to inhibit additional sperm from entering an already fertilized egg (Fig. 3-6) (*72*).

3.3.1 Variations in fast block recordings

Previous studies showed that fertilization-evoked depolarizations vary with respect to amplitude and shape, even when recorded under control conditions (*9*, *43*, *97*). Our study further demonstrates that the rate of depolarization varies for each unique fertilization event. Because the depolarization rate is directly proportional to the number of TMEM16A channels that open (*72*), our data imply that fertilization of every egg is unique and leads to the opening of different numbers of channels. The variance in numbers of TMEM16A channels activated in response to fertilization may reflect variance in the amount of Ca^{2+} released from the ER in different eggs. For example, if fertilization opens TMEM16A by a pathway that involves receptor activation and second-messenger signaling, variation may reveal that some sperm activate multiple receptors whereas others activate only one. Alternatively, if the sperm donates a compound to initiate the fast block pathway, variation may reveal that sperm contain varying amounts of that compound.

3.3.2 Membrane-localized Ca^{2+} channels do not signal the fast block in *X. laevis*

To uncover the source of Ca^{2+} that signals the fast block, we first explored whether Ca^{2+}-permeant channels on the eggs plasma membrane were required for this fertilization-signaled depolarization. We have recently demonstrated that the jelly layer surrounding *X. laevis* eggs is enriched with 6.3 mM freely diffusing Ca^{2+} (*53*), thereby indicating that fertilization could signal

Ca^{2+} entry even with changing environmental conditions. By mining existing proteomics and RNA-seq datasets (*64, 74*), we uncovered that *X. laevis* eggs express two Ca^{2+}-permeant channels on the plasma membrane, TRPV4 and PKD2 (Fig. 3-2). A possible role for either channel in the fast block was attractive because both are known to transduce physical stress into cationic signaling (*120, 121*), and sperm-egg fusion at fertilization theoretically exerts forces on the membrane of the egg that could trigger the activation of these channels to induce the fast block. We found, however, that fertilization evoked normal depolarizations in the presence of the broad-spectrum Ca^{2+} channel inhibitors Gd^{3+} or SK&F-96365, which are known to block both TRPV4 (*112, 114*) and PKD2 (*114*) (Fig. 3-3). These results reveal that Ca^{2+} entry into the egg is unessential for the fast block, a surprising finding given that Ca^{2+} enters eggs from other external fertilizers at fertilization to initiate the fast block. In starfish and sea urchins, for example, the depolarization of the fast block is driven by nicotinic acid-adenine dinucleotide phosphate (NAADP) and voltage-gated Ca^{2+} channels (*122-124*); this pathway has been shown to be sensitive to SK&F-96265 and verapamil in starfish (*125*).

3.3.3 PLC induces IP_3 production to initiate the fast block in *X. laevis*

To explore a possible role for Ca^{2+} release from an intracellular store in the fast block, we tested the hypothesis that Ca^{2+} release from the ER via IP_3R was required for the fertilization-evoked depolarization. A prominent role for an IP_3-signaled Ca^{2+} release from the ER was particularly attractive because *X. laevis* eggs lack other prominent ER Ca^{2+} signaling mechanisms, such as ryanodine receptors (Fig. 3-2) (*126, 127*). Moreover, in eggs from nearly all species examined thus far, fertilization increases the IP_3 content in eggs to activate Ca^{2+} release from the ER and signal the cortical granule exocytosis of the slow block to polyspermy (*21, 128-130*).

Because the slow polyspermy block occurs minutes after sperm entry (*5, 21*), we worried that employing a second messenger cascade would be too slow to initiate the fast block. To test whether IP_3 signals the fast block in *X. laevis*, we inseminated eggs in the presence of IP_3R inhibitors Xesto or 2-APB. We found that inhibition of IP_3Rs diminished the fast block and increased the incidence of polyspermy (Fig. 3-4). These results demonstrate that IP_3 signals both the fast and the slow blocks to polyspermy in *X. laevis*. Furthermore, other intracellular Ca^{2+} stores, such as mitochondria or lysosomes, are not sufficient to induce the fast block in the absence of IP_3-medaited Ca^{2+} release from the ER.

Finally, we explored a possible role for PLC in signaling the fast block. Theoretically, sperm could bypass the need for PLC activity by entering eggs preloaded with enough IP_3 to stimulate for the fast block. However, fertilization failed to depolarize *X. laevis* eggs in the presence of the broad-spectrum PLC inhibitor U73122 (Fig. 3-5) (*118*). By contrast, depolarizations were unaltered in eggs inseminated in the presence of the U73122 inactive analog, U73343 (Fig. 3-5) (*118*). Together these results demonstrate a requirement for PLC activity for the fast block and reveal that IP_3 is created *de novo* in this pathway. Given that IP_3 synthesis is necessary for the fast block, the alternate hypothesis that fertilizing sperm release sufficient IP_3 to activate IP_3Rs is rejected.

3.3.4 Summary

In summary, fertilization quickly activates PLC to generate the IP_3 needed to induce Ca^{2+} release from the ER. This pathway culminates in a depolarizing efflux of Cl^- from the channel TMEM16A (*72*), thereby resulting in the fast, electrical polyspermy block in *X. laevis*. Many

questions remain regarding the upstream components of this pathway. For example, do sperm activate the depolarization by binding to a receptor on the extracellular surface of the egg to trigger a signaling cascade, or is sperm entry into the egg required to donate a fast block activating compound? How does egg membrane depolarization prevent sperm entry? Answering these questions will not only reveal the first events of new life but will also uncover the voltage dependence of fertilization.

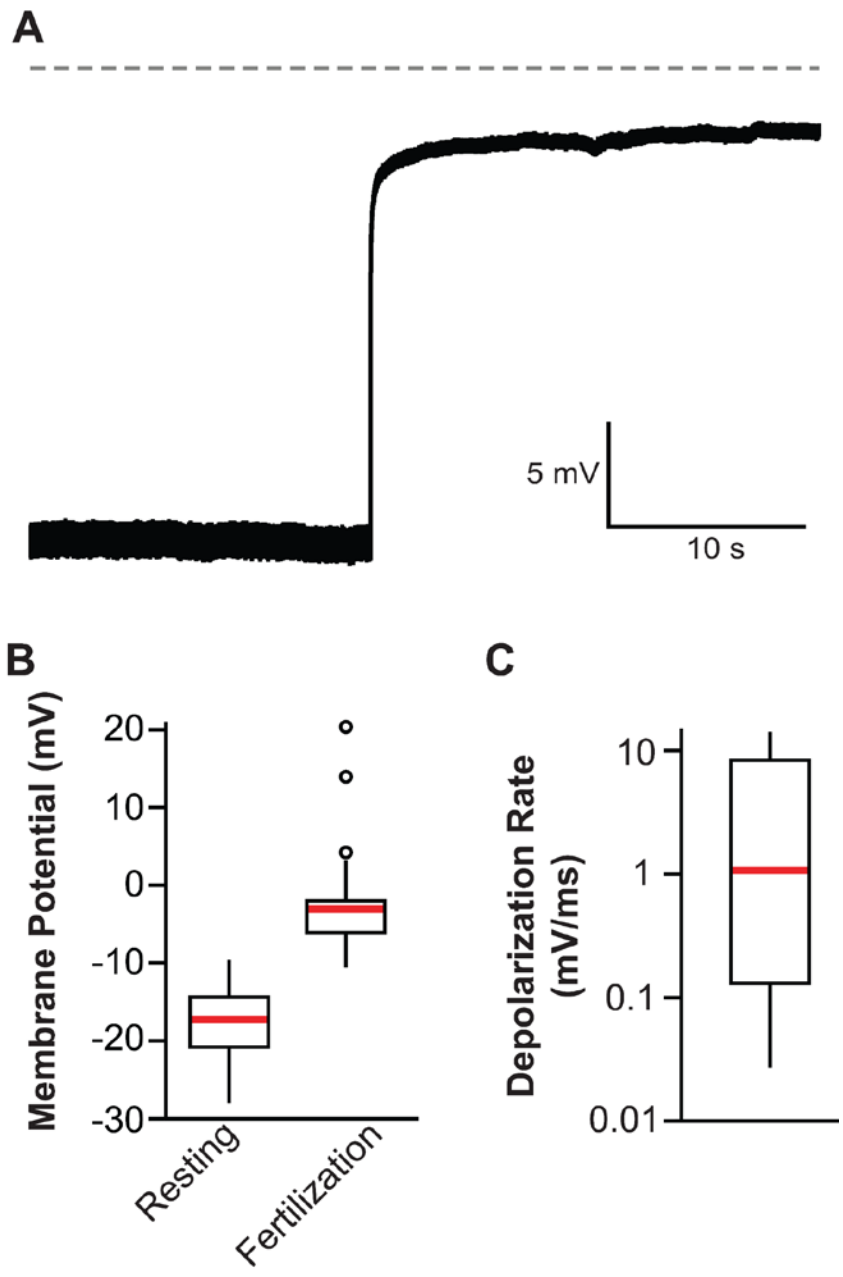

Figure 3-1. Fertilization signals a depolarization in *X. laevis* eggs

A) Representative whole-cell recordings made during fertilization in control conditions (in MR/5 solution). Dashed line denotes 0 mV. Tukey box plot distributions of the B) resting and fertilization potentials in control conditions and C) depolarization rate (N=31, recorded over 22 experiment days).

Table 3-1. Biophysical properties of fertilization-evoked depolarizations using various Ca^{2+} channel and PLC inhibitors

	Resting Potential (mV)	Fertilization Potential (mV)	Sperm addition to depolarization time (min)	Depolarization Rate (mV/ms)	N
Control (MR/5)	-17.9 ± 0.9	-2.6 ± 1.2	5.3 ± 0.5	3.9 ± 0.8	31
10 µM $GdCl_3$	-17.0 ± 2.3	-2.6 ± 0.7	3.5 ± 0.8	10.6 ± 7.9	8
20 µM SK&F-96365	-13.6 ± 2.0	-6.4 ± 1.9	3.8 ± 1.0	6.1 ± 3.6	6
500 nM Xesto	-11.0 ± 1.4	---	---	---	5
2% DMSO	-21.5 ± 4.2	-6.6 ± 2.3	8.0 ± 1.4	5.8 ± 3.4	5
100 µM 2-APB	-19.6 ± 1.4	-4.8 ± 2.0	6.6 ± 1.8	0.6 ± 0.3	8
1 µM U73122	-22.1 ± 4.1	---	---	---	7
1 µM U73343	-20.8 ± 2.3	-3.7 ± 1.2	1.9 ± 0.4	14.9 ± 6.6	8

Average ± SEM for the indicated measurement before, during, and after the fertilization-signaled depolarization.

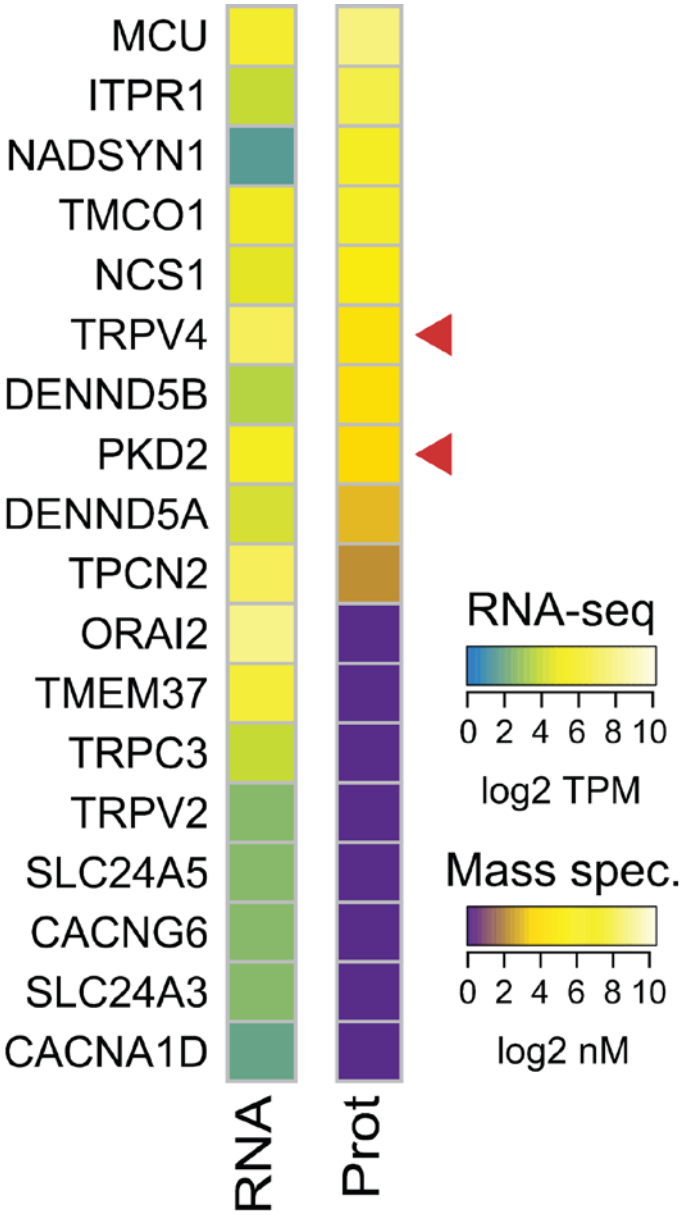

Figure 3-2. Expression of Ca^{2+} channels in *X. laevis* eggs

Heatmaps of RNA (*left)* and protein *(right)* expression levels of Ca^{2+} channels. Transcript levels (shown as transcripts per million (TPM)) from (*74*). Protein concentrations from (*64*) as determined by mass spectrometry-based proteomics in $\log_2$ nanomolar. Red arrows highlight plasma membrane localized Ca^{2+} channels found in eggs. *This data was collected in collaboration with Wesley Phelps and Miler Lee.*

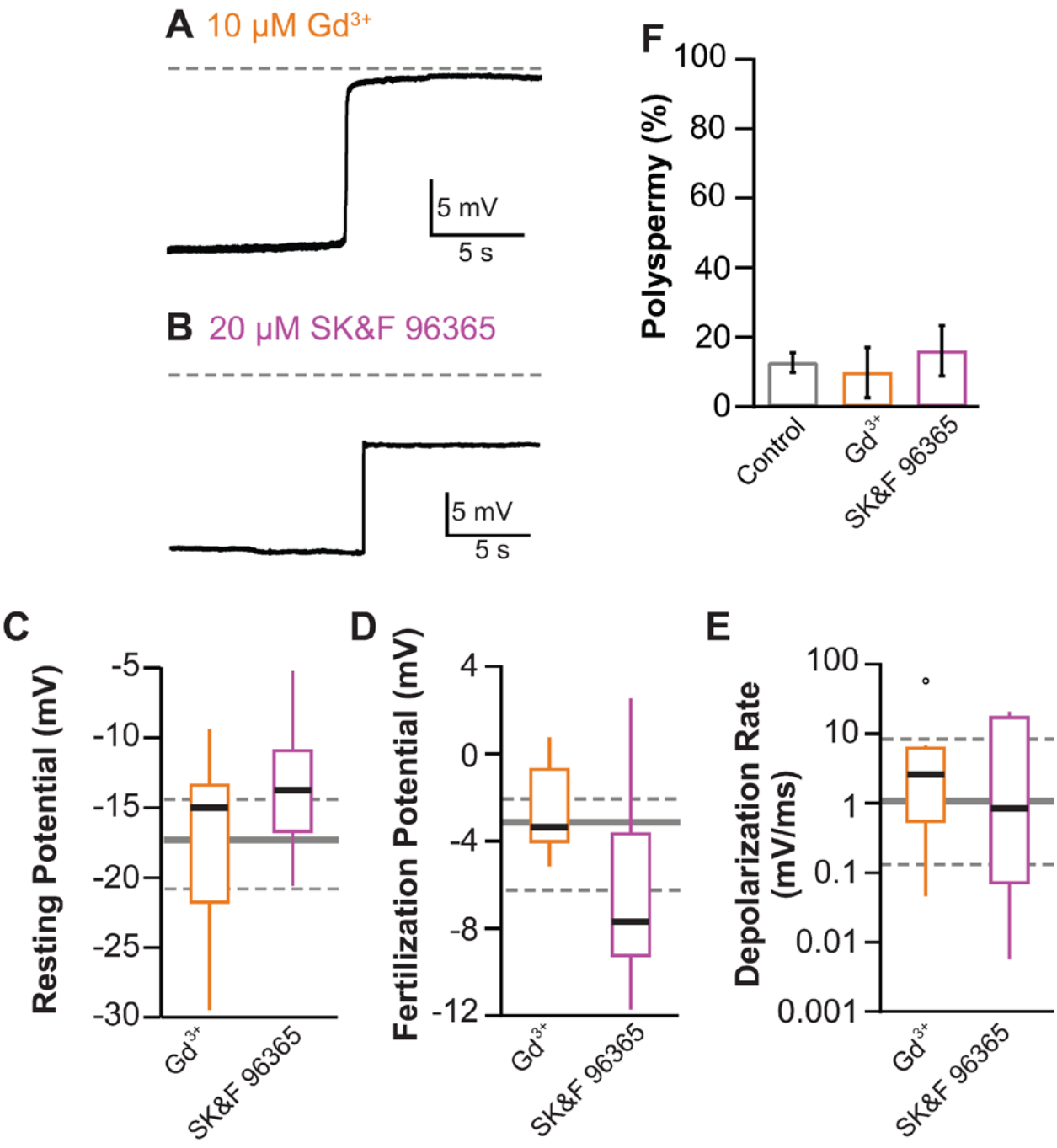

Figure 3-3. Fertilization-signaled depolarization does not require Ca^{2+} entry into *X. laevis* eggs

A-B) Representative fertilization recordings made in solutions with 10 µM $GdCl_3$ (A) and 20 µM SK&F-96365 (B). Dashed lines denote 0 mV. C-E) Tukey box plot distributions of the

resting (C) and fertilization (D) potentials, and depolarization rate (E), for indicated treatments (N=8-12, recorded over 3 experiment days/treatment). (D-E) The grey lines denote the Tukey box plot distributions for recordings made in control conditions (MR/5 solution). F) Proportion of polyspermic embryos out of total developed embryos in control, Gd^{3+}, and SK&F-96365 (N=3-6, recorded over 3-6 experiment days per treatment).

Table 3-2. Development assays using various Ca^{2+} channel and PLC inhibitors

	Undeveloped (%)	Developed (%)	Polyspermic (%)	N
Control	3 ± 2	97 ± 2	13 ± 3	6
10 µM Gd	5 ± 5	95 ± 5	10 ± 7	3
20 µM SK&F 96365	23 ± 11	77 ± 11	16 ± 7	3
Control	46 ± 15	54 ± 15	13 ± 4	3
500 nM Xesto	32 ± 8	68 ± 8	34 ± 6	3
Control	6 ± 5	94 ± 5	8 ± 4	3
100 µM 2-APB	19 ± 10	81 ± 10	69 ± 17	3
Control	18 ± 9	82 ± 9	11 ± 7	3
1 µM U73343	26 ± 16	74 ± 16	12 ± 3	3
1 µM U73122	35 ± 13	65 ± 13	60 ± 11	3

Average ± SEM for each fertilization condition. Out of the zygotes that initiated embryonic development, embryos were categorized as monospermic or polyspermic based on cleavage furrow symmetry (*see Fig. 2-3 for examples).* Control development for Xesto was MR/3 with 2% DMSO.

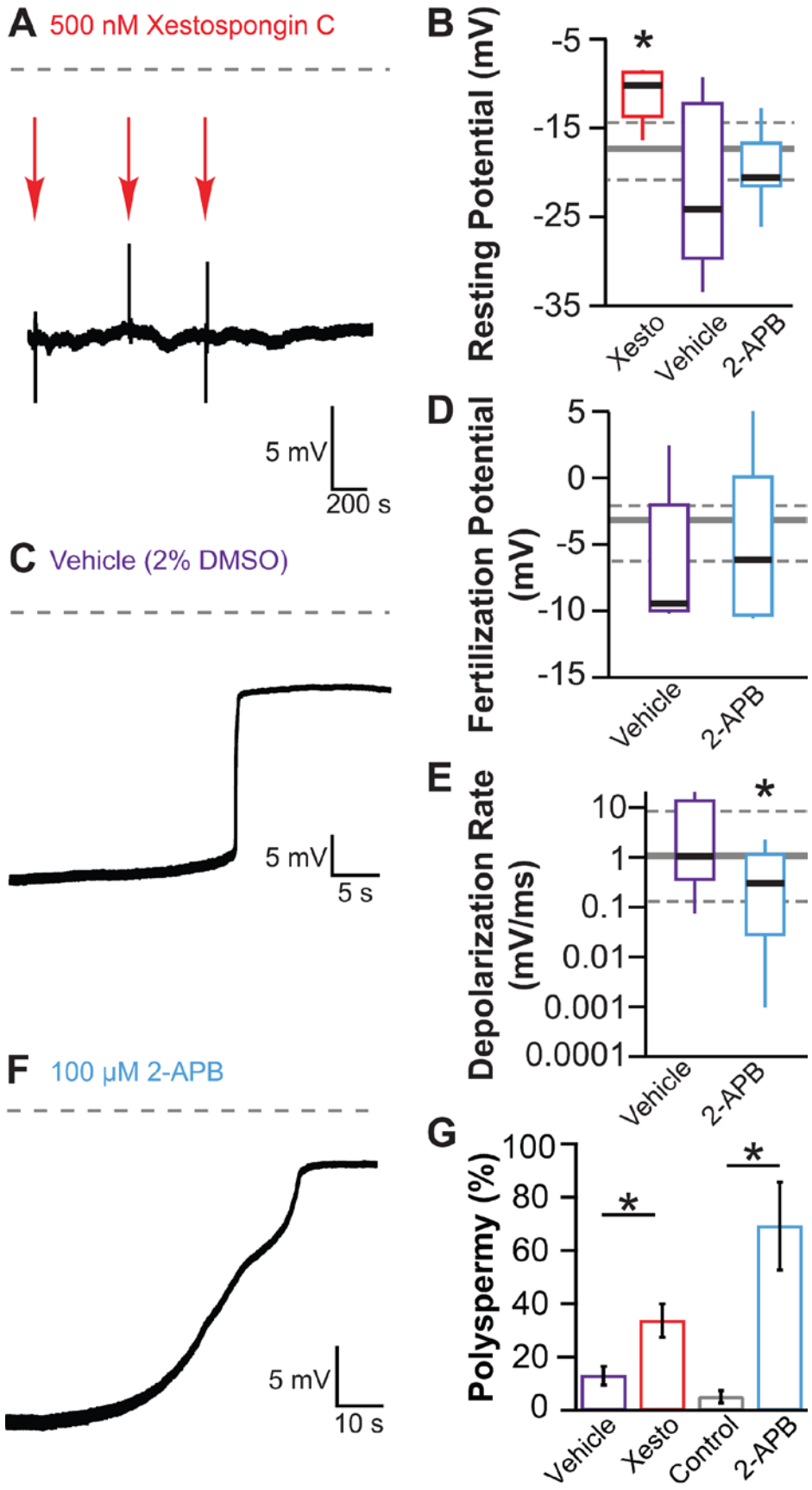
A
500 nM Xestospongin C
5 mV
200 s
C
Vehicle (2% DMSO)
5 mV
5 s
F
100 µM 2-APB
5 mV
10 s
B
Resting Potential (mV)
-5
-15
-25
-35
*
Xesto
Vehicle
2-APB
D
Fertilization Potential (mV)
5
0
-5
-10
-15
Vehicle
2-APB
E
Depolarization Rate (mV/ms)
10
1
0.1
0.01
0.001
0.0001
*
Vehicle
2-APB
G
Polyspermy (%)
100
80
60
40
20
0
*
*
Vehicle
Xesto
Control
2-APB

Figure 3-4. ER-released Ca^{2+} is essential for the fast polyspermy block

Representative fertilization recordings made in the presence of 500 nM Xesto (A), vehicle (2% DMSO) (C), or 100 μM 2-APB (F). Dashed line denotes 0 mV and arrows indicate sperm additions. Tukey box plot distributions of the resting (B) and fertilization (D) potentials, as well as the depolarization rates (E), from recordings made in the indicated treatments (N=5-8, 2-4 experiment days/treatment). (B-D) The grey lines behind the box plots represent the Tukey box plot distributions for the control (MR/5) data. G) Proportion of polyspermic embryos out of total developed embryos in vehicle (2% DMSO in MR/5), Xesto, control (MR/5), and 2-APB (N=3 recorded over 3 experiment days per treatment). * represents $P < 0.05$. *Some of the 2-APB and control recordings were collected by Wase Tembo.*

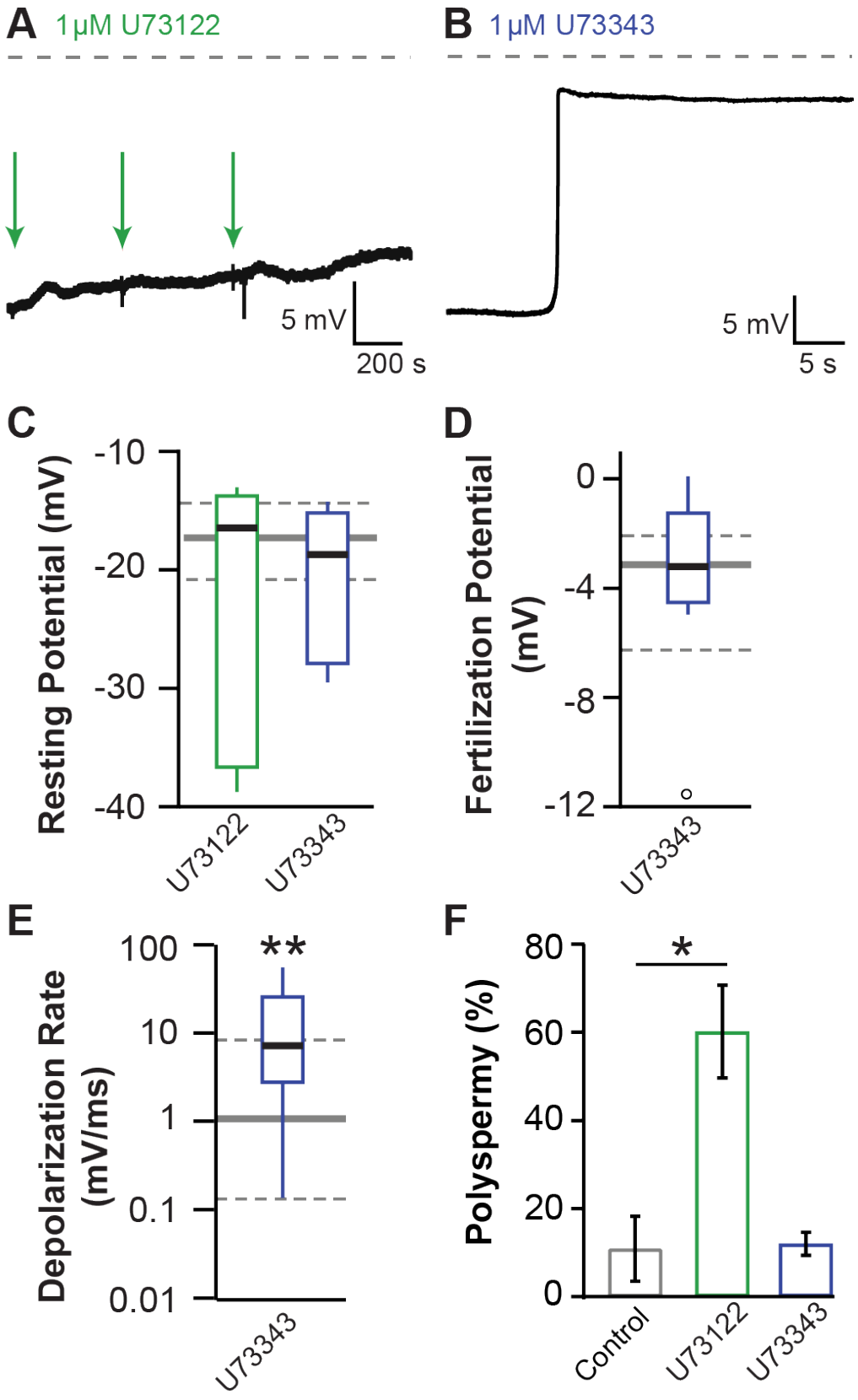
A
1 µM U73122
5 mV
200 s
B
1 µM U73343
5 mV
5 s
C
Resting Potential (mV)
-10
-20
-30
-40
U73122
U73343
D
Fertilization Potential (mV)
0
-4
-8
-12
U73343
E
Depolarization Rate (mV/ms)
100
10
1
0.1
0.01
**
U73343
F
Polyspermy (%)
80
60
40
20
0
*
Control
U73122
U73343

Figure 3-5. PLC is required for the fast block

A-B) Representative fertilization recordings made in 1 μM U73122 (A) or 1 μM U73343 (B). Dashed line denotes 0 mV and arrows indicate sperm additions. C-E) Tukey box plot distributions of the resting (C) and fertilization (D) potentials, and the depolarization rates (E), made in indicated treatments (N=7-8, recorded over 3-5 experiment days/treatment). The grey lines behind the box plots represent the Tukey box plot distributions for the control (MR/5) data. F) Percent polyspermic embryos out of total developed embryos in control (MR/5), U73122, and U73343. ** represents $P < 0.01$ and * represents $P < 0.05$.

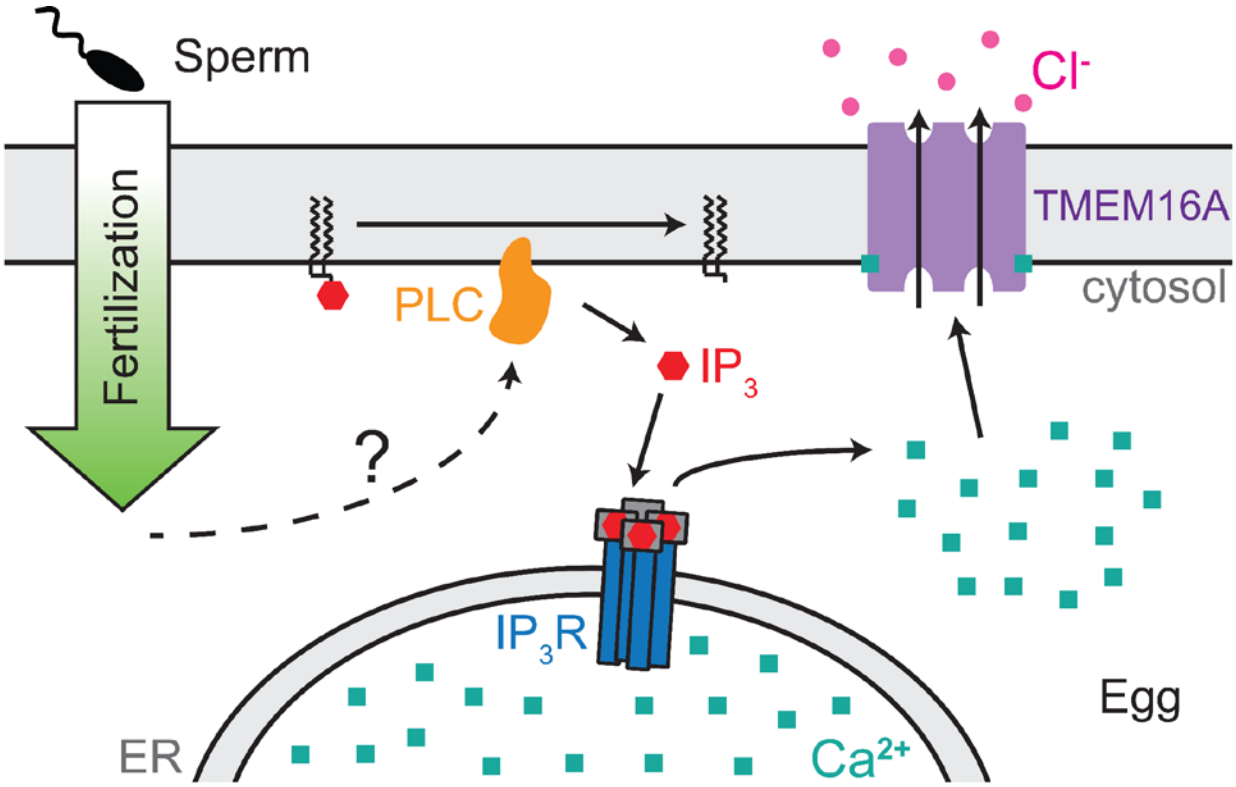

Figure 3-6. Model for the fast polyspermy block in *X. laevis*

In the fast block to polyspermy in *X. laevis* eggs, fertilization activates a PLC, which then cleaves PIP_2 to create IP_3. Increased IP_3 then activates its cognate receptor on the ER to evoke a Ca^{2+} release through the pore of the IP_3R. This ER-derived Ca^{2+} then activates the Cl^- channel TMEM16A, which conducts a Cl^- efflux to depolarize the egg.

4.0 The TMEM16A channel mediates the fast polyspermy block in *Xenopus laevis*

The contents of this chapter are adapted from a recently published article (*72*): © 2018 Wozniak et al. originally published in The Journal of General Physiology https://doi.org/10.1085/jgp.201812071

4.1 Introduction

Fertilization of an egg by more than one sperm, a condition known as polyspermy, presents one of the earliest and most prevalent barriers to successful reproduction. In most sexually reproducing species, polyspermy causes chromosomal abnormalities that are embryonic lethal (*5*). Eggs have evolved multiple strategies to combat the entry of sperm into an already fertilized egg and to thereby avoid such catastrophic consequences (*5, 21*). One mechanism commonly used by external fertilizers is the fast polyspermy block. Within seconds of fertilization, the fast block induces a depolarization of the egg membrane that acts as an electrical barrier to polyspermy (*7*). Sperm can bind to, but not enter, a depolarized egg (*7*). We are just beginning to uncover the molecular pathways that prevent sperm entry into a depolarized egg.

As in all frogs, the *Xenopus laevis* fast block requires an increase of cytosolic Ca^{2+} and a depolarizing efflux of Cl^- (*9, 43, 96, 97*); an event hypothesized to be mediated by a Ca^{2+}-activated Cl^- channel (CaCC) (*71, 131*). We have recently demonstrated that this cytosolic Ca^{2+} increase is caused by inositol 1,4,5-trisphosphate (IP_3)-induced Ca^{2+} release from the endoplasmic reticulum

(ER) (*73*) (*see chapter 3)*. Here we sought to identify the CaCC that mediates the fast block in *X. laevis*.

The channels expressed in the fertilization-competent *X. laevis* egg are not well studied, which is in stark contrast to the well-characterized channels found in the immature oocyte (e.g. *84*). Indeed, the oocytes and eggs of *X. laevis* are vastly different cells (Fig. 1-1) (*132*). Immature *oocytes* are located in the ovary, arrested in prophase I, and cannot be fertilized. By contrast, *eggs* are ovulated and laid by mature *X. laevis* females, are arrested in metaphase II, and are fertilization-competent. As the oocyte matures into an egg, many plasma membrane localized ion channels and transporters are internalized, including: the pore-forming subunit of the store-operated Ca^{2+} entry channel (ORAI1) (*133*); the plasma membrane Ca^{2+}-ATPase (PMCA) (*134*); and Na^{+}/K^{+} ATPase (*135*). In addition, oocyte maturation induces changes in intracellular proteins that closely interact with the plasma membrane, including components of the cytoskeleton, to thereby facilitate structural transformations (*136*). Therefore, experimental findings regarding prominent CaCCs in *X. laevis* oocytes, namely TMEM16A (*84*), cannot be directly applied to eggs in the absence of further testing, and thus it was necessary to study the CaCCs in eggs directly.

We sought to identify the Cl^{-} channel that mediates the fertilization-evoked depolarization of the fast block in *X. laevis* eggs. Using existing proteomic and transcriptomic data from *X. laevis* oocytes and eggs (*64, 74*), we identified two candidate CaCCs: transmembrane protein 16a (TMEM16A) (*84, 98, 99*) and bestrophin 2a (BEST2A) (*137, 138*). To distinguish between the currents produced by the *X. laevis* orthologs of these channels (xTMEM16A and xBEST2A), we exogenously expressed each channel in *A. mexicanum* oocytes, which lack endogenous Ca^{2+}-

activated currents. Using this isolated system, we independently characterized each channel using pharmacological inhibitors. By applying the most potent inhibitors to whole-cell recordings of *X. laevis* eggs during fertilization, we demonstrate that xTMEM16A, and not xBEST2A, conducts the depolarizing current of the fast block to polyspermy. Furthermore, these inhibitors led to an increased incidence of polyspermy in *X. laevis* eggs. Thus, we describe the first known ion channel that mediates the fast block.

4.2 Results

4.2.1 Two candidate CaCCs accumulate in the egg and are candidates for the trigger of the fast block

To identify candidate CaCCs that may trigger the fast block in *X. laevis*, we interrogated two previously published high-throughput gene expression datasets. First, we examined the proteome of fertilization-competent eggs (*64*) and queried for all known ion channels (Fig. 2-3). Three protein families containing CaCCs have been characterized to date: the CLCAs, the bestrophins (BEST), and the transmembrane protein 16s (TMEM16/ANO) (*139*). We discovered that only one member of the BEST family, xBEST2A, and three members of the TMEM16 family, xTMEM16A, xTMEM16E and xTMEM16K, are represented in the egg proteome (Fig. 4-1). Second, we examined an RNA-seq time course in *X. laevis* oocytes and unfertilized eggs (*74*). All four types of mRNA show increasing levels through gamete development, culminating in the egg, thereby suggesting that these CaCCs may be important for early development (Fig. 4-1). Although *tmem16f* and *clca3p-like* mRNA are present, it is likely that they are expressed after fertilization

to guide the developing embryo through the maternal-to-zygotic transition, since their proteins are not detected in the unfertilized egg (*140, 141*).

The CaCC responsible for the fast block needs to be plasma membrane-localized in eggs to mediate the depolarizing Cl^- efflux. Both xBEST2A and xTMEM16A were originally cloned from fertilization-incompetent, *X. laevis* oocytes (*84, 142*), and each has been characterized as plasma membrane-localized (*84, 142-144*). Moreover, xTMEM16A is the prominent CaCC in *X. laevis* oocytes (*84*). In contrast, TMEM16E localizes to the ER where it functions as a Ca^{2+}-activated scramblase (*145, 146*). TMEM16K similarly localizes to the ER (*147, 148*). Because both TMEM16E and TMEM16K proteins localize to the ER, they were both excluded from further consideration. Together, these analyses suggest that the fast block to polyspermy in *X. laevis* eggs is mediated by either xBEST2A or xTMEM16A.

4.2.2 Uncaging IP_3 activates xTMEM16A and xBEST2A

Having discovered two CaCCs as candidate channels that may mediates the fast block in *X. laevis* eggs, we sought to distinguish between their currents in the context of fertilization. Studying the activities of xTMEM16A and xBEST2A independently necessitated their exogenous expression. For this purpose, we chose a highly tractable system that lacks endogenous Ca^{2+}-activated currents: oocytes from the axolotl *Ambystoma mexicanum*.

Although xTMEM16A was previously expressed in *A. mexicanum* oocytes and their currents generated in this context have been recorded [18], this is not the case for xBEST2A. We first confirmed that the exogenously expressed xBEST2A is localized to the plasma membrane of

these oocytes. Confocal imaging of *A. mexicanum* oocytes expressing both Ruby-tagged xBEST2A and the eGFP-tagged membrane marker MemE (*94*) revealed that xBEST2A was indeed expressed in these cells, and that it was transported to the plasma membrane (Fig. 4-2 A). As expected, no fluorescence was detected in water-injected control oocytes (Fig. 4-2 A).

To study the currents conducted by xTMEM16A and xBEST2A, we exploited their shared regulation by Ca^{2+} (*84, 137, 138*). Specifically, we photoactivated myo-inositol 1,4,5-trisphosphate, P4(5)-1-(2-nitrophenyl) ethyl ester (caged-IP_3) by exposing the oocytes to ultraviolet light. Uncaging of IP_3 induces Ca^{2+} release from the ER, thereby increasing the cytosolic Ca^{2+} concentration and activating the channels. Importantly, we used the splice variants of xTMEM16A and xBEST2A channels that are present in *X. laevis* eggs (*64, 84, 142*). Using the two-electrode voltage clamp (TEVC) technique, we recorded Ca^{2+}-activated Cl^- currents ranging from 0.2 to 17 µA, with an average of 5.6 ± 1.0 µA (N=12) for xTMEM16A in *A. mexicanum* oocytes, and 0.47 ± 0.7 µA for xBEST2A in *A. mexicanum* oocytes, as well as 6.9 ± 1.5 µA in *X. laevis* oocytes (N=16). As shown previously (*84*), uncaging IP_3 in wild-type *A. mexicanum* oocytes does not elicit any Ca^{2+}-induced currents (Fig. 4-2 B).

Using the uncaging system in conjunction with TEVC, we recorded whole-cell currents in the presence or absence of known Cl^- channel inhibitor molecules. To determine the effect of a given inhibitor, we recorded and compared sequential currents in the absence and presence of each inhibitor. Our initial assessment of the effects of sequential uncaging events in the absence of inhibitors revealed no differences in current between *A. mexicanum* oocytes expressing either of the channels or *X. laevis* oocytes expressing the endogenous channels (Table 4-1). This finding

indicated that differences in Ca^{2+}-evoked currents measured in the presence or absence of an inhibitor in this system would reflect the efficacy of that inhibitor; therefore, this experimental design would enable us to characterize the efficacy of inhibitors in reducing xTMEM16A- or xBEST2A-mediated currents.

Using this experimental configuration, we quantified the effects of five inhibitors on xTMEM16A- and xBEST2A-mediated currents (Table 4-1). Three of these – MONNA, Ani9, and $T16a_{inh}$-A01 – were previously reported to target human and/or mouse TMEM16A (*149-151*), whereas $CaCC_{inh}$-A01 is a general inhibitor of CaCCs (*149*, *152*). Although no BEST-specific inhibitor has been characterized to date, we included the broad-spectrum Cl^- channel inhibitor DIDS because it reportedly inhibits human bestrophin 1 channels with an affinity 160-fold higher than that for mouse TMEM16A (*153*).

4.2.3 MONNA and Ani9 inhibit xTMEM16A currents

To characterize the effects of each inhibitor, we applied them to oocytes during sequential uncaging events. In the case of xTMEM16A, both MONNA and Ani9 effectively reduced currents in the *A. mexicanum* oocytes by over 70% (Figs. 4-2 C & 4-3, Table 4-1), whereas $T16A_{inh}$-A01 and $CaCC_{inh}$-A01 were much less effective (Table 4-1, Fig. 4-3). Unexpectedly, we found that 7.5 μM DIDS, a concentration well below the reported IC_{50} for the drug on mouse TMEM16A (*153*), reduced xTMEM16A by almost 50% (Table 4-1, Fig. 4-3).

In *X. laevis* oocytes, the prominent Ca^{2+}-activated Cl^- current is known to be generated by xTMEM16A channels (*84*). Comparison of the effects on exogenously expressed xTMEM16A

current in the *A. mexicanum* oocytes to the endogenous TMEM16A currents generated in *X. laevis* oocytes revealed that in nearly all cases the efficacy of the inhibitors was very similar in the two test groups (Figs. 4-2 D & 4-3, Table 4-1). However, MONNA blocked significantly more xTMEM16A current in the *X. laevis* oocyte (87 ± 2%) than in the *A. mexicanum* oocytes (72 ± 3%) ($P < 0.05$ ANOVA; Table 4-1). Collectively, these data demonstrate that only MONNA and Ani9 effectively inhibit xTMEM16A.

4.2.4 MONNA and Ani9 discriminate between currents generated by xTMEM16A and xBEST2A

Comparison of the effects of the five assayed inhibitors on xBEST2A currents revealed that none significantly altered these currents ($P > 0.05$, ANOVA; Figs. 4-2 F & 4-3 and Table 4-1). Most notably, currents generated in the presence of MONNA or Ani9 were no different than those produced in the control, confirming that these two compounds are specific for xTMEM16A. Furthermore, the lack of xBEST2A inhibition by MONNA and Ani9 demonstrates that these inhibitors do not interfere with the IP_3-induced Ca^{2+} release pathway. Together, these results demonstrate that MONNA and Ani9 effectively target xTMEM16A channels but have only minimal effects on xBEST2A and the IP_3R, thereby providing a mechanism for discerning between xTMEM16A and xBEST2A currents during the fast block.

4.2.5 The TMEM16A mediated-current produces the fast block in *X. laevis*

To study the fast block to polyspermy in *X. laevis*, we conducted whole-cell voltage recording of eggs during fertilization and recorded up to 40 minutes after fertilization or until the

cortex contracted (Fig. 2-3). Fig. 4-4 A depicts a typical fertilization-evoked depolarization that occurred after sperm addition. For eggs inseminated under control conditions, we found that: the resting potential was -19.2 ± 1.0 mV; the fertilization potential was 3.7 ± 2.3 mV (N=30, Fig. 4-4 B); the time between the addition of sperm and the onset of membrane depolarization was 4.9 ± 0.7 minutes (N=30, Fig. 4-4 C); and the average rate of depolarization was 9.0 ± 3.4 mV/ms (N=30) (Fig. 4-4 D, Table 4-2).

To determine whether xTMEM16A or xBEST2A conducts the depolarizing current responsible for the fast block, we inseminated *X. laevis* eggs in the presence of MONNA or Ani9, each of which was expected to inhibit xTMEM16A but to have minimal effect on xBEST2A or IP_3Rs (Fig. 4-2 F, Table 4-1). In *X. laevis* eggs, inhibition of xTMEM16A using either inhibitor effectively diminished the fast block. In the presence of 10 μM MONNA, fertilization failed to evoke depolarizations in seven independent experiments (Fig. 4-4 E); thus, this inhibitor completely abolished the fast block. Eggs incubated in MONNA had a significantly more positive resting potential than that of control eggs (-12.8 ± 0.8 mV vs. -19.2 ± 1.0 mV, T-test, $P < 0.001$) (Fig. 4-4 B). However, this elevated resting potential did not interfere with fertilization, as visual assessment revealed contraction of the animal pole followed by the appearance of a cleavage furrows (Fig. 2-3), thereby demonstrating that all eggs inseminated in the presence of MONNA initiated embryonic development. Additionally, it has been shown that the majority of eggs fertilize at -11 mV in *X. laevis (96)*. To determine whether inhibiting TMEM16A effected the prevalence of polyspermy, we compared the incidence of polyspermy in embryos inseminated under control conditions (MR/3 solution) or with 10 μM MONNA (Table 4-3, Fig. 4-4 F). Polyspermic fertilization was assessed based on the appearance of asymmetric cleavage furrows; whereas,

symmetric furrows reveal monospermic fertilization (Fig. 2-3) (*43*, *87*). Significantly more embryos inseminated in MONNA were polyspermic compared to control (56 ± 9% (N=3) vs. 9 ± 4% (N=5), ANOVA, $P < 0.01$).

In the presence of 1 μM Ani9, the rate of depolarization for inseminated eggs was significantly reduced, and thereby attenuated the fast block (1.2 ± 1.1 mV/ms with Ani9 (N=5) vs 9.0 ± 3.4 mV/ms in control (N=30), T-test, $P < 0.05$) (Figs. 4-4 F-G). Because the rate of depolarization is proportional to the number of channels that are open, a slower depolarization rate reflects fewer channels being activated by fertilization. Based on the rates measured, we estimate that in the presence of 1 μM Ani9, 7.5-fold fewer channels were triggered to open by fertilization; i.e., only 13% of the channels that would be activated under normal conditions opened in this context. This 87% reduction in the number of open channels is similar to the 80% inhibition of xTMEM1Aa channels measured when IP_3 was uncaged in *X. laevis* and *A. mexicanum* oocytes (Fig. 4-3, Table 4-1). No other metrics of the fast block differed significantly in recordings made in the presence versus absence of Ani9 (Fig. 4-4 B-D). Moreover, embryos inseminated in Ani9 had a higher incidence of polyspermy compared to control (17 ± 5% (N=3) versus 9 ± 4% (N=5)); however, this difference was not statistically significant (Fig. 4-4 F) ($P > 0.05$, ANOVA).

Collectively, the ability of MONNA and Ani9 to effectively diminish fertilization-evoked depolarizations and increase the incidence of polyspermy demonstrate that TMEM16A channels produce the depolarizing current that mediates the fast block in *X. laevis* eggs.

4.3 Discussion

The fast block to polyspermy is one of the earliest developmental events that arises in species that undergo external fertilization. We have recently demonstrated that fertilization-signaled depolarization in *X. laevis* eggs requires activation of a PLC that induces Ca^{2+} release from the ER in an IP_3-mediated pathway (*73*). Here we identify the CaCC that mediates the fast block in the African clawed frog *X. laevis*: TMEM16A (Fig. 4-5).

4.3.1 xBEST2A and xTMEM16A are abundantly expressed in *X. laevis* eggs

Our identification of xTMEM16A and xBEST2A as candidate CaCCs that may mediate the fast block is based on proteomics and transcriptomics. Indeed, both proteins are translated in high concentrations: approximately 22 x 10^9 xTMEM16A channels and 2 x 10^9 xBEST2A channels in mature eggs. Given that both channel proteins are present in the egg, it was feasible that either or both could mediate the Ca^{2+}-activated Cl^- efflux that drives the fertilization-evoked depolarization of the fast block in *X. laevis.*

Despite the gross changes that the plasma membrane of a *X. laevis* oocyte undergoes as it matures into a fertilization-competent egg, it is evident that xTMEM16A channels are retained. Although proteomics data reveal that *X. laevis* eggs express the xBEST2A channel, our data demonstrate that this channel does not contribute to the fast block. Based on its presence in the mature egg (*64*) and its lack of contribution to the fast block, we speculate that xBEST2A is either desensitized or absent from the plasma membrane, as is the case for ORAI1 (*133*), PMCA (*134*), and Na^+/K^+ ATPase (*135*).

4.3.2 MONNA and Ani9 selectively inhibit xTMEM16A

Our finding that 10 μM MONNA and 1 μM Ani9, concentrations higher than their published IC_{50} (*150, 151*), inhibit >70% of xTMEM16A channels in both *A. mexicanum* and *X. laevis* oocytes, yet that they are largely ineffective at reducing currents conducted by xBEST2A, demonstrate that these inhibitors discriminate between our two candidate CaCCs. Both of these inhibitors are known to be highly specific for TMEM16A, with Ani9 failing to block even the closest relative of TMEM16A, TMEM16B (*151*). In contrast, $T16_{inh}$-A01, and $CaCC_{inh}$-A01 were much less effective at inhibiting either xTMEM16A or xBEST2A. The similarity between the pharmacological profiles of xTMEM16A currents recorded in *A. mexicanum* oocytes and endogenous Ca^{2+}-activated currents in *X. laevis* oocytes supports the hypothesis that the native Ca^{2+}-activated Cl^- currents in *X. laevis* oocytes are generated by xTMEM16A channels (*84*).

Although MONNA and Ani9 inhibited exogenously expressed xTMEM16A in *A. mexicanum* oocytes to similar extents, MONNA was significantly more effective in reducing the endogenous Ca^{2+}-activated currents of *X. laevis* oocytes (Fig. 4-4 D, $P < 0.05$, ANOVA). The increased efficacy of MONNA with respect to endogenous xTMEM16A in the egg is consistent with the observed difference in its fertilization-induced electrical profile over that of Ani9 (*i.e.* with MONNA completely blocking depolarization and Ani9 merely slowing it). Although the mechanisms underlying TMEM16A inhibition by these chemically distinct agents have not yet been elucidated, we hypothesize that the differing effects of these inhibitors on *X. laevis* oocytes and eggs may reflect the strikingly different membrane environments of these two cell types. Furthermore, we speculate that the elevated resting potential recorded from eggs inseminated in

the presence of MONNA reflects the altered resting state of these cells, consistent with a recent demonstration that TMEM16A activity plays a prominent role in Cl^- homeostasis (*154*).

4.3.3 Conservation of fast block signaling pathway in anurans

Given that an increase of cytosolic Ca^{2+} and an efflux of Cl^- are required for the fast block in all frogs and toads studied thus far (*9, 155*), we propose that the current produced by TMEM16A channels triggers the fertilization-evoked depolarization in all anurans with a fast block. Interestingly, not all anurans reside in freshwater; for example, the crab-eating frog *Rana cancrivora* can reside in both freshwater and saltwater (*156*). In saltwater, opening of TMEM16A could trigger a Cl^- influx resulting in a hyperpolarization of the egg membrane potential, thereby inducing polyspermy (*43*). As *R. cancrivora* are external fertilizers (*157*), it is unclear if these eggs have a fast block or if a slow block is sufficient to inhibit polyspermy. Similarly, not all anurans are external fertilizers, thus they may not require a fast block. For example, the common coqui frog *Eleutherodactylus coqui* is an internal fertilizer (*158*). Given the limited number of sperm that reach these eggs, it is unknown whether a fast block is required to prevent polyspermy. Remarkably, it has been suggested that *E. coqui* may have evolved to be physiologically polyspermic (*159*), thereby not requiring any polyspermy block. While TMEM16a may mediate the fast block in most frogs and toads, the varying life histories of anurans lend themselves to adaptive evolutionary changes.

4.3.4 Summary

In conclusion, the fertilization-induced activation of PLC leading to opening of TMEM16A channels in *X. laevis* is the earliest known signaling event evoked by sperm-egg interaction (Fig. 4-5). The discovery of a critical role for TMEM16A channels in fertilization lays a foundation for understanding how the membrane potential regulates fertilization. More broadly, TMEM16A channels regulate diverse processes ranging from epithelial secretions (*99*) to smooth muscle contraction (*160, 161*). These CaCCs are indispensable for human health (*162*), yet we are only beginning to understand the complex gating mechanisms of TMEM16A (*163*). Due to their large size, ease and reproducibility for electrophysiology recordings, and years of study by developmental biologists and biophysicists alike, we propose that *X. laevis* fertilization may serve as a straightforward model system to study the physiologic regulation of TMEM16A.

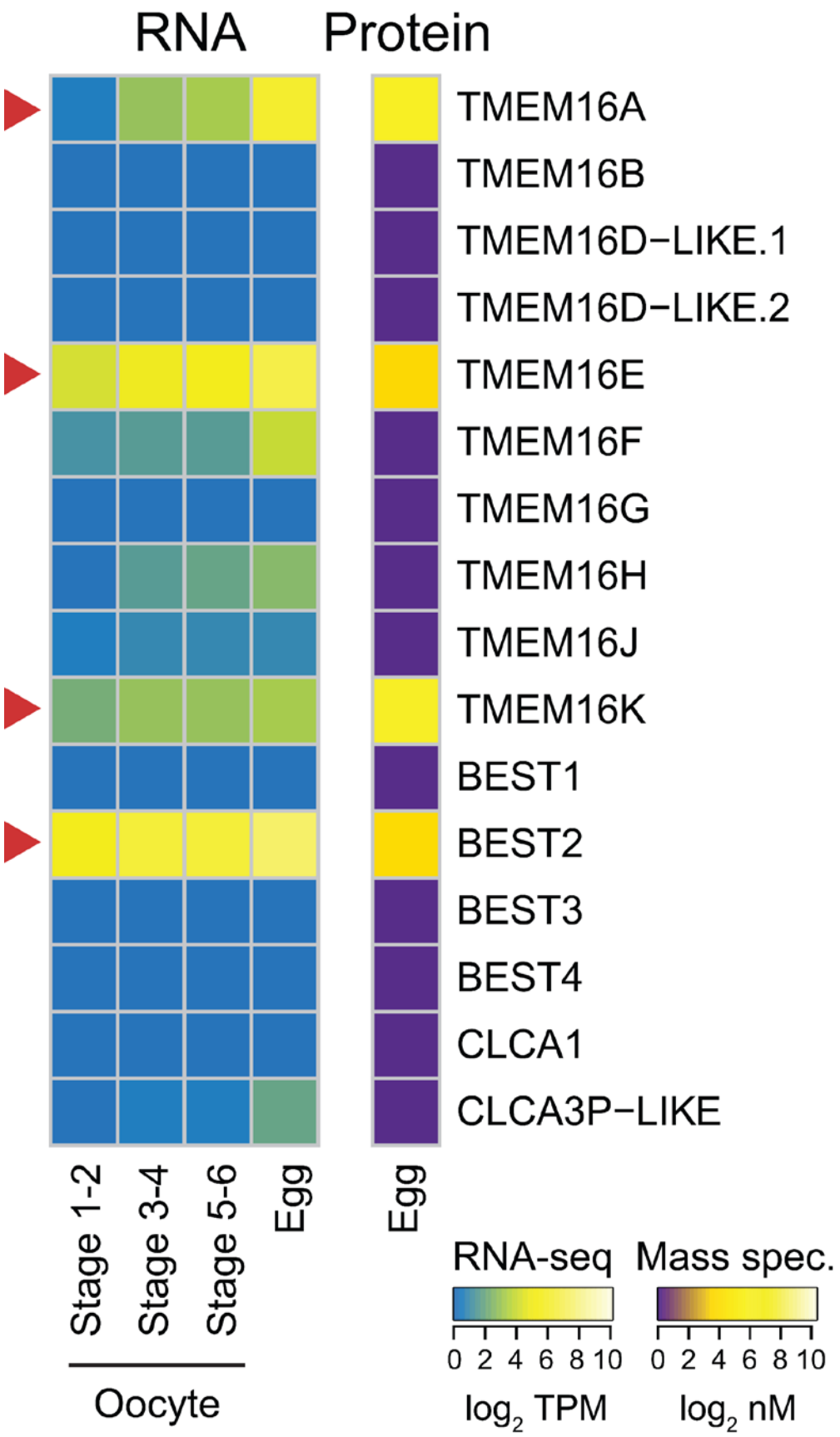
RNA
Protein
TMEM16A
TMEM16B
TMEM16D−LIKE.1
TMEM16D−LIKE.2
TMEM16E
TMEM16F
TMEM16G
TMEM16H
TMEM16J
TMEM16K
BEST1
BEST2
BEST3
BEST4
CLCA1
CLCA3P−LIKE
Stage 1-2
Stage 3-4
Stage 5-6
Egg
Egg
Oocyte
RNA-seq
Mass spec.
0 2 4 6 8 10
0 2 4 6 8 10
log2 TPM
log2 nM

Figure 4-1. Expression of CaCCs in *X. laevis* oocytes and eggs

Heatmaps of expression levels of CaCCs at the developmental stages indicated. (*Right*) Protein concentrations (from (*64*)) as determined by mass spectrometry-based proteomics study, in $\log_2$ nanomolar. (*Left*) Transcript levels (shown as transcripts per million (TPM)) from (*74*), as determined by RNA-seq-based transcriptome study). Red arrowheads highlight CaCCs with proteins found in eggs. *This data was collected in collaboration with Wesley Phelps and Miler Lee.*

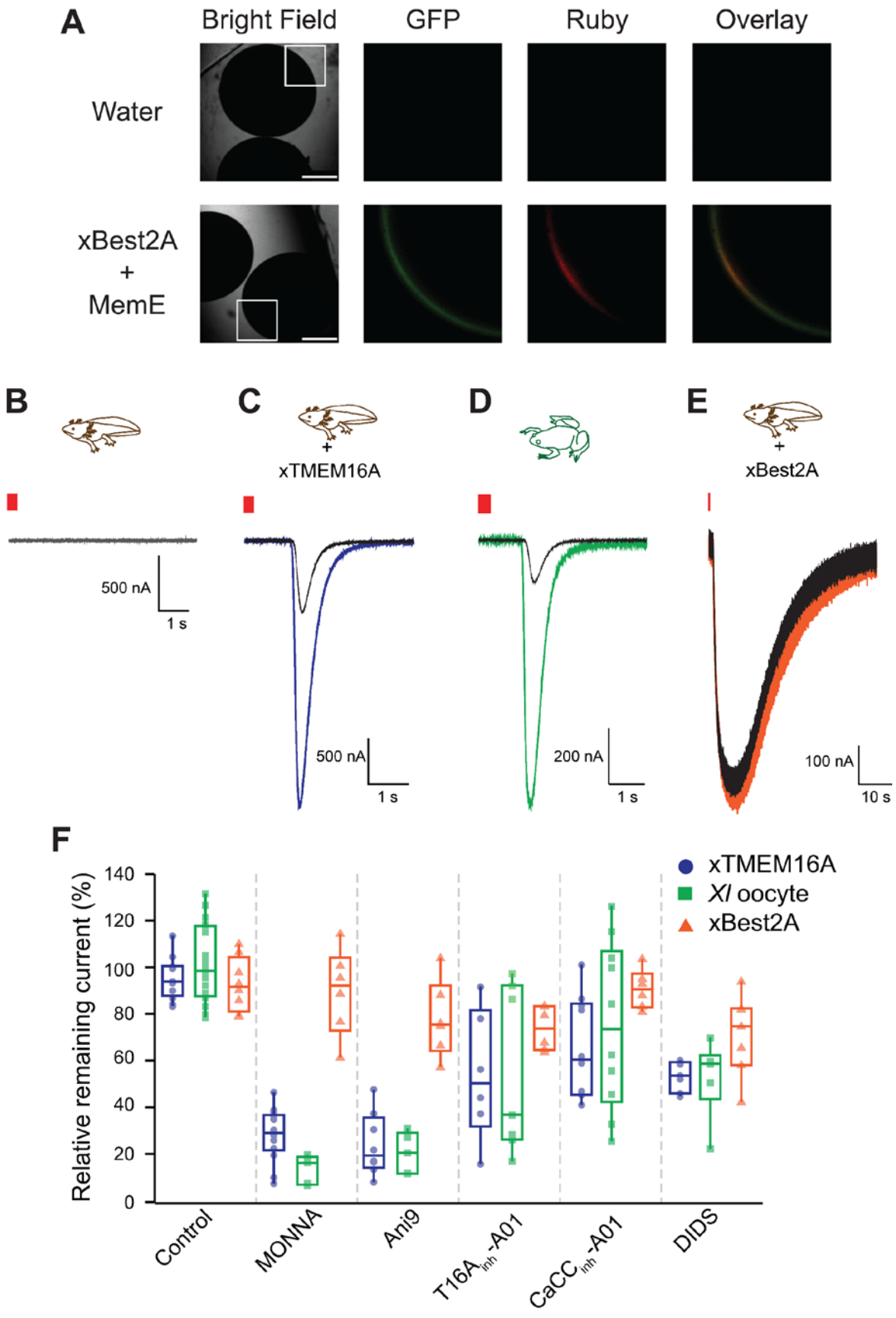
A
Bright Field
GFP
Ruby
Overlay
Water
xBest2A
+
MemE
B
C
xTMEM16A
D
E
xBest2A
500 nA
1 s
500 nA
1 s
200 nA
1 s
100 nA
10 s
F
Relative remaining current (%)
140
120
100
80
60
40
20
0
xTMEM16A
Xl oocyte
xBest2A
Control
MONNA
Ani9
T16A inh -A01
CaCC inh -A01
DIDS

Figure 4-2. MONNA and Ani9 inhibit TMEM16A-conducted Cl^- currents

A) Representative bright-field and fluorescence images of *A. mexicanum* oocytes expressing Ruby-tagged xBEST2A and eGFP-tagged MemE (reporter of plasma membrane). Boxes denote portions included in fluorescence images, and scale bar denotes 750 μm. Overlay is of GFP and Ruby images. B-E) TEVC current recordings from oocytes of *A. mexicanum* (B-C & E) or *X. laevis* (D), following injection with a photolabile caged-IP_3 analog, with clamping at -80 mV. *A. mexicanum* oocytes expressed no transgene (B), xTMEM16A (C), or xBEST2A (E). Wild-type *X. laevis* oocytes expressed endogenous channels (D). Typical current traces before and after uncaging, during control treatment (colored) and in the presence of 10 μM MONNA (black). Red bar denotes the 250 ms duration of UV exposure. (F) Averaged proportion of current remaining after application of the indicated inhibitors, in *A. mexicanum* oocytes expressing xTMEM16A (N=6-14) or xBEST2A (N=6-8), and in *X. laevis* oocytes expressing endogenous channels (N=5-16).

Table 4-1. Inhibition of Ca^{2+}-activated current using Cl^- channel inhibitors

	Control	10 µM MONNA	1 µM Ani9	30 µM $T16a_{inh}$-A01	10 µM $CaCC_{inh}$-A01	7.5 µM DIDS
xTMEM16A in *Am* oocytes	5 ± 3	72 ± 3	76 ± 5	46 ± 11	35 ± 7	46 ± 2
***Xl* oocytes**	2 ± 4	87 ± 2	80 ± 4	45 ± 13	25 ± 11	47 ± 7
xBEST2A in *Am* oocytes	7 ± 4	10 ± 8	22 ± 7	26 ± 4	9 ± 3	29 ± 7

Average ± SEM percentage (%) of current inhibition seen for uncaging experiments. The number of independent observations for each treatment is: MONNA (N=8-16); Ani9 (N=5-8); $T16a_{inh}$-A01 (N=6-7); $CaCC_{inh}$-A01 (N=6-10); DIDS (N=6-7). *Am* and *Xl* denote *A. mexicanum* and *X. laevis*, respectively.

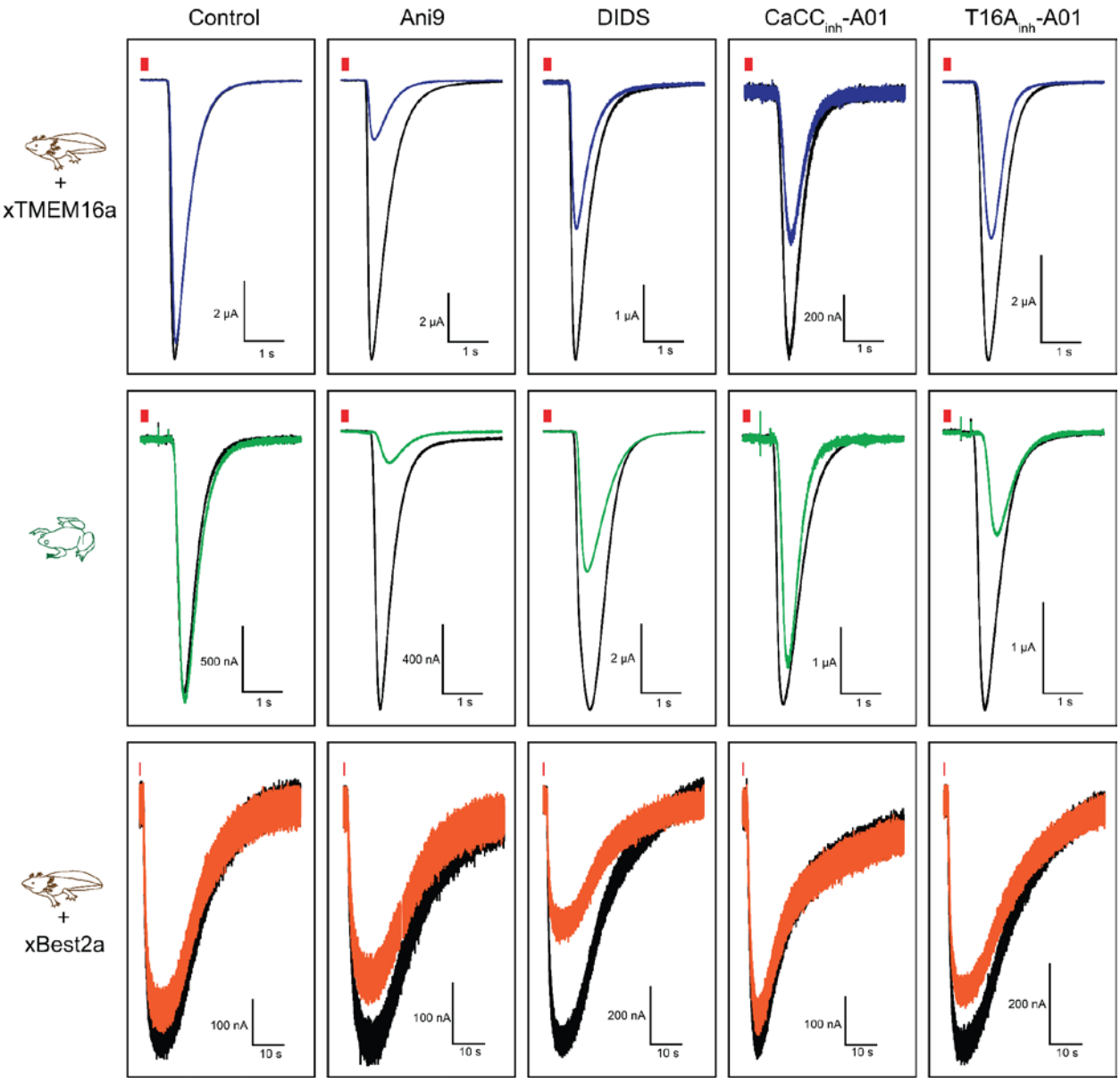

Figure 4-3. Representative current traces evoked by IP_3 uncaging using Cl^- channel inhibitors

Recordings from *A. mexicanum* oocytes expressing xTMEM16A (top) or xBEST2A (bottom), and wild-type *X. laevis* oocytes (middle). Shown are typical traces before (black) and after (colored) application of a control solution, Ani9, DIDS, $CaCC_{inh}$-A01, or $T16A_{inh}$-A01. The red bars denote the 250 ms UV-exposure.

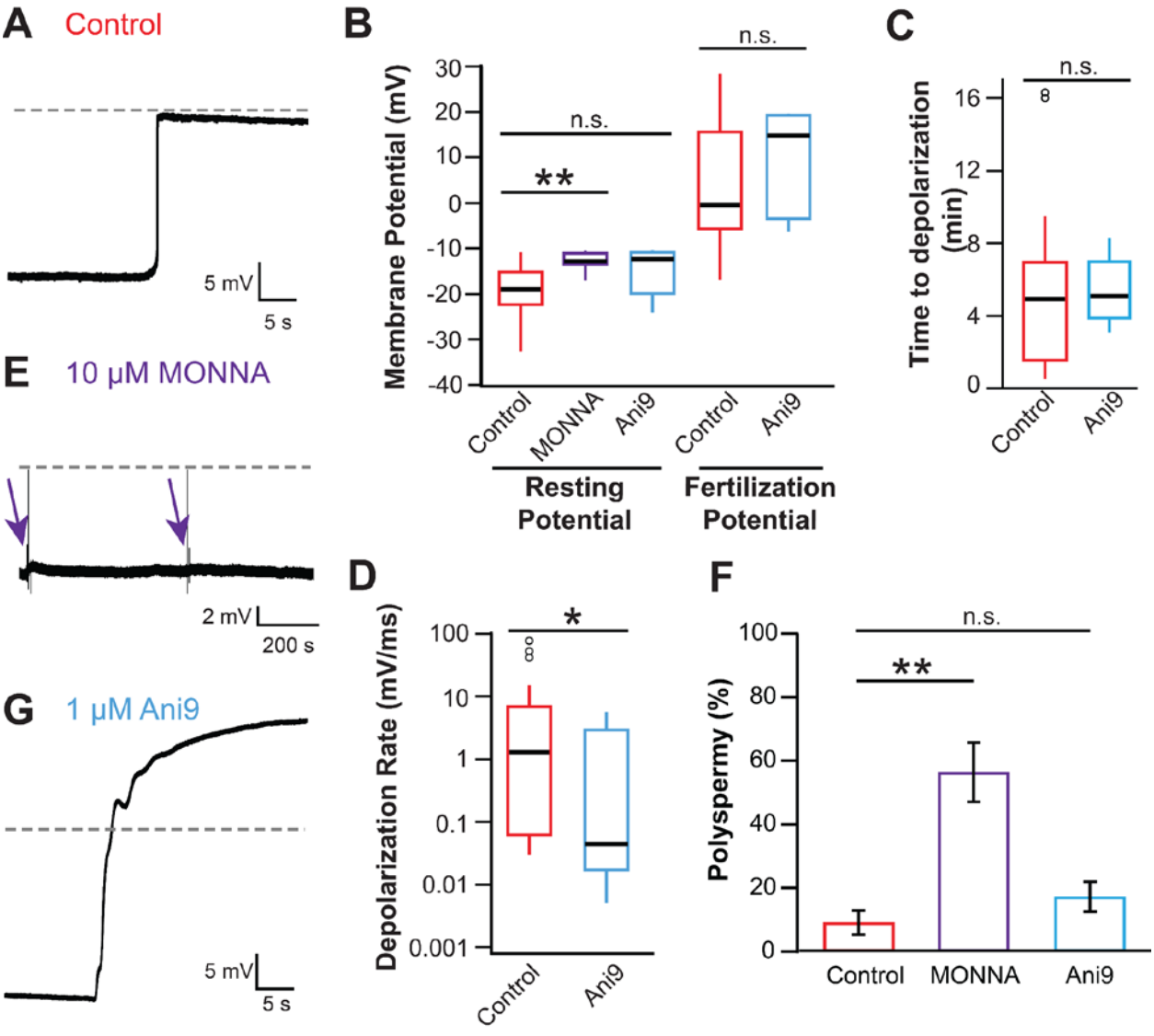

Figure 4-4. Fertilization activates TMEM16A to depolarize the egg

A, E, G) Representative whole-cell recordings made during fertilization in control conditions (A), the presence of 10 µM MONNA (E), or the presence of 1 µM Ani9 (G). Dashed lines denote 0 mV, arrows denote times at which sperm was applied to eggs. B-D) Tukey box plot distributions of the resting and fertilization potentials in control conditions and with MONNA or Ani9 (B), the time between sperm application and depolarization in the absence and presence of Ani9 (C), and

the depolarization rate in the absence and presence of Ani9 (D) (N=5-30, recorded over 2-16 experimental days per treatment). (F) Proportion of polyspermic embryos out of total developed embryos in control, MONNA, and Ani9 (N=3, recorded over 3 experiment days/treatment). ** denotes $P < 0.001$, * denotes $P < 0.05$, and n.s. denotes $P > 0.05$.

Table 4-2. Biophysical properties of fertilization-evoked depolarizations using TMEM16A inhibitors

	Resting Potential (mV)	Fertilization Potential (mV)	Sperm addition to depolarization time (min)	Depolarization Rate (mV/ms)	N
Control (MR/5)	-19.2 ± 1.0	3.7 ± 2.3	4.9 ± 0.7	9.0 ± 3.4	30
10 µM MONNA	-12.8 ± 0.8	---	---	---	7
1 µM Ani9	-14.7 ± 2.5	9.3 ± 5.2	5.4 ± 0.8	1.21 ± 1.15	5

Average ± SEM for the indicated measurement before, during, and after the fertilization-signaled depolarization.

Table 4-3. Developmental assays using TMEM16A inhibitors

Condition	Undeveloped (%)	Developed (%)	Polyspermic (%)	N
Control (MR/3)	0 ± 0	100 ± 0	9 ± 4	5
10 µM MONNA	7 ± 2	93 ± 2	56 ± 9	3
1 µM Ani9	2 ± 2	98 ± 2	17 ± 5	3

Average ± SEM for each fertilization condition. Out of the zygotes that initiated embryonic development, embryos were categorized as monospermic or polyspermic based on cleavage furrow symmetry (*see Fig. 2-3 for examples)*

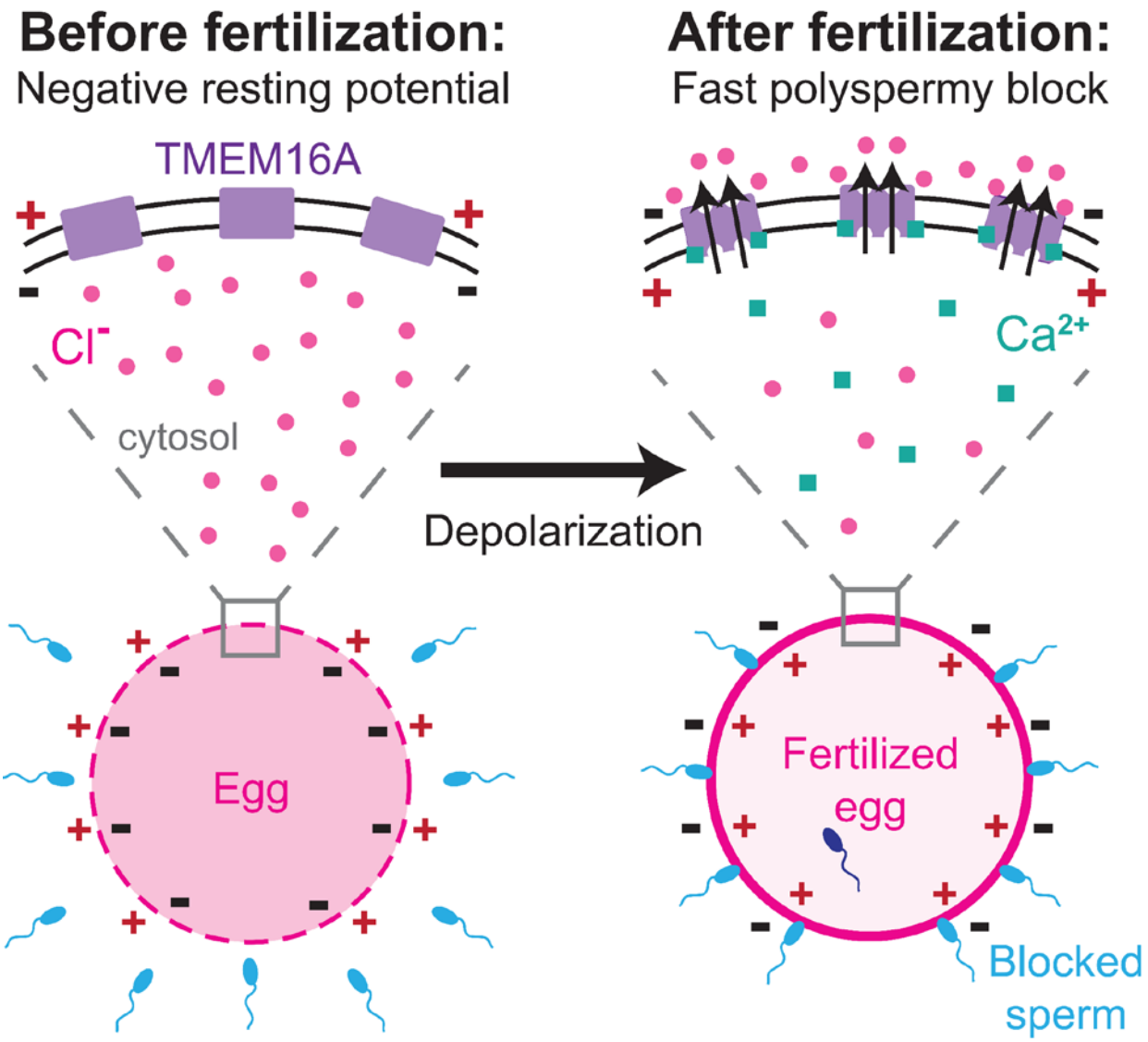

Figure 4-5. Proposed model for fertilization signaled activation of TMEM16A in *X. laevis*

Before fertilization, *X. laevis* eggs have a negative resting potential; thereby electrically signaling to sperm that they can receive a male gamete. After fertilization, cytosolic Ca^{2+} increases to activate TMEM16A. An efflux of Cl^- then depolarizes the egg, and this change in membrane potential blocks supernumerary sperm from entering the fertilized egg.

5.0 Fertilization-induced Zn^{2+} release is conserved in eggs from non-mammalian species and contributes to the slow polyspermy block in *Xenopus laevis*

5.1 Introduction

The divalent, transition metal zinc (Zn^{2+}) plays a commanding role in the life cycle of an egg. Female gametes accumulate Zn^{2+} as they mature from prophase I arrested oocytes into fertilization-competent, metaphase II arrested eggs (*164*). Zn^{2+} is enriched in eggs of mammals, non-mammalian vertebrates, and echinoderms (*164-166*). Inhibiting Zn^{2+} accumulation in mouse and frog oocytes halts maturation prior to metaphase II arrest thereby revealing the importance of this transition metal in oogenesis (*164*, *167-170*). Furthermore, fertilization signals the release of Zn^{2+} ions from mammalian eggs (*29, 30*), an event that is both necessary and sufficient for meiotic resumption and egg activation (*30, 171-173*). Despite these demonstrated critical roles for Zn^{2+} in egg maturation and early embryonic development, we are only just beginning to understand the mechanisms that underlie how this Zn^{2+} is regulated and what role Zn^{2+} plays in these critical processes.

Cortical granules docked at the plasma membrane of mouse eggs are enriched with Zn^{2+} that is accumulated during maturation (*174*). Upon fertilization, this Zn^{2+} is released from the egg during the cortical granule exocytosis of the slow polyspermy block (*5, 23*). Exocytosis of cortical granules from the egg is signaled by a fertilization-evoked increase in intracellular Ca^{2+} (*21, 22, 175*). Given that multiple cytosolic Ca^{2+} oscillations occur in fertilized mammalian eggs (*176*), and Zn^{2+}release mimics this oscillatory pattern (*29, 30*), fertilization-induced Zn^{2+} release has been

coined "Zn^{2+} sparks" (*29*). Zn^{2+} sparks have been observed in various mammalian eggs including mouse, bovine, non-human primate, and human (*29-31*). These Zn^{2+} sparks represent the release of a significant amount of Zn^{2+} into the extracellular milieu. In mice, for example, fertilization-induces the release of one billion Zn^{2+} ions per egg (*29*). It has been proposed that the Zn^{2+} released from cortical granules contributes to transformation of the extracellular structures surrounding eggs from readily passable by sperm before fertilization to an impenetrable barrier after (*32*).

Two lines of experimentation suggest that elevated extracellular Zn^{2+} might protect the nascent zygote from polyspermy. First, Zn^{2+} application altered the ultrastructure of the zona pellucida surrounding mammalian eggs as observed by electron microscopy and reduced sperm binding to this glycoprotein matrix (*177*). Second, *in vitro* fertilization in the presence of extracellular Zn^{2+} impaired the motility of mouse, frog, and sea urchin sperm (*24, 178, 179*). In mice, zinc-induced motility changes limited the number of sperm that penetrated the zona pellucida and reached the egg during *in vitro* fertilization (*24*). While Zn^{2+} plays a critical role in mammalian egg development and sperm motility, the impact of extracellular Zn^{2+} on non-mammalian fertilization remains unexplored.

We sought to determine whether fertilization signals the release of Zn^{2+} from non-mammalian eggs. Using confocal microscopy to image and fluorometry to quantify extracellular Zn^{2+} released during fertilization, we found that eggs from the African clawed frog *Xenopus laevis* release Zn^{2+} upon fertilization or parthenogenic activation. To determine if increased extracellular Zn^{2+} serves as a polyspermy block, we fertilized *X. laevis* eggs in varying concentration of extracellular Zn^{2+}. Indeed, Zn^{2+} inhibited the appearance of cleavage furrows in a concentration-

dependent manner. This Zn^{2+} mediated interference of early embryonic development did not require continued presence of the ion, as incubation of *X. laevis* eggs with Zn^{2+} prior to insemination was sufficient to block cleavage furrow development. These data are consistent with the hypothesis that Zn^{2+} alters the extracellular matrix (ECM) around eggs to make it impenetrable to sperm. To explore whether the fertilization-induced Zn^{2+} release is conserved, we monitored extracellular Zn^{2+} upon activating oocytes from the axolotl *Ambystoma mexicanum* and eggs from the zebrafish *Danio rerio.* Indeed, both gamete types released Zn^{2+} upon parthenogenic activation. To determine whether extracellular Zn^{2+} regulates fertilization and embryonic development in more diverse species, we fertilized eggs from the sea urchin *Strongylocentrotus purpuratus* and the cnidaria *Hydractinia symbiolongicarpus* in varying concentrations of extracellular Zn^{2+}. Similar to *X. laevis*, elevated extracellular Zn^{2+} inhibited fertilization and development in these eggs. Taken together, these findings suggest a prominent role for Zn^{2+} in the slow polyspermy block in non-mammalian vertebrates, echinoderms, and cnidarians.

5.2 Results

5.2.1 *X. laevis* fertilization and parthenogenic activation induce Zn^{2+} release

Zn^{2+} release following fertilization of dejellied eggs from *X. laevis* was monitored using confocal microscopy with the cell-impermeant, fluorescent Zn^{2+} indicator FluoZin-3. Fertilization-induced Zn^{2+} release began 251 ± 39 seconds after insemination (Fig. 5-1 A&B, N=11 eggs). Zn^{2+} was released as a single wave that wraps around the egg and that lasted a total of 137 ± 14 seconds (Fig. 5-1 A&B, N=11 eggs). The localization and timing of Zn^{2+} release followed the pattern of

the fertilization envelope lifting, as seen in the brightfield images collected concurrently (Fig. 5-1 A red arrows). Cortical granule exocytosis stimulates lifting of the fertilization envelope due to release of proteases that cleave contacts between the envelope and plasma membrane (*5*, *22*); therefore, Zn^{2+} released in this pattern is consistent with the hypothesis that cortical granules exocytose Zn^{2+} following fertilization of *X. laevis* eggs. Accordingly, lifting of the envelope is a sign of successful fertilization and egg activation. Consistently, all eggs that underwent *in vitro* fertilization contracted at their animal poles following fluorescent imaging (Fig. 2-3), which is yet another mark of successful fertilization and egg activation.

To determine whether sperm were required to induce Zn^{2+} release from *X. laevis* eggs, we used confocal microscopy and FluoZin-3 to monitor extracellular Zn^{2+} before and after parthenogenic activation. *X. laevis* eggs can be parthenogenically activated using the Ca^{2+} ionophore ionomycin (*59*). Ionomycin-induced activation evokes cortical granule exocytosis, resumption of the cell cycle, and the appearance of abortive cleavages (Fig. 2-3). Consistently, parthenogenic activation of dejellied *X. laevis* eggs with 10 µM ionomycin evoked Zn^{2+} release (Fig. 5-1 C, N=12 eggs). The Zn^{2+} released from these activated eggs followed a similar pattern of Zn^{2+} release from fertilized eggs, where Zn^{2+} appeared around the circumference of the egg in a single wave and followed the lifting of the fertilization envelope (Fig. 5-1 C red arrows). These results are consistent with the hypothesis that this Zn^{2+} is released from cortical granules. Envelope lifting and animal pole contraction from fluorescently imaged eggs was used to confirmed successful activation. Furthermore, to test the robustness of ionomycin activation, we compared the appearance of abortive cleavages in dejellied eggs treated with 0 or 10 µM ionomycin. We observed 100 ± 0% activation from dejellied *X. laevis* eggs treated with 10 µM ionomycin (N=5

experimental trials), compared to 4 ± 2% activation from the dejellying process alone (N=5 experimental trials). These results indicate that the Zn^{2+} release observed by confocal microscopy was the direct result of egg activation.

The amount of Zn^{2+} released from *X. laevis* eggs was quantified by collecting the solution surrounding dejellied eggs after fertilization or parthenogenic activation and performing fluorometry using FluoZin-3 (Table 5-1). We found that fertilization induces an average release of $1.0 \pm 0.5 \times 10^{14}$ Zn^{2+} ions per *X. laevis* egg (N=8 experimental trials). Parthenogenic activation evoked a slightly smaller release of $2.5 \pm 1.5 \times 10^{13}$ Zn^{2+} ions per *X. laevis* egg (N=4 experimental trials). Together, these results confirm that Zn^{2+} is released from *X. laevis* eggs following fertilization and parthenogenic activation. If we assume that the Zn^{2+} released by a fertilized *X. laevis* egg remains in the envelope and jelly around the egg, the concentration of Zn^{2+} would be 2 ± 1 mM immediately surrounding the egg. These calculations suggest that immediately following fertilization, a high local concertation of Zn^{2+} may exists around *X. laevis* eggs.

5.2.2 Extracellular Zn^{2+} inhibits early embryonic development in *X. laevis*

We inseminated *X. laevis* eggs in varying concentrations of extracellular $ZnSO_4$ to explore whether Zn^{2+} may aid in preventing polyspermy. Using the appearance of cleavage furrows as an indicator of successful fertilization and development (Figs. 2-3), we found that $ZnSO_4$ inhibited embryonic development in a concentration-dependent manner (Fig. 5-2 A). Fitting plots of embryo development versus the concentration of $ZnSO_4$ with a sigmoidal function, we found that the half-maximal inhibitory concentration (IC_{50}) was 31 ± 10 µM (Table 5-2, N=7 experimental trails). To confirm that Zn^{2+} was responsible for this inhibition of development, and not SO_4^{2-}, *X. laevis* eggs

were fertilized in varying concentrations of $ZnCl_2$ and $MgSO_4$ (Fig. 5-2 B&C). $ZnCl_2$ inhibited development with a similar IC_{50} of 30 ± 8 µM (Table 5-2, N=8 experimental trials); whereas, $MgSO_4$ had no effect (N=5 experimental trials). Collectively, these results demonstrate that excess extracellular Zn^{2+} inhibits development of *X. laevis* eggs.

To hone in on the timeframe of developmental inhibition by Zn^{2+}, *X. laevis* eggs were inseminated in saturating concentrations of $ZnSO_4$ (1 mM) or control solution (MR/3) and then transferred 30 minutes after sperm addition to either $ZnSO_4$ or MR/3. We found that eggs inseminated in $ZnSO_4$ failed to develop whereas those inseminated in MR/3 developed normally, even when transferred to $ZnSO_4$ 30 min after sperm addition (Fig. 5-2 D). These results reveal that Zn^{2+} is acting during the first 30 minutes of insemination, on the egg and/or sperm, to inhibit development.

To determine if Zn^{2+} disrupts fertilization and embryonic development by modifying the egg, rather than acting on the sperm, we explored whether pre-treating eggs with Zn^{2+} and then applying sperm in the absence of Zn^{2+} interfered with fertilization. *X. laevis* eggs were pre-treated with saturating concentrations of $ZnSO_4$ (300 µM) or control solution (MR/3) and then transferred to either $ZnSO_4$ or MR/3 solutions for insemination and development. Eggs pretreated in $ZnSO_4$ failed to develop cleavage furrows, even when inseminated in the control solution with no added Zn^{2+} (MR/3). By contrast, eggs pretreated in MR/3 and transferred to MR/3 developed normally (Fig. 5-3 A). Consistent with our previous experiments (Fig. 5-2 D), eggs pretreated with the control solution (MR/3) and inseminated in $ZnSO_4$ failed to develop (Fig. 5-3 A). Together, these results document that Zn^{2+} alters the egg to interfere with fertilization and the earliest events of

embryonic development. These results are consistent with a role for extracellular Zn^{2+} in altering the ECM surrounding the egg to create a barrier that prevents sperm penetration.

5.2.3 Zn^{2+} alters the ECM of *X. laevis* eggs

The ECM of *X. laevis* eggs has two layers (Fig. 5-6 A). Immediately adjacent to the plasma membrane is the vitelline envelope, which contains conserved glycoproteins analogous to those found in the zona pellucida surrounding mammalian eggs (*18-20*). Cortical granules contain conserved proteases that cleave these glycoproteins to make the envelope impenetrable by sperm (*5, 23, 28*). Outside of the vitelline envelope of *X. laevis* eggs is the jelly coat, which is enriched in various ions, glycoproteins, and contains the chemoattractant allurin (*53, 180-185*).

To explore whether Zn^{2+} alters the *X. laevis* egg jelly coat, eggs were incubated in saturating concentrations of $ZnSO_4$ (1 mM) or control solution (MR/3), then they were placed in a reducing MR/3 solution with β-mercaptoethanol (BME) to remove the jelly coat. An average *X. laevis* egg with a jelly coat is 2.0 mm in diameter; whereas, eggs lacking jelly are 1.4 mm in diameter (*53*). We found that eggs pre-treated with $ZnSO_4$ had an average egg diameter of 1.93 ± 0.07 mm after BME treatment (N = 15 eggs from 7 frogs). By contrast, eggs pre-treated with MR/3 had an average diameter of 1.45 ± 0.01 mm after BME treatment (N = 22 eggs from 7 frogs). These results demonstrate that Zn^{2+} is stabilizing the jelly coat to prevent dejellying with BME. These data are consistent with the hypothesis that extracellular Zn^{2+} hardens the jelly to make it impenetrable to sperm.

To determine whether the jelly layer is required for Zn^{2+} to interfere with fertilization and development, *X. laevis* eggs were dejellied and fertilized in the presence of varying concentrations of extracellular $ZnSO_4$ (Fig. 5-3 B). Indeed, $ZnSO_4$ interfered with the appearance of cleavage furrows, with an IC_{50} of 23 ± 3 µM (N=6 experimental trials, Table 5-2). Because Zn^{2+} inhibited development similarly with and without the jelly coat, we predict that Zn^{2+} is acting on the vitelline envelope to cease fertilization and development, and/or Zn^{2+} inhibits the sperm from fertilizing regardless of the vestments surrounding the egg.

5.2.4 Parthenogenic activation induces Zn^{2+} release from non-mammalian vertebrate eggs

To establish the conservation of fertilization-induced Zn^{2+} release, we explored whether eggs from other non-mammalian vertebrates known to have cortical granules release Zn^{2+} during egg activation. First, we tested for activation-induced Zn^{2+} release from another amphibian: the axolotl *A. mexicanum.* Given that *A. mexicanum* are internal fertilizers and collecting an abundance of mature eggs is challenging, we used fertilization-incompetent *A. mexicanum* oocytes that were surgically removed from the animal. Unlike most urodeles (*3, 4*), *A. mexicanum* female gametes have cortical granules docked at their plasma membrane (*186*). Because *A. mexicanum* cortical granules are released after fertilization to modify the ECM surrounding the egg (*186*), we hypothesized that they may also contain Zn^{2+}. Similar to *X. laevis*, urodele eggs are activated by increased intracellular Ca^{2+} (*3*). Thus, we activated *A. mexicanum* oocytes with ionomycin application and used confocal microscopy to image extracellular Zn^{2+} with FluoZin-3. We found that *A. mexicanum* oocytes released Zn^{2+} in response to 300 µM ionomycin application (Fig. 5-4 A, N=5 oocytes); whereas, *X. laevis* eggs release Zn^{2+} with only 10 µM ionomycin (Fig. 5-1 C). A high concentration of ionomycin was required to activate these cells because oocytes are much

less sensitive to internal Ca^{2+} changes compared to eggs (*187*); a phenomenon that we also observed with *X. laevis* oocytes (data not shown). Given the abundance of Ca^{2+} that was loaded into these *A. mexicanum* oocytes, the eventual Zn^{2+} release was abrupt and did follow a distinct pattern.

We next used eggs from the zebrafish *D. rerio*, which are oviparous and lay their eggs externally prior to fertilization. *D. rerio* eggs are activated by osmotic shock upon spawning, meaning water is sufficient to awaken the quiescent egg to resume cellular processes such as meiosis (*85, 188*). Blastodisc formation occurs within 90 minutes of hydration, and abortive cleavages are observed within 120 minutes (Fig. 2-3). We observed 100 ± 0% activation, indicated by abortive cleavages, from dry eggs placed in water (N=12 experimental trials). When *D. rerio* eggs were hydrated in the presence of the Zn^{2+} indicator FluoZin-3, activation-induced Zn^{2+} release was observed in all eggs (Fig. 5-4 B, N=7 eggs). Because there is no visual indicator of polarity in unfertilized zebrafish eggs (*85*), the pattern of Zn^{2+} release could not be determined; therefore, a correlation between cortical granule exocytosis and Zn^{2+} release cannot be made.

5.2.5 Extracellular Zn^{2+} inhibits fertilization and embryonic development in echinoderms and cnidaria

To determine the conservation of zinc-inhibition of fertilization and early embryonic development in invertebrates, we fertilized eggs from the sea urchin *S. purpuratus* and the cnidarian *H. symbiolongicarpus* in varying concentration of $ZnSO_4$. By monitoring the appearance of cleavage furrows (Fig. 2-3), we found that fertilization and development were blocked in a concentration-dependent manner for both *S. purpuratus* and *H. symbiolongicarpus* (Fig. 5-5). The

IC_{50} for *S. purpuratus* was 9 ± 2 µM (N=3 experimental trials) and for *H. symbiolongicarpus* was 4 ± 2 µM (N=3 experimental trials, Table 5-2). The results reveal that Zn^{2+} can inhibit fertilization and development in non-mammalian species too.

5.3 Discussion

Zn^{2+} is an important regulator of egg maturation and early embryonic development in vertebrate systems. Here we demonstrate that, like mammals, fertilization and parthenogenic egg activation induces Zn^{2+} release from frog, axolotl, and fish eggs. Zn^{2+} release from *X. laevis* eggs likely serves as a polyspermy prevention mechanism, given that increased extracellular Zn^{2+} inhibits fertilization in a concentration-dependent manner (Fig. 5-6 A). Furthermore, we show that elevated extracellular Zn^{2+} inhibits fertilization and development in more distantly related invertebrates, including sea urchins and cnidarians (Fig. 5-6 B). Together, these results suggest that fertilization-induced Zn^{2+} release is a conserved mechanism in animals whose eggs have cortical granules and that this Zn^{2+} contributes to the slow polyspermy block.

5.3.1 Zn^{2+} released from *X. laevis* eggs mimics internal Ca^{2+} dynamics

The original reports of fertilization-induced Zn^{2+} sparks in mice, non-human primates, humans, and bovine show that the pattern of Zn^{2+} released mimics that of Ca^{2+} changes in the egg, where Zn^{2+} is released in short, repetitive spurts (*29-31*). In *X. laevis* eggs, we also demonstrate that Zn^{2+} release follows the pattern of Ca^{2+} changes in the egg, namely Zn^{2+} release begins at one point on the egg and traverses radially until the entire egg has released (Fig. 5-1 A). There is only

one Zn^{2+} wave in *X. laevis* eggs, in accordance with a singular fertilization-induced rise in intracellular Ca^{2+}. Similarly, we speculate that fertilization-induced Zn^{2+} release follows the pattern of Ca^{2+} dynamics in fertilized eggs of other animals too.

5.3.2 Zn^{2+} modifies the *X. laevis* ECM

We found that fertilization induces the release of $1.0 \pm 0.5 \times 10^{14}$ (Table 5-1) Zn^{2+} ions per *X. laevis* egg. Similar variability in the amount of Zn^{2+} released from individual eggs has also been reported in mice and bovine (*29, 31*). Consistent with this variation, mammalian eggs retain 100-500 µM Zn^{2+} in their ECM (zona pellucida) surround their eggs post-fertilization (*32*). Similarly, if the Zn^{2+} released by a fertilized *X. laevis* egg were to remain in the ECM (envelope and jelly), we calculate that the concentration of Zn^{2+} would be 2 ± 1 mM immediately surrounding the egg. We found that the IC_{50} for $ZnSO_4$ inhibition of fertilization was 31 ± 10 µM in *X. laevis* (Table 5-2). Taken together, these data suggest that the Zn^{2+} release upon fertilization is sufficient to alter the ECM and inhibit fertilization and development of *X. laevis* eggs.

Extracts from *X. laevis* egg cortical granules induce hardening of the vitelline envelope and jelly layer to inhibit fertilization (*189*). We speculate that this effect may be due, in part, to the Zn^{2+} found in cortical granules. Consistent with this hypothesis, we found that exposure of *X. laevis* eggs to Zn^{2+} prior to fertilization made the eggs unfertilizable (Fig. 5-2 D and 5-3 A). By fertilizing dejellied eggs in varying concentrations of $ZnSO_4$, we demonstrate that Zn^{2+} acts directly on the vitelline envelope (Fig. 5-3 B). Given that the envelope is made of highly glycosylated proteins, we speculate that Zn^{2+} is oxidizing these glycoproteins in the envelope to inhibit sperm binding. Additionally, we showed that Zn^{2+} is altering the jelly coat of *X. laevis* eggs,

as zinc-treated eggs were incapable of being dejellied under standard conditions used to dejelly unfertilized eggs. There are three distinct jelly layers surrounding the *X. laevis* egg, which are comprised of various ions, highly glycosylated proteins and the sperm chemoattractant allurin (*28, 53, 182-185*). We suspect that Zn^{2+} could be acting on glycoproteins in the jelly layers similarly to how it is interacting with the envelope. Together our *X. laevis* fertilization data suggest that Zn^{2+} is likely released from cortical granules to modify the ECM and contribute to the slow polyspermy block.

5.3.3 Conservation of extracellular Zn^{2+} affecting fertilization and development

To investigate the conservation of fertilization-induced Zn^{2+} release, we parthenogenically activated oocytes from the axolotl *A. mexicanum* and eggs from the zebrafish *D. rerio*. Indeed, we found that artificially activating these gametes induced Zn^{2+} release (Fig. 5-4). Similarly, we wanted to investigate the conservation of zinc-induced inhibition of fertilization and development. In addition to *X. laevis*, we found that Zn^{2+} caused a concentration-dependent inhibition of development from eggs of the sea urchin *S. purpuratus* and the cnidaria *H. symbiolongicarpus* (Fig. 5-5). Frogs, zebrafish, axolotls, and sea urchins contain homologous ZP proteins that could be similarly altered by Zn^{2+} (*20*), thus it is likely that Zn^{2+} modification of ZP proteins is conserved. Accordingly, exposure to Zn^{2+} causes a thickening of the egg envelope in mice (*32*); this Zn^{2+}-induced physical barrier is suggested to contribute to the slow polyspermy block. However, *H. symbiolongicarpus* eggs lack an envelope with conserved ZP proteins (*190*), thus it is unknown how Zn^{2+} is altering fertilization in this organism.

In addition to contributing to the slow polyspermy block, fertilization-induced Zn^{2+} release may play other physiological roles. For example, we know that the presence of extracellular Zn^{2+} in *in vitro* fertilization media impairs the motility of mouse, frog, and sea urchin sperm (*24*, *178*, *179*). Thus, the effects of Zn^{2+} released from mammalian eggs following fertilization has recently been coined the "zinc shield" (*191*). This shield encompasses the protective modifications to the egg envelope, as well as the motility effects that deter additional sperm from reaching the nascent zygote (*191*). Additionally, the zinc shield effect may support safe passage of the embryo to the implantation site. Zn^{2+} is a ligand for the mammalian oviduct receptor GPR39, and it is speculated that Zn^{2+} released from eggs following fertilization may stimulate this receptor to aid in transport of the embryo from the oviduct to the implantation site (*192*). Taken together, it seems that Zn^{2+} is an important developmental regulator immediately after fertilization in all species studied this far, and Zn^{2+} may contribute to maintaining early embryo health and viability in mammals.

5.3.4 Summary

In summary, we have shown that Zn^{2+} plays a prominent role post-fertilization in *X. laevis*, which may contribute to the slow polyspermy block. Based on our experiments with zebrafish, axolotls, and sea urchins, it seems that fertilization-induced Zn^{2+} release and zinc-induced inhibition of fertilization and development is a conserved feature of the slow polyspermy block in mammalian and non-mammalian systems. Continued use of tractable fertilization models, such as *X. laevis*, will allow us to more readily study these conserved processes.

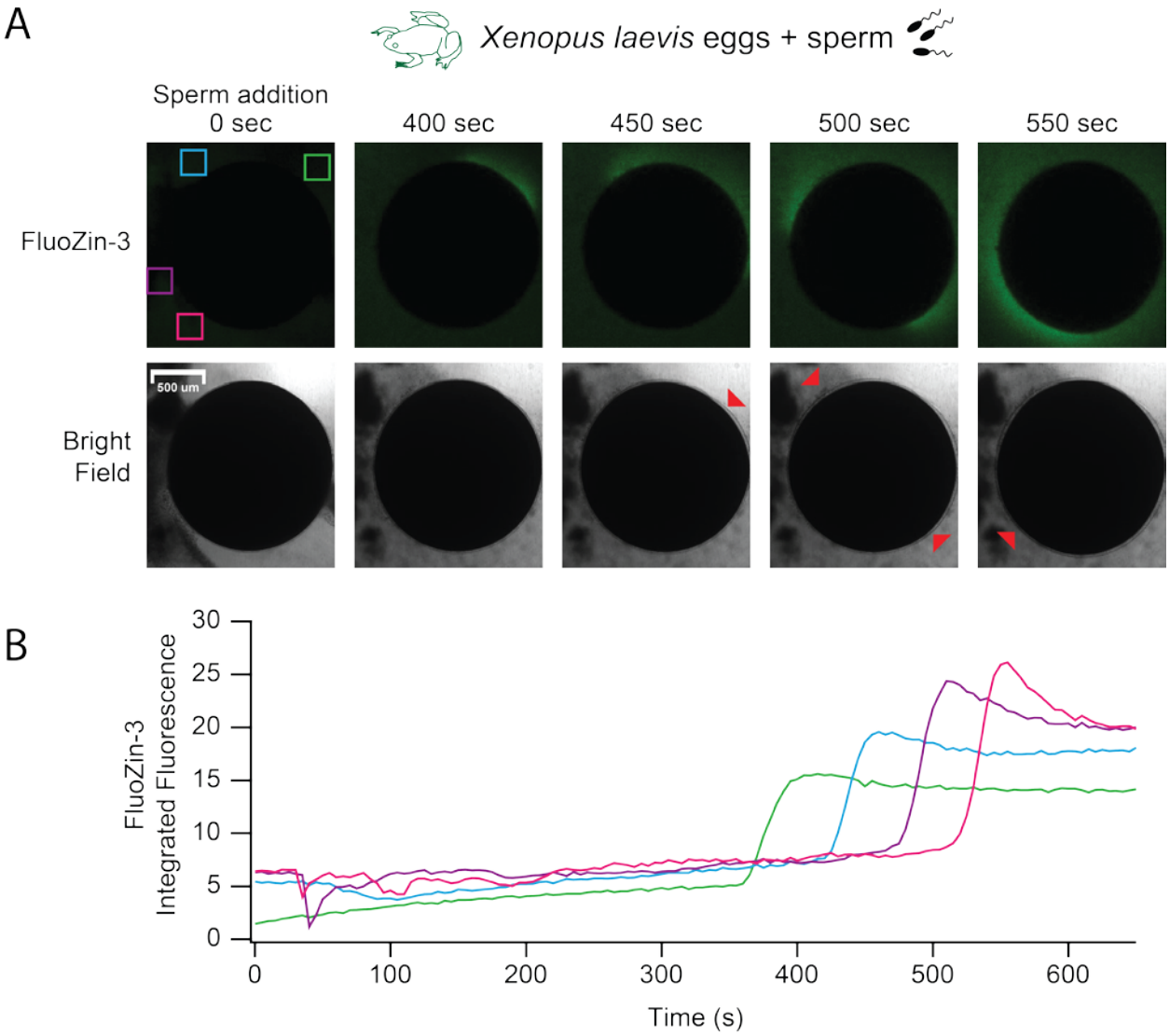
A
Xenopus laevis eggs + sperm
Sperm addition
0 sec
400 sec
450 sec
500 sec
550 sec
FluoZin-3
Bright Field
500 um
B
FluoZin-3 Integrated Fluorescence
30
25
20
15
10
5
0
0
100
200
300
400
500
600
Time (s)
C
Xenopus laevis eggs + 10 µM ionomycin
Ionomycin addition
0 sec
100 sec
125 sec
175 sec
225 sec
FluoZin-3
Bright Field
500 um

Figure 5-1. Fertilization and parthenogenic activation-induced Zn^{2+} release in *X. laeivs*

A) Representative bright field and fluorescent images of *X. laevis* eggs releasing Zn^{2+} upon fertilization with sperm (N=11 eggs), which was detected with the Zn^{2+}-indicator FluoZin-3. B) Increase in FluoZin-3 fluorescence upon *in vitro* fertilization was detected by ROI analysis (shown as colored boxes in A). C) Parthenogenic activation of *X. laevis* eggs with 10 µM ionomycin in the presence of Fluozin-3 also induced Zn^{2+} exocytosis (N=12 eggs). The pattern of Zn^{2+} release corresponds with lifting of the fertilization envelope (red arrowheads), indicating successful egg activation (A&C). All eggs were placed in 50 µM FluoZin-3 and imaged every 5 seconds via confocal microscopy. Scale bars in bright field images represents 500 µm. *Monica Sauer and Maddy Czekalski helped collect these images.*

Table 5-1. Quantification of the Zn^{2+} released from *X. laevis* eggs

	Fertilization	**Parthenogenic activation**
X. laevis	$1.0 \pm 0.5 \times 10^{14}$ N = 8	$2.5 \pm 1.5 \times 10^{13}$ N = 4

Average ± SEM Zn^{2+} ions released per egg after fertilization or activation. Activation was induced with 10 µM ionomycin. N represents the number of experimental trials.

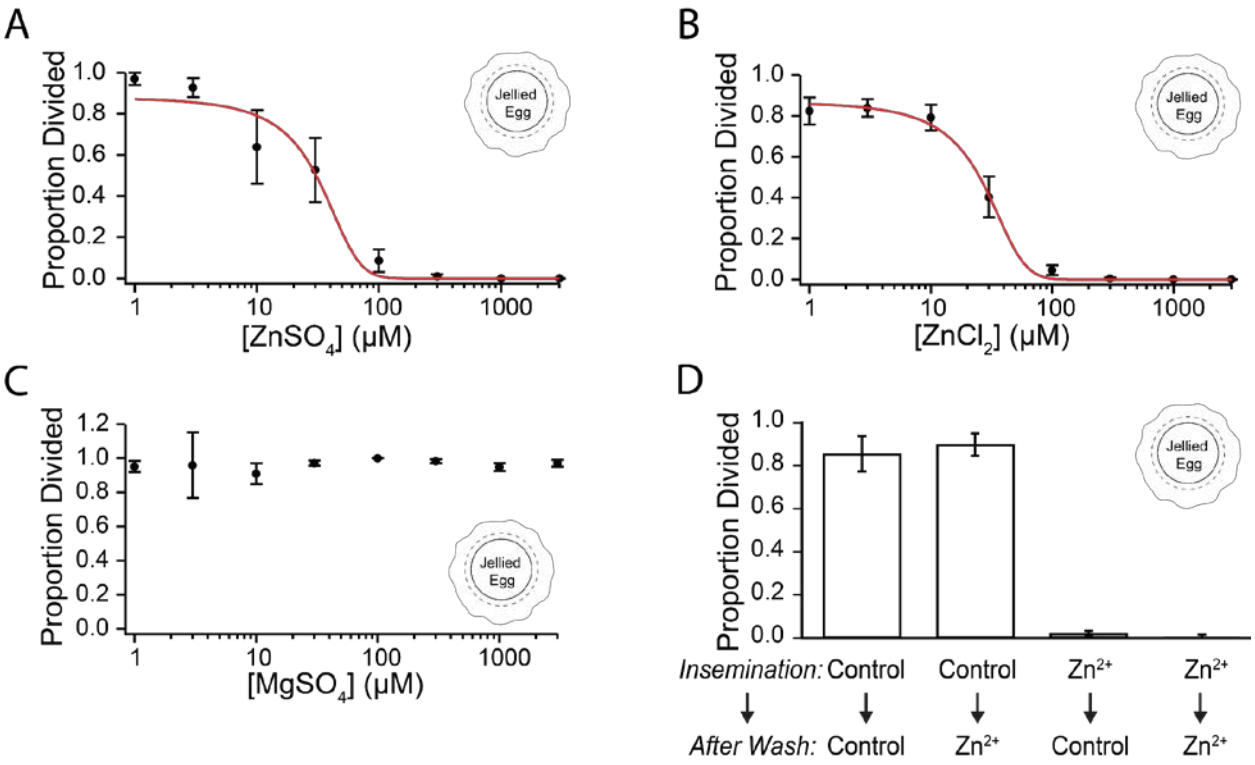

Figure 5-2. Extracellular Zn^{2+} blocks fertilization and development of *X. laevis* eggs

A-C) Development was blocked in a concentration-dependent manner for jellied eggs inseminated in extracellular $ZnSO_4$ (A, N = 7 experimental trials) and $ZnCl_2$ (B, N = 8 experimental trials), whereas $MgSO_4$ had no effect on development (C, N = 5 experimental trials). D) Post-fertilization transfer assays were conducted by inseminating in either control solution (MR/3) or saturating Zn^{2+} (1 mM $ZnSO_4$). Eggs were switched to the transfer solution 30-minutes post-fertilization (N = 6 experimental trials). Averaged data ± S.E.M. are displayed for each condition and were fit sigmoidal function, when possible (A-D). *Data for panels A-D was collected by Monica Sauer, Ben Wisner, Meli Linderman, Meghan Hanson, and Kavya Pasumarthy.*

Table 5-2. Concentration-responses for eggs fertilized in extracellular Zn^{2+}

	$ZnSO_4$	**$ZnSO_4$ (dejellied)**	**$ZnCl_2$**
X. laevis	31 ± 10 µM N = 7	23 ± 3 µM N = 6	30 ± 8 µM N = 8
S. purpuratus	9 ± 2 µM N = 3	---	---
H. symbiolongicarpus	4 ± 2 µM N = 3	---	---

Average ± SEM IC_{50} for each fertilization condition. The ECM of the eggs was unaltered unless noted otherwise. N represents the number of experimental trials.

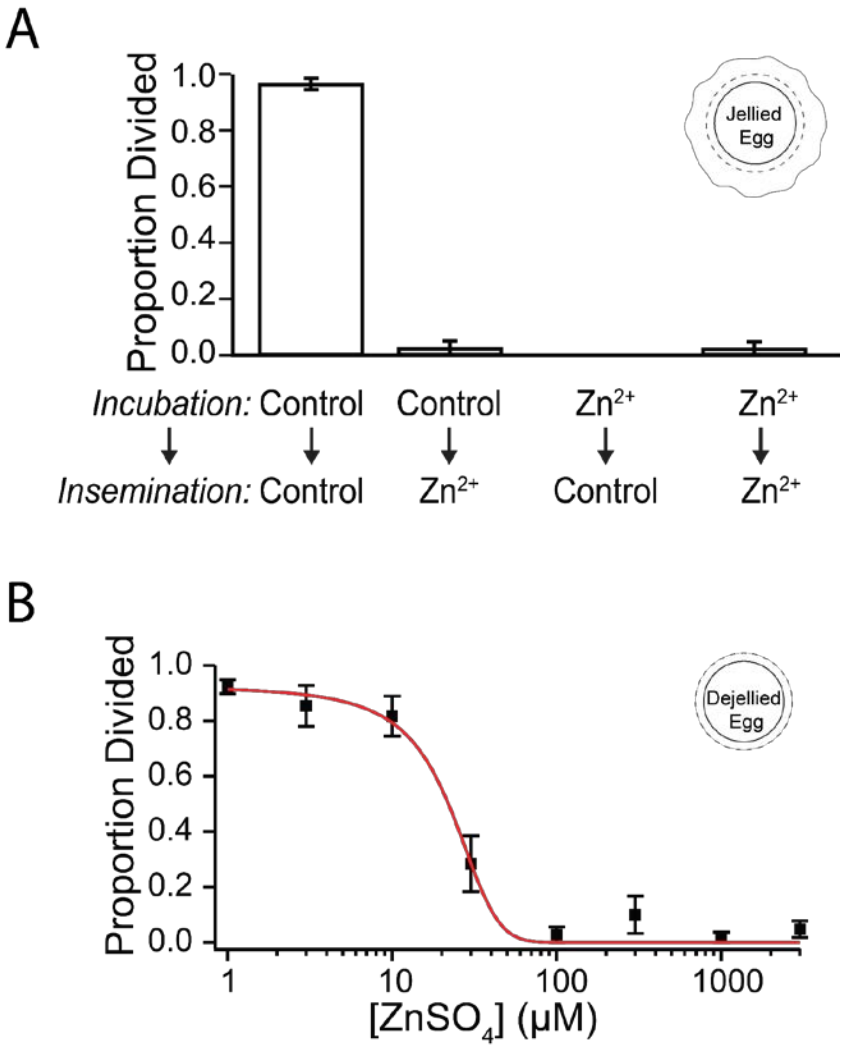

Figure 5-3. Extracellular Zn^{2+} alters the ECM of *X. laevis* eggs to inhibit fertilization

A) Pre-fertilization transfer assays were conducted by incubating eggs in either control solution (MR/3) or saturating Zn^{2+} (300 µM $ZnSO_4$) and switching the eggs to the transfer solution for insemination (N = 5-6 experimental trials). B) Development of dejellied eggs was inhibited in a concentration-dependent manner by $ZnSO_4$ (N=6 experimental trials). Averaged data ± S.E.M. are displayed for each condition and were fit sigmoidal function, when possible (A-B). *Data for panel A was collected by Monica Sauer, Ben Wisner, Meli Linderman, Meghan Hanson, and Kavya Pasumarthy.*

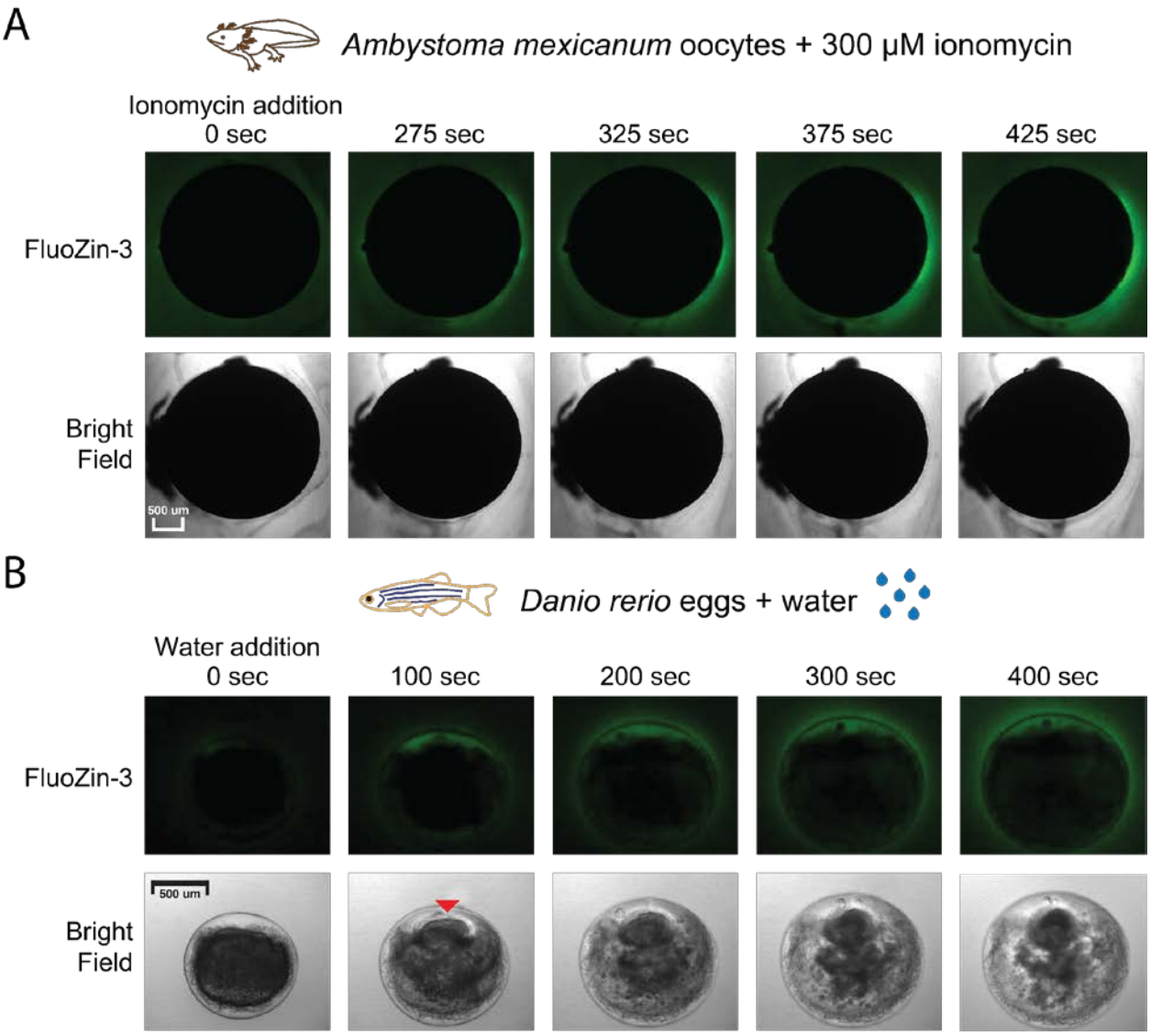

Figure 5-4. Parthenogenic activation-induced Zn^{2+} release in *D. rerio* eggs and *A. mexicanum* oocytes

A) *A. mexicanum* oocytes exocytose Zn^{2+} upon activation with 300 µM ionomycin (N = 5 eggs). All eggs and oocytes were placed in 50 µM FluoZin-3 and imaged every 5 seconds via confocal microscopy. Scale bars in bright field images represents 500 µm. B) Representative bright field and fluorescent images of *D. rerio* eggs releasing Zn^{2+} upon activation with water (N = 7 eggs).

Blastodisc formation (red arrowhead) indicates successful egg activation. *Wesley Phelps and Maddy Czekalski helped collect these images.*

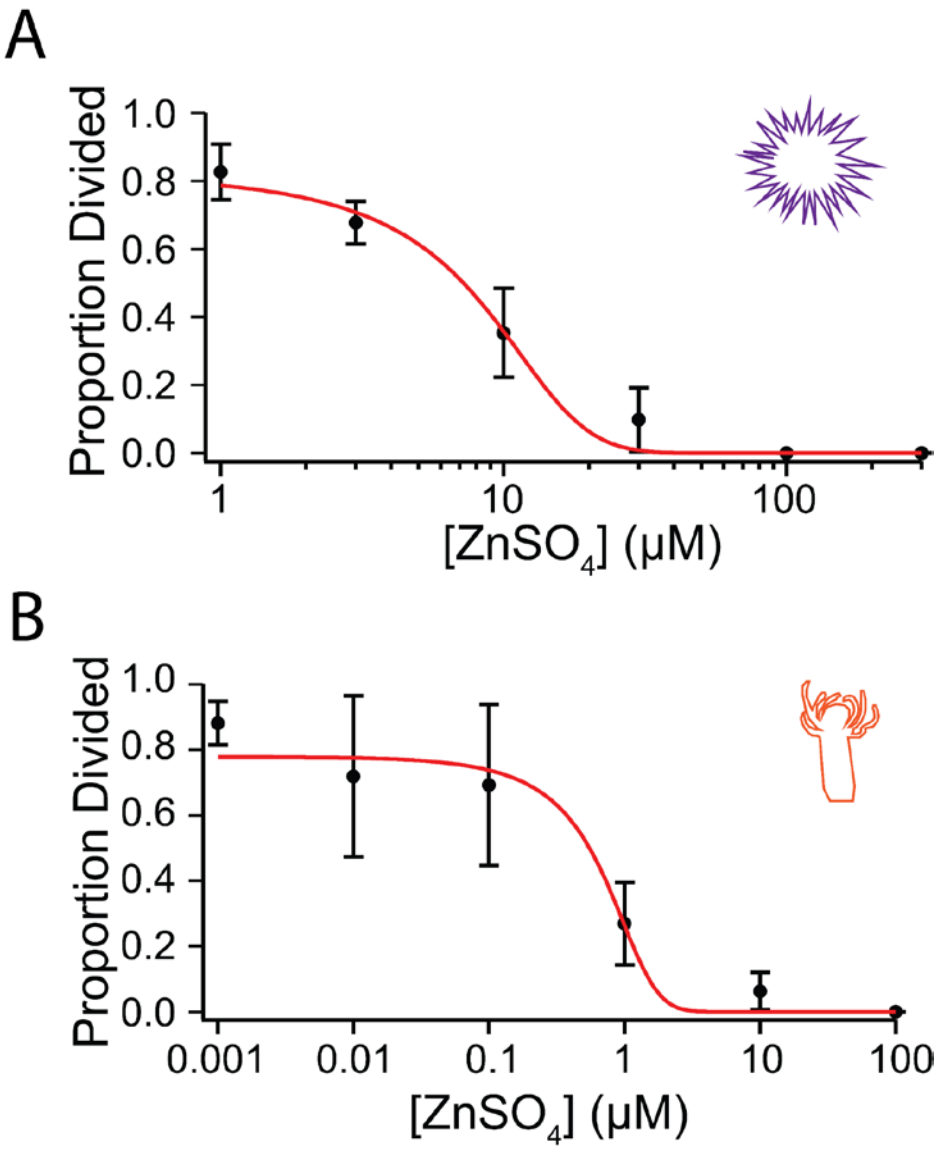

Figure 5-5. Fertilization of *S. purpuratus* and *H. symbiolongicarpus* egg in the presence of Zn^{2+}

A-B) Development was blocked in a concentration-dependent manner for *S. purpuratus* (A, N=3 experimental trials) and *H. symbiolongicarpus* (B, N=3-4 experimental trials) eggs inseminated in extracellular $ZnSO_4$. *Rachel Bainbridge helped to collect data for this figure.*

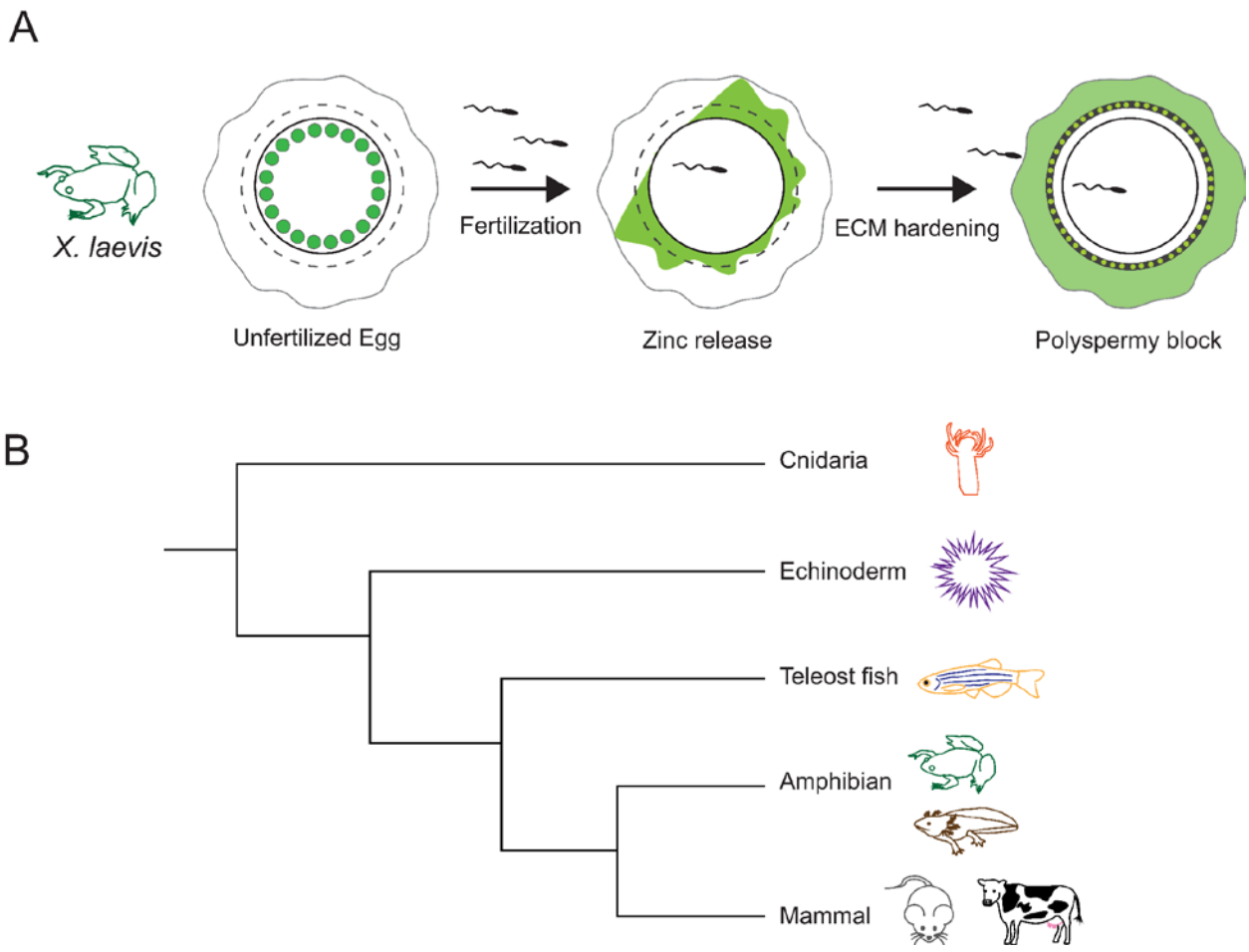

Figure 5-6. Conservation of fertilization-induced Zn^{2+} release model

A) In *X. laevis*, fertilization stimulates the release of cortical granules (green spheres) from eggs, which release Zn^{2+} in a wave pattern to modify the envelope (dashed line) and jelly coat (squiggly line) to inhibit sperm entry. B) Phylogenetic tree of organisms that release Zn^{2+} following fertilization and/or artificial activation, as well as organisms that exhibit a zinc-induced fertilization and development block.

6.0 Conclusions and future directions

6.1 Overview

Over the course of my dissertation research, I have investigated polyspermy prevention mechanisms used by the African clawed frog, *Xenopus laevis.* Briefly, I have shown that the Ca^{2+} needed to stimulate the fast polyspermy block originates from the endoplasmic reticulum (ER) in a phospholipase C (PLC) and inositol 1,4,5-trisphosphate (IP_3)-dependent pathway. Additionally, I have demonstrated that this increase in cytosolic Ca^{2+} activates the transmembrane protein 16A (TMEM16A) channel to conduct the depolarizing Cl^- current of the fast block. This depolarization of the egg membrane electrically inhibits supernumerary sperm from entering an already fertilized *X. laevis* egg. Furthermore, I established that the extracellular Zn^{2+} released by eggs upon fertilization contributes to slow polyspermy block in *X. laevis* and other non-mammalian organisms. Specifically, I have shown that *X. laevis* eggs release Zn^{2+} at fertilization and that increased extracellular Zn^{2+} modified the egg's extracellular matrix (ECM) to inhibit fertilization and development. I have also demonstrated that zinc-induced inhibition of fertilization is conserved in other non-mammalian species including sea urchins, zebrafish, axolotls, and cnidaria. Here I will discuss possible future directions for investigation of the fast and slow block pathways in *X. laevis* and other organisms.

6.2 Future studies

6.2.1 Elucidating the PLC that initiates the fast polyspermy block in *X. laevis*

I have established that the fast polyspermy block in *X. laevis* is initiated by PLC activation. We do not yet know the identity of the PLC that signals the fast block, how it is activated by fertilization, or if the same signaling mechanisms are employed to activate the fast and slow blocks in *X. laevis*. Yet, we do know that *X. laevis* eggs contain two PLC isoforms β and γ (*64*), which are activated by different stimuli (*65*). If fertilization triggers the fast block by PLCγ activation, one ought to be able to inhibit the fertilization-evoked depolarization with tyrosine kinase inhibitors such as PP1 or lavendustin A. Alternatively, the importance of PLCβ in inducing the fast block in *X. laevis* can be tested by inhibiting G_q protein coupled receptor signaling.

Alternatively, one might speculate that a sperm-derived PLCζ could activate the fast block, similar to how the slow block is activated in mammals (*193-195*). Intriguingly, PLCζ is expressed in the testes of the teleost fish medaka but in the eggs of pufferfish (*196, 197*). A gene encoding PLCζ, however, has not been annotated in the *X. laevis* or *X. tropicalis* genomes (*74, 198*). Due to the incomplete nature of the annotations for the most recent *X. laevis* genome (*74*), it is possible that a PLCζ gene exists but has not been identified. Using conserved PLC sequences (*65*), one could search for novel PLCs in the *X. laevis* genome. If any new PLCs are identified, transcriptomics could be used to test for testes-specific expression.

6.2.2 Exploring the diversity of organisms that release Zn^{2+} from their eggs at fertilization

My own data demonstrates that frog, axolotl, and zebrafish eggs all release Zn^{2+} in response to fertilization and/or parthenogenic activation. I hypothesize that this Zn^{2+} resides in the eggs' cortical granules and is exocytosed during the slow polyspermy block. Fertilization induces a Zn^{2+} release from cortical granules in mammalian eggs (*29-31*). To determine whether this phenomenon is conserved, it would be interesting to expand these studies to include non-mammalian invertebrates known to release cortical granules following fertilization, such as sea urchins and ascidians (*199, 200*). One limitation for visualizing Zn^{2+} release in species that spawn in the ocean is that artificial sea water (ASW) contains tens of mM of Ca^{2+} and Mg^{2+} (*86*), which could bind to the Zn^{2+} indicator FluoZin-3 and skew the Zn^{2+} signal (*201*). However, my preliminary experiments testing FluoZin-3 in ASW suggest that the Zn^{2+} signal should surpass that of Ca^{2+} or Mg^{2+} (data not shown).

6.2.3 Determine the breadth of organisms whose fertilization is inhibited by increased extracellular Zn^{2+}

Here I have shown evidence that increased extracellular Zn^{2+} inhibits fertilization and development in frogs, sea urchins, and cnidarians. Moreover, in frogs I have demonstrated that Zn^{2+} likely alters the ECM of the egg to block fertilization and development. Given the conservation of envelope proteins (known as ZP proteins) ranging from mammals to echinoderms to mollusks, which are modified by cortical granule components during the slow polyspermy block (*5, 6, 20, 23*), it is likely that Zn^{2+} released from cortical granules also contributes to the slow polyspermy block. The impact of extracellular Zn^{2+} on envelope proteins from diverse organisms

is yet to be determined. Future experiments could explore fertilization in other deuterostomes such as ascidians, as well as the protostomes abalone and marine worms. It will be important to distinguish whether Zn^{2+} is acting on the sperm and/or eggs of these organisms. Additionally, direct tests will need to be performed to determine if Zn^{2+} treatment is inhibiting sperm entry into these eggs or ceasing the resumption of development after successful fertilization.

6.2.4 Explore the structural changes to the *X. laevis* ECM upon Zn^{2+} exposure

My data suggests that Zn^{2+} alters the ECM of *X. laevis* eggs to inhibit fertilization and development. Consistently, we know that Zn^{2+} makes the ECM of mouse eggs denser and less penetrable by sperm (*32*). Whether Zn^{2+} similarly alters the *X. laevis* ECM is yet to be determined. To investigate the Zn^{2+}-induced structural changes to the vitelline envelope and jelly coat of *X. laevis* eggs, future experiments could focus on comparing isolated jelly and envelope proteins before and after Zn^{2+} exposure using western blot analysis, mass spectrometry, and electron microscopy.

6.3 Significance of studying polyspermy

In most sexually reproducing species, polyspermy is embryonic lethal due to an unviable amount of DNA and an abundance of centrioles. Even with polyspermy prevention mechanisms, 1-2% of mammalian *in vivo* fertilization results in polyspermy (*33*). Furthermore, aged eggs have an increased incidence of polyspermy (*33*). By increasing our knowledge of polyspermy blocks in

mammalian and non-mammalian species, we expand our understanding of how to best prevent polyspermy.

6.4 Research applications

The overall goal of my dissertation has been to expand our understanding of polyspermy prevention mechanisms in the model organism *X. laevis*. Understanding how fertilization successfully propagates new life in multiple systems broadens our knowledge regarding the proliferation of sexually reproducing species. Furthermore, *X. laevis* fertilization is a robust, easily manipulatable system to study conserved processes, like fertilization-induced Zn^{2+} release. Accordingly, this research will introduce novel insight into human family planning. By understanding the molecular mechanisms regulating fertilization, efforts can be made to design novel contraceptive options, as well as infertility treatments. In the United States alone, 5% of reproductive age women have unintended pregnancies yearly (*202*). In addition to contraception development, understanding the early events of fertilization can help develop diagnosis of and treatments for infertility. Infertility affects up of 12% of married couples in the United States, and many of the currently available treatments are invasive and cost-prohibitive for many families (*203*).

Bibliography

1. R. R. Snook, D. J. Hosken, T. L. Karr, The biology and evolution of polyspermy: insights from cellular and functional studies of sperm and centrosomal behavior in the fertilized egg. *Reproduction (Cambridge, England)* **142**, 779-792 (2011).
2. E. Bianchi, G. J. Wright, Sperm Meets Egg: The Genetics of Mammalian Fertilization. *Annual review of genetics* **50**, 93-111 (2016).
3. Y. Iwao, Egg activation in physiological polyspermy. *Reproduction (Cambridge, England)* **144**, 11-22 (2012).
4. S. Mizushima, Fertilization 2: Polyspermic Fertilization. *Advances in experimental medicine and biology* **1001**, 105-123 (2017).
5. J. L. Wong, G. M. Wessel, Defending the zygote: search for the ancestral animal block to polyspermy. *Current topics in developmental biology* **72**, 1-151 (2006).
6. L. A. Jaffe, M. Gould, in *Biology of Fertilization*. (Academic Press, New York, London, UK, 1985), vol. 3, pp. 223 - 250.
7. L. A. Jaffe, Fast block to polyspermy in sea urchin eggs is electrically mediated. *Nature* **261**, 68-71 (1976).
8. L. A. Jaffe, A. P. Sharp, D. P. Wolf, Absence of an electrical polyspermy block in the mouse. *Developmental biology* **96**, 317-323 (1983).
9. N. L. Cross, R. P. Elinson, A fast block to polyspermy in frogs mediated by changes in the membrane potential. *Developmental biology* **75**, 187-198 (1980).
10. S. Miyazaki, Y. Igusa, Fertilization potential in golden hamster eggs consists of recurring hyperpolarizations. *Nature* **290**, 702-704 (1981).

11. S. H. Brawley, The fast block against polyspermy in fucoid algae is an electrical block. *Developmental biology* **144**, 94-106 (1991).

12. D. Kline, L. A. Jaffe, R. P. Tucker, Fertilization potential and polyspermy prevention in the egg of the nemertean, Cerebratulus lacteus. *The Journal of experimental zoology* **236**, 45-52 (1985).

13. H. Goudeau, Y. Depresle, A. Rosa, M. Goudeau, Evidence by a voltage clamp study of an electrically mediated block to polyspermy in the egg of the ascidian Phallusia mammillata. *Developmental biology* **166**, 489-501 (1994).

14. S. Miyazaki, S. Hirai, Fast polyspermy block and activation potential. Correlated changes during oocyte maturation of a starfish. *Developmental biology* **70**, 327-340 (1979).

15. E. Bianchi, B. Doe, D. Goulding, G. J. Wright, Juno is the egg Izumo receptor and is essential for mammalian fertilization. *Nature* **508**, 483-487 (2014).

16. A. D. Burkart, B. Xiong, B. Baibakov, M. Jimenez-Movilla, J. Dean, Ovastacin, a cortical granule protease, cleaves ZP2 in the zona pellucida to prevent polyspermy. *The Journal of cell biology* **197**, 37-44 (2012).

17. E. Just, The Fertilization Reaction in Echinarachnius Parma. *Biological Bulletin* **36**, 1-10 (1919).

18. J. M. Feng, H. F. Tian, Q. M. Hu, Y. Meng, H. B. Xiao, Evolution and multiple origins of zona pellucida genes in vertebrates. *Biology open* **7**, (2018).

19. H. Kubo, M. Kotani, H. Suzuki, N. Yoshizaki, Immunohistochemical localisation of gp69/64 molecules in Xenopus egg envelopes in relation to their sperm binding activity. *Zygote (Cambridge, England)* **10**, 131-140 (2002).

20. K. G. Claw, W. J. Swanson, Evolution of the egg: new findings and challenges. *Annual review of genomics and human genetics* **13**, 109-125 (2012).

21. S. A. Stricker, Comparative biology of calcium signaling during fertilization and egg activation in animals. *Developmental biology* **211**, 157-176 (1999).

22. L. L. Runft, L. A. Jaffe, L. M. Mehlmann, Egg activation at fertilization: where it all begins. *Developmental biology* **245**, 237-254 (2002).

23. M. Liu, The biology and dynamics of mammalian cortical granules. *Reproductive biology and endocrinology : RB&E* **9**, 149 (2011).

24. K. Tokuhiro, J. Dean, Glycan-Independent Gamete Recognition Triggers Egg Zinc Sparks and ZP2 Cleavage to Prevent Polyspermy. *Developmental cell*, (2018).

25. Y. Shibata *et al.*, Identification and cDNA cloning of alveolin, an extracellular metalloproteinase, which induces chorion hardening of medaka (Oryzias latipes) eggs upon fertilization. *The Journal of biological chemistry* **275**, 8349-8354 (2000).

26. Y. Shibata *et al.*, An oocyte-specific astacin family protease, alveolin, is released from cortical granules to trigger egg envelope hardening during fertilization in medaka (Oryzias latipes). *Developmental biology* **372**, 239-248 (2012).

27. L. L. Lindsay, J. L. Hedrick, Proteolysis of Xenopus laevis egg envelope ZPA triggers envelope hardening. *Biochemical and biophysical research communications* **324**, 648-654 (2004).

28. N. Oulhen, D. Xu, G. M. Wessel, Conservation of sequence and function in fertilization of the cortical granule serine protease in echinoderms. *Biochemical and biophysical research communications* **450**, 1135-1141 (2014).

29. A. M. Kim *et al.*, Zinc sparks are triggered by fertilization and facilitate cell cycle resumption in mammalian eggs. *ACS chemical biology* **6**, 716-723 (2011).

30. F. E. Duncan *et al.*, The zinc spark is an inorganic signature of human egg activation. *Scientific reports* **6**, 24737 (2016).

31. F. E. D. Emily L. Que, Hoi Chang Lee, Jessica E .Hornick, Stefan Vogt, Rafael Fissored, Thomas V. O'Halloran, and Teresa K.Woodruff, Bovine eggs release zinc in response to parthenogenetic and sperm-induced egg activation. *Theriogenology* **Available Online**, (2018).

32. E. L. Que *et al.*, Zinc sparks induce physiochemical changes in the egg zona pellucida that prevent polyspermy. *Integrative biology : quantitative biosciences from nano to macro*, (2017).

33. A. J. Gardner, J. P. Evans, Mammalian membrane block to polyspermy: new insights into how mammalian eggs prevent fertilisation by multiple sperm. *Reproduction, fertility, and development* **18**, 53-61 (2006).

34. T. Albert, A. Monroy, C. Y. Kao, H. Grundfest, Membrane Potential and resistance of the starfish egg before and after fertilization. *Biol. Bull. (Woods Hole, Mass.)* **111**, 152-177 (1956).

35. T. Maeno, Electrical characteristics and activation potential of Bufo eggs. *The Journal of general physiology* **43**, 139-157 (1959).

36. Y. Hiramoto, Changes in electrical properties upon fertilization in the sea urchin egg. *Experimental Cell Research* **16**, 421-424 (1958).

37. K. S. Cole, Dynamic electrical characteristics of the squid axon membrane. *Archives des sciences physiologiques* **3**, 253-258 (1949).

38. A. L. Hodgkin, A. F. Huxley, B. Katz, Ionic currents underlying activity in the giant axon of the squid. *Arch. Sci. Physiol.* **3**, 129-150 (1949).

39. G. Marmont, Studies on the axon membrane; a new method. *J Cell Comp Physiol* **34**, 351-382 (1949).

40. R. A. Steinhardt, L. Lundin, D. Mazia, Bioelectric responses of the echinoderm egg to fertilization. *Proceedings of the National Academy of Sciences of the United States of America* **68**, 2426-2430 (1971).

41. M. Charbonneau, M. Moreau, B. Picheral, J. P. Vilain, P. Guerrier, Fertilization of amphibian eggs: a comparison of electrical responses between anurans and urodeles. *Developmental biology* **98**, 304-318 (1983).

42. R. Nuccitelli, R. D. Grey, Controversy over the fast, partial, temporary block to polyspermy in sea urchins: a reevaluation. *Developmental biology* **103**, 1-17 (1984).

43. R. D. Grey, M. J. Bastiani, D. J. Webb, E. R. Schertel, An electrical block is required to prevent polyspermy in eggs fertilized by natural mating of Xenopus laevis. *Developmental biology* **89**, 475-484 (1982).

44. J. W. Lynn, D. H. McCulloh, E. L. Chambers, Voltage clamp studies of fertilization in sea urchin eggs. II. Current patterns in relation to sperm entry, nonentry, and activation. *Developmental biology* **128**, 305-323 (1988).

45. B. Hille, *Ion Channels of Excitable Membranes*. (Sinauer Associates, Inc., Sunderland, MA, 2001).

46. N. D. a. I. Lotan, *Expression of Exogenous Ion Channels and Neurotransmitter Receptors in RNA-Injected Xenopus Oocytes. In: Longstaff A., Revest P. (eds) Protocols in Molecular Neurobiology.*, (Springer, Totowa, NJ, 1992).

47. R. L. Papke, C. Smith-Maxwell, High throughput electrophysiology with Xenopus oocytes. *Combinatorial chemistry & high throughput screening* **12**, 38-50 (2009).

48. J. N. Dumont, Oogenesis in Xenopus laevis (Daudin). I. Stages of oocyte development in laboratory maintained animals. *Journal of morphology* **136**, 153-179 (1972).

49. K. Sobczak, N. Bangel-Ruland, G. Leier, W. M. Weber, Endogenous transport systems in the Xenopus laevis oocyte plasma membrane. *Methods (San Diego, Calif.)* **51**, 183-189 (2010).

50. J. M. Gomez-Hernandez, W. Stuhmer, A. B. Parekh, Calcium dependence and distribution of calcium-activated chloride channels in Xenopus oocytes. *The Journal of physiology* **502 (Pt 3)**, 569-574 (1997).

51. W. Weber, Ion currents of Xenopus laevis oocytes: state of the art. *Biochimica et biophysica acta* **1421**, 213-233 (1999).

52. R. G. Hazel Sive, and Richard Harland, *Early Development of Xenopus laevis: A laboratory manual*. (Cold Spring Harbor Laboratory Press, Cold Spring Harbor, New York, 2000).

53. K. L. Wozniak *et al.*, Extracellular Ca2+ Is Required for Fertilization in the African Clawed Frog, Xenopus laevis. *PloS one* **12**, e0170405 (2017).

54. G. N. Wheeler, A. W. Brandli, Simple vertebrate models for chemical genetics and drug discovery screens: lessons from zebrafish and Xenopus. *Developmental dynamics : an official publication of the American Association of Anatomists* **238**, 1287-1308 (2009).

55. K. Sato, Y. Fukami, B. J. Stith, Signal transduction pathways leading to Ca2+ release in a vertebrate model system: lessons from Xenopus eggs. *Seminars in cell & developmental biology* **17**, 285-292 (2006).

56. M. Watabe *et al.*, The electrical block to polyspermy induced by an intracellular Ca(2+) increase at fertilization of the clawed frogs, Xenopus laevis and Xenopus tropicalis. *Molecular reproduction and development*, (2019).

57. D. Kline, Calcium-dependent events at fertilization of the frog egg: injection of a calcium buffer blocks ion channel opening, exocytosis, and formation of pronuclei. *Developmental biology* **126**, 346-361 (1988).

58. K. Sato, A. A. Tokmakov, T. Iwasaki, Y. Fukami, Tyrosine kinase-dependent activation of phospholipase Cgamma is required for calcium transient in Xenopus egg fertilization. *Developmental biology* **224**, 453-469 (2000).

59. P. Snow, D. L. Yim, J. D. Leibow, S. Saini, R. Nuccitelli, Fertilization stimulates an increase in inositol trisphosphate and inositol lipid levels in Xenopus eggs. *Developmental biology* **180**, 108-118 (1996).

60. B. J. Stith, M. Goalstone, S. Silva, C. Jaynes, Inositol 1,4,5-trisphosphate mass changes from fertilization through first cleavage in Xenopus laevis. *Molecular biology of the cell* **4**, 435-443 (1993).

61. W. B. Busa, R. Nuccitelli, An elevated free cytosolic Ca2+ wave follows fertilization in eggs of the frog, Xenopus laevis. *The Journal of cell biology* **100**, 1325-1329 (1985).

62. R. Nuccitelli, D. L. Yim, T. Smart, The sperm-induced Ca2+ wave following fertilization of the Xenopus egg requires the production of Ins(1, 4, 5)P3. *Developmental biology* **158**, 200-212 (1993).

63. L. L. Runft, J. Watras, L. A. Jaffe, Calcium release at fertilization of Xenopus eggs requires type I IP(3) receptors, but not SH2 domain-mediated activation of PLCgamma or G(q)-mediated activation of PLCbeta. *Developmental biology* **214**, 399-411 (1999).

64. M. Wuhr *et al.*, Deep proteomics of the Xenopus laevis egg using an mRNA-derived reference database. *Current biology : CB* **24**, 1467-1475 (2014).

65. S. G. Rhee, Regulation of phosphoinositide-specific phospholipase C. *Annual review of biochemistry* **70**, 281-312 (2001).

66. L. L. Runft, J. Watras, L. A. Jaffe, Calcium release at fertilization of *Xenopus* eggs requires type I IP_3 receptors, but not SH2 domain-mediated activation of PLCγ or G_q-mediated activation of PLCβ. *Dev Biol* **214**, 399-411 (1999).

67. D. Glahn, S. D. Mark, R. K. Behr, R. Nuccitelli, Tyrosine kinase inhibitors block sperm-induced egg activation in Xenopus laevis. *Developmental biology* **205**, 171-180 (1999).

68. Y. Iwao, An electrically mediated block to polyspermy in the primitive urodele Hynobius nebulosus and phylogenetic comparison with other amphibians. *Developmental biology* **134**, 438-445 (1989).

69. E. M. Wright, J. M. Diamond, Anion selectivity in biological systems. *Physiol Rev* **57**, 109-156 (1977).

70. R. Y. Tsien, New calcium indicators and buffers with high selectivity against magnesium and protons: design, synthesis, and properties of prototype structures. *Biochemistry* **19**, 2396-2404 (1980).

71. H. C. Hartzell, K. Yu, Q. Xiao, L. T. Chien, Z. Qu, Anoctamin/TMEM16 family members are Ca^{2+}-activated Cl^- channels. *J Physiol* **587**, 2127-2139 (2009).

72. K. L. Wozniak, W. A. Phelps, M. Tembo, M. T. Lee, A. E. Carlson, The TMEM16A channel mediates the fast polyspermy block in Xenopus laevis. *The Journal of general physiology*, (2018).

73. K. L. Wozniak, M. Tembo, W. A. Phelps, M. T. Lee, A. E. Carlson, PLC and IP3-evoked Ca(2+) release initiate the fast block to polyspermy in Xenopus laevis eggs. *The Journal of general physiology*, (2018).

74. A. M. Session *et al.*, Genome evolution in the allotetraploid frog Xenopus laevis. *Nature* **538**, 336-343 (2016).

75. D. Kim, B. Langmead, S. L. Salzberg, HISAT: a fast spliced aligner with low memory requirements. *Nature methods* **12**, 357-360 (2015).

76. Y. Liao, G. K. Smyth, W. Shi, featureCounts: an efficient general purpose program for assigning sequence reads to genomic features. *Bioinformatics (Oxford, England)* **30**, 923-930 (2014).

77. J. D. Brunner, N. K. Lim, S. Schenck, A. Duerst, R. Dutzler, X-ray structure of a calcium-activated TMEM16 lipid scramblase. *Nature* **516**, 207-212 (2014).

78. V. Kane Dickson, L. Pedi, S. B. Long, Structure and insights into the function of a Ca(2+)-activated Cl(-) channel. *Nature* **516**, 213-218 (2014).

79. T. Yang *et al.*, Structure and selectivity in bestrophin ion channels. *Science (New York, N.Y.)* **346**, 355-359 (2014).

80. S. C. Murray *et al.*, Validation of cryo-EM structure of IP(3)R1 channel. *Structure (London, England : 1993)* **21**, 900-909 (2013).

81. S. J. Ludtke *et al.*, Flexible architecture of IP3R1 by Cryo-EM. *Structure (London, England : 1993)* **19**, 1192-1199 (2011).

82. J. Heasman, S. Holwill, C. C. Wylie, Fertilization of cultured Xenopus oocytes and use in studies of maternally inherited molecules. *Methods Cell Biol* **36**, 213-230 (1991).

83. R. A. Wallace, D. W. Jared, J. N. Dumont, M. W. Sega, Protein incorporation by isolated amphibian oocytes. 3. Optimum incubation conditions. *J Exp Zool* **184**, 321-333 (1973).

84. B. C. Schroeder, T. Cheng, Y. N. Jan, L. Y. Jan, Expression cloning of TMEM16A as a calcium-activated chloride channel subunit. *Cell* **134**, 1019-1029 (2008).

85. K. W. Lee, S. E. Webb, A. L. Miller, A wave of free cytosolic calcium traverses zebrafish eggs on activation. *Developmental biology* **214**, 168-180 (1999).

86. S. S. Shen, W. R. Buck, Sources of calcium in sea urchin eggs during the fertilization response. *Developmental biology* **157**, 157-169 (1993).

87. R. P. Elinson, Site of sperm entry and a cortical contraction associated with egg activation in the frog Rana pipiens. *Developmental biology* **47**, 257-268 (1975).

88. P. T. Kroeger, Jr. *et al.*, Production of haploid zebrafish embryos by in vitro fertilization. *Journal of Visualized Experiments : JoVE*, (2014).

89. S. M. Sanders *et al.*, CRISPR/Cas9-mediated gene knockin in the hydroid Hydractinia symbiolongicarpus. *BMC genomics* **19**, 649 (2018).

90. C. Y. Seiler *et al.*, DNASU plasmid and PSI:Biology-Materials repositories: resources to accelerate biological research. *Nucleic Acids Res* **42**, D1253-1260 (2014).

91. S. Kredel *et al.*, mRuby, a bright monomeric red fluorescent protein for labeling of subcellular structures. *PLoS One* **4**, e4391 (2009).

92. A. E. Carlson *et al.*, Identical phenotypes of CatSper1 and CatSper2 null sperm. *The Journal of biological chemistry* **280**, 32238-32244 (2005).

93. I. Marszalek *et al.*, Revised stability constant, spectroscopic properties and binding mode of Zn(II) to FluoZin-3, the most common zinc probe in life sciences. *Journal of inorganic biochemistry* **161**, 107-114 (2016).

94. K. Moriyoshi, L. J. Richards, C. Akazawa, D. D. O'Leary, S. Nakanishi, Labeling neural cells using adenoviral gene transfer of membrane-targeted GFP. *Neuron* **16**, 255-260 (1996).

95. C. A. Schneider, W. S. Rasband, K. W. Eliceiri, NIH Image to ImageJ: 25 years of image analysis. *Nat Methods* **9**, 671-675 (2012).

96. D. Glahn, R. Nuccitelli, Voltage-clamp study of the activation currents and fast block to polyspermy in the egg of Xenopus laevis. *Development, growth & differentiation* **45**, 187-197 (2003).

97. D. J. Webb, R. Nuccitelli, Fertilization potential and electrical properties of the Xenopus laevis egg. *Developmental biology* **107**, 395-406 (1985).

98. A. Caputo *et al.*, TMEM16A, a membrane protein associated with calcium-dependent chloride channel activity. *Science (New York, N.Y.)* **322**, 590-594 (2008).

99. Y. D. Yang *et al.*, TMEM16A confers receptor-activated calcium-dependent chloride conductance. *Nature* **455**, 1210-1215 (2008).

100. M. J. Berridge, Inositol trisphosphate and calcium signalling mechanisms. *Biochim Biophys Acta* **1793**, 933-940 (2009).

101. P. J. Calcraft *et al.*, NAADP mobilizes calcium from acidic organelles through two-pore channels. *Nature* **459**, 596-600 (2009).

102. D. De Stefani, A. Raffaello, E. Teardo, I. Szabo, R. Rizzuto, A forty-kilodalton protein of the inner membrane is the mitochondrial calcium uniporter. *Nature* **476**, 336-340 (2011).

103. S. J. Pitt *et al.*, TPC2 is a novel NAADP-sensitive Ca2+ release channel, operating as a dual sensor of luminal pH and Ca2+. *J Biol Chem* **285**, 35039-35046 (2010).

104. Q. C. Wang *et al.*, TMCO1 Is an ER Ca(2+) Load-Activated Ca(2+) Channel. *Cell* **165**, 1454-1466 (2016).

105. R. Bobe *et al.*, Identification, expression, function, and localization of a novel (sixth) isoform of the human sarco/endoplasmic reticulum Ca2+ATPase 3 gene. *J Biol Chem* **279**, 24297-24306 (2004).

106. A. Sakuntabhai *et al.*, Mutations in ATP2A2, encoding a Ca2+ pump, cause Darier disease. *Nat Genet* **21**, 271-277 (1999).

107. Z. Sun *et al.*, TMCO1 is essential for ovarian follicle development by regulating ER Ca(2+) store of granulosa cells. *Cell Death Differ*, (2018).

108. S. L. Zhang *et al.*, STIM1 is a Ca2+ sensor that activates CRAC channels and migrates from the Ca2+ store to the plasma membrane. *Nature* **437**, 902-905 (2005).

109. Y. Bourne, J. Dannenberg, V. Pollmann, P. Marchot, O. Pongs, Immunocytochemical localization and crystal structure of human frequenin (neuronal calcium sensor 1). *J Biol Chem* **276**, 11949-11955 (2001).

110. T. Y. Nakamura *et al.*, A role for frequenin, a Ca2+-binding protein, as a regulator of Kv4 K+-currents. *Proc Natl Acad Sci U S A* **98**, 12808-12813 (2001).

111. S. Gonzalez-Perrett *et al.*, Polycystin-2, the protein mutated in autosomal dominant polycystic kidney disease (ADPKD), is a Ca2+-permeable nonselective cation channel. *Proc Natl Acad Sci U S A* **98**, 1182-1187 (2001).

112. M. Suzuki, A. Mizuno, K. Kodaira, M. Imai, Impaired pressure sensation in mice lacking TRPV4. *The Journal of biological chemistry* **278**, 22664-22668 (2003).

113. D. E. Clapham, SnapShot: mammalian TRP channels. *Cell* **129**, 220 (2007).

114. T. C. Ho, N. A. Horn, T. Huynh, L. Kelava, J. B. Lansman, Evidence TRPV4 contributes to mechanosensitive ion channels in mouse skeletal muscle fibers. *Channels (Austin, Tex.)* **6**, 246-254 (2012).

115. J. Gafni *et al.*, Xestospongins: potent membrane permeable blockers of the inositol 1,4,5-trisphosphate receptor. *Neuron* **19**, 723-733 (1997).

116. H. Kanki *et al.*, Activation of inositol 1,4,5-trisphosphate receptor is essential for the opening of mouse TRP5 channels. *Molecular pharmacology* **60**, 989-998 (2001).

117. T. Maruyama, T. Kanaji, S. Nakade, T. Kanno, K. Mikoshiba, 2APB, 2-aminoethoxydiphenyl borate, a membrane-penetrable modulator of Ins(1,4,5)P3-induced Ca2+ release. *Journal of biochemistry* **122**, 498-505 (1997).

118. J. E. Bleasdale *et al.*, Selective inhibition of receptor-coupled phospholipase C-dependent processes in human platelets and polymorphonuclear neutrophils. *J Pharmacol Exp Ther* **255**, 756-768 (1990).

119. W. Jin, T. M. Lo, H. H. Loh, S. A. Thayer, U73122 inhibits phospholipase C-dependent calcium mobilization in neuronal cells. *Brain Res* **642**, 237-243 (1994).

120. T. L. Toft-Bertelsen, D. Krizaj, N. MacAulay, When size matters: transient receptor potential vanilloid 4 channel as a volume-sensor rather than an osmo-sensor. *The Journal of physiology* **595**, 3287-3302 (2017).

121. P. Delmas, Polycystins: polymodal receptor/ion-channel cellular sensors. *Pflugers Archiv : European journal of physiology* **451**, 264-276 (2005).

122. G. C. Churchill *et al.*, Sperm deliver a new second messenger: NAADP. *Current biology : CB* **13**, 125-128 (2003).

123. D. Lim, K. Kyozuka, G. Gragnaniello, E. Carafoli, L. Santella, NAADP+ initiates the Ca2+ response during fertilization of starfish oocytes. *FASEB journal : official publication of the Federation of American Societies for Experimental Biology* **15**, 2257-2267 (2001).

124. F. Moccia, D. Lim, G. A. Nusco, E. Ercolano, L. Santella, NAADP activates a Ca2+ current that is dependent on F-actin cytoskeleton. *FASEB journal : official publication of the Federation of American Societies for Experimental Biology* **17**, 1907-1909 (2003).

125. F. Moccia, D. Lim, K. Kyozuka, L. Santella, NAADP triggers the fertilization potential in starfish oocytes. *Cell calcium* **36**, 515-524 (2004).

126. J. B. Parys *et al.*, Isolation, characterization, and localization of the inositol 1,4,5-trisphosphate receptor protein in Xenopus laevis oocytes. *The Journal of biological chemistry* **267**, 18776-18782 (1992).

127. C. C. Petersen, M. J. Berridge, The regulation of capacitative calcium entry by calcium and protein kinase C in Xenopus oocytes. *The Journal of biological chemistry* **269**, 32246-32253 (1994).

128. M. C. Gould, J. L. Stephano, Peptides from sperm acrosomal protein that initiate egg development. *Dev Biol* **146**, 509-518 (1991).

129. S. Kume *et al.*, The Xenopus IP3 receptor: structure, function, and localization in oocytes and eggs. *Cell* **73**, 555-570 (1993).

130. S. A. Stricker, V. E. Centonze, R. F. Melendez, Calcium dynamics during starfish oocyte maturation and fertilization. *Dev Biol* **166**, 34-58 (1994).

131. S. Cruz-Rangel *et al.*, Gating modes of calcium-activated chloride channels TMEM16A and TMEM16B. *The Journal of physiology* **593**, 5283-5298 (2015).

132. M. A. Rasar, S. R. Hammes, The physiology of the Xenopus laevis ovary. *Methods in molecular biology (Clifton, N.J.)* **322**, 17-30 (2006).

133. F. Yu, L. Sun, K. Machaca, Constitutive recycling of the store-operated Ca2+ channel Orai1 and its internalization during meiosis. *The Journal of cell biology* **191**, 523-535 (2010).

134. W. El-Jouni, B. Jang, S. Haun, K. Machaca, Calcium signaling differentiation during Xenopus oocyte maturation. *Dev Biol* **288**, 514-525 (2005).

135. B. K. Mohanty, B. L. Gupta, A marked animal-vegetal polarity in the localization of Na+,K+-ATPase activity and its down-regulation following progesterone-induced maturation. *Mol Reprod Dev* **79**, 138-160 (2012).

136. C. C. Wylie, D. Brown, S. F. Godsave, J. Quarmby, J. Heasman, The cytoskeleton of Xenopus oocytes and its role in development. *Journal of embryology and experimental morphology* **89 Suppl**, 1-15 (1985).

137. V. Kane Dickson, L. Pedi, S. B. Long, Structure and insights into the function of a Ca2+-activated Cl- channel. *Nature* **516**, 213-218 (2014).

138. Z. Qu, C. Hartzell, Determinants of anion permeation in the second transmembrane domain of the mouse bestrophin-2 chloride channel. *The Journal of general physiology* **124**, 371-382 (2004).

139. F. Huang, X. Wong, L. Y. Jan, International Union of Basic and Clinical Pharmacology. LXXXV: Calcium-Activated Chloride Channels. *Pharmacological Reviews* **64**, 1-15 (2012).

140. M. T. Lee, A. R. Bonneau, A. J. Giraldez, Zygotic genome activation during the maternal-to-zygotic transition. *Annu Rev Cell Dev Biol* **30**, 581-613 (2014).

141. W. Tadros, H. D. Lipshitz, The maternal-to-zygotic transition: a play in two acts. *Development* **136**, 3033-3042 (2009).

142. Z. Qu, R. W. Wei, W. Mann, H. C. Hartzell, Two bestrophins cloned from Xenopus laevis oocytes express Ca(2+)-activated Cl(-) currents. *The Journal of biological chemistry* **278**, 49563-49572 (2003).

143. Y. Gao da *et al.*, Coupling of TRPV6 and TMEM16A in epithelial principal cells of the rat epididymis. *The Journal of general physiology* **148**, 161-182 (2016).

144. X. Jin *et al.*, Activation of the Cl- channel ANO1 by localized calcium signals in nociceptive sensory neurons requires coupling with the IP3 receptor. *Science signaling* **6**, ra73 (2013).

145. S. Gyobu *et al.*, A Role of TMEM16E Carrying a Scrambling Domain in Sperm Motility. *Mol Cell Biol* **36**, 645-659 (2015).

146. T. T. Tran *et al.*, TMEM16E (GDD1) exhibits protein instability and distinct characteristics in chloride channel/pore forming ability. *J Cell Physiol* **229**, 181-190 (2014).

147. C. Hammer *et al.*, A Coding Variant of ANO10, Affecting Volume Regulation of Macrophages, Is Associated with Borrelia Seropositivity. *Mol Med* **21**, 26-37 (2015).

148. P. Wanitchakool *et al.*, Cellular defects by deletion of ANO10 are due to deregulated local calcium signaling. *Cell Signal* **30**, 41-49 (2017).

149. W. Namkung, P. W. Phuan, A. S. Verkman, TMEM16A inhibitors reveal TMEM16A as a minor component of calcium-activated chloride channel conductance in airway and intestinal epithelial cells. *The Journal of biological chemistry* **286**, 2365-2374 (2011).

150. S. J. Oh *et al.*, MONNA, a potent and selective blocker for transmembrane protein with unknown function 16/anoctamin-1. *Molecular pharmacology* **84**, 726-735 (2013).

151. Y. Seo *et al.*, Ani9, A Novel Potent Small-Molecule ANO1 Inhibitor with Negligible Effect on ANO2. *PloS one* **11**, e0155771 (2016).

152. R. De La Fuente, W. Namkung, A. Mills, A. S. Verkman, Small-molecule screen identifies inhibitors of a human intestinal calcium-activated chloride channel. *Molecular pharmacology* **73**, 758-768 (2008).

153. Y. Liu *et al.*, Characterization of the effects of Cl- channel modulators on TMEM16A and bestrophin-1 Ca2+ activated Cl- channels. *Pflugers Arch* **467**, 1417-1430 (2015).

154. M. He *et al.*, Cytoplasmic Cl(-) couples membrane remodeling to epithelial morphogenesis. *Proceedings of the National Academy of Sciences of the United States of America* **114**, E11161-e11169 (2017).

155. N. L. Cross, Initiation of the activation potential by an increase in intracellular calcium in eggs of the frog, Rana pipiens. *Developmental biology* **85**, 380-384 (1981).

156. P. Wright *et al.*, The crab-eating frog, Rana cancrivora, up-regulates hepatic carbamoyl phosphate synthetase I activity and tissue osmolyte levels in response to increased salinity. *Journal of experimental zoology. Part A, Comparative experimental biology* **301**, 559-568 (2004).

157. A. C. Alcala, Breeding behaviour and early development of frogs of Negros, Philippine Islands. *Copeia*, 679-726 (1962).

158. D. S. Townsend, M. M. Stewart, F. H. Pough, P. F. Brussard, Internal fertilization in an oviparous frog. *Science (New York, N.Y.)* **212**, 469-471 (1981).

159. R. P. Elinson, Fertilization and aqueous development of the puerto rican terrestrial-breeding frog, Eleutherodactylus coqui. *Journal of morphology* **193**, 217-224 (1987).

160. S. Bulley *et al.*, TMEM16A/ANO1 channels contribute to the myogenic response in cerebral arteries. *Circulation research* **111**, 1027-1036 (2012).

161. F. Huang *et al.*, Studies on expression and function of the TMEM16A calcium-activated chloride channel. *Proc Natl Acad Sci U S A* **106**, 21413-21418 (2009).

162. J. R. Rock, C. R. Futtner, B. D. Harfe, The transmembrane protein TMEM16A is required for normal development of the murine trachea. *Developmental biology* **321**, 141-149 (2008).

163. Q. Ji *et al.*, Recent advances in TMEM16A: Structure, function, and disease. *Journal of cellular physiology*, (2018).

164. A. M. Kim, S. Vogt, T. V. O'Halloran, T. K. Woodruff, Zinc availability regulates exit from meiosis in maturing mammalian oocytes. *Nature chemical biology* **6**, 674-681 (2010).

165. K. H. Falchuk, M. Montorzi, Zinc physiology and biochemistry in oocytes and embryos. *Biometals : an international journal on the role of metal ions in biology, biochemistry, and medicine* **14**, 385-395 (2001).

166. J. G. Shiber, Heavy metals in Ras Beirut prawns and sea urchin eggs. *Journal of environmental science and health. Part. B, Pesticides, food contaminants, and agricultural wastes* **14**, 73-95 (1979).

167. S. Schaefer-Ramadan, S. Hubrack, K. Machaca, Transition metal dependent regulation of the signal transduction cascade driving oocyte meiosis. *Journal of cellular physiology* **233**, 3164-3175 (2018).

168. L. Sun, Y. Chai, R. Hannigan, V. K. Bhogaraju, K. Machaca, Zinc regulates the ability of Cdc25C to activate MPF/cdk1. *Journal of cellular physiology* **213**, 98-104 (2007).

169. M. L. Bernhardt, A. M. Kim, T. V. O'Halloran, T. K. Woodruff, Zinc requirement during meiosis I-meiosis II transition in mouse oocytes is independent of the MOS-MAPK pathway. *Biology of reproduction* **84**, 526-536 (2011).

170. B. Y. Kong, M. L. Bernhardt, A. M. Kim, T. V. O'Halloran, T. K. Woodruff, Zinc maintains prophase I arrest in mouse oocytes through regulation of the MOS-MAPK pathway. *Biology of reproduction* **87**, 11, 11-12 (2012).

171. T. Suzuki, N. Yoshida, E. Suzuki, E. Okuda, A. C. Perry, Full-term mouse development by abolishing Zn2+-dependent metaphase II arrest without Ca2+ release. *Development (Cambridge, England)* **137**, 2659-2669 (2010).

172. M. L. Bernhardt, B. Y. Kong, A. M. Kim, T. V. O'Halloran, T. K. Woodruff, A zinc-dependent mechanism regulates meiotic progression in mammalian oocytes. *Biology of reproduction* **86**, 114 (2012).

173. K. Lee *et al.*, Pig oocyte activation using a Zn(2)(+) chelator, TPEN. *Theriogenology* **84**, 1024-1032 (2015).

174. E. L. Que *et al.*, Quantitative mapping of zinc fluxes in the mammalian egg reveals the origin of fertilization-induced zinc sparks. *Nature chemistry* **7**, 130-139 (2015).

175. M. Whitaker, Calcium at fertilization and in early development. *Physiological reviews* **86**, 25-88 (2006).

176. Y. L. Miao, C. J. Williams, Calcium signaling in mammalian egg activation and embryo development: the influence of subcellular localization. *Molecular reproduction and development* **79**, 742-756 (2012).

177. E. L. Que *et al.*, Zinc sparks induce physiochemical changes in the egg zona pellucida that prevent polyspermy. *Integr Biol (Camb)* **9**, 135-144 (2017).

178. L. G. Young, L. Nelson, The effects of heavy metal ions on the motility of sea urchin spermatozoa. *The Biological bulletin* **147**, 236-246 (1974).

179. J. R. Christensen, C. A. Bishop, J. S. Richardson, B. Pauli, J. Elliott, Validation of an amphibian sperm inhibition toxicological test method using zinc. *Environmental toxicology and chemistry* **23**, 2950-2955 (2004).

180. L. A. Burnett, S. Boyles, C. Spencer, A. L. Bieber, D. E. Chandler, Xenopus tropicalis allurin: expression, purification, and characterization of a sperm chemoattractant that exhibits cross-species activity. *Developmental biology* **316**, 408-416 (2008).

181. N. Tholl *et al.*, Swimming of Xenopus laevis sperm exhibits multiple gears and its duration is extended by egg jelly constituents. *The Biological bulletin* **220**, 174-185 (2011).

182. X. Xiang, A. Kittelson, J. Olson, A. Bieber, D. Chandler, Allurin, a 21 kD sperm chemoattractant, is rapidly released from the outermost jelly layer of the Xenopus egg by diffusion and medium convection. *Molecular reproduction and development* **70**, 344-360 (2005).

183. Y. Guerardel *et al.*, O-glycan variability of egg-jelly mucins from Xenopus laevis: characterization of four phenotypes that differ by the terminal glycosylation of their mucins. *The Biochemical journal* **352 Pt 2**, 449-463 (2000).

184. B. S. Bonnell, D. E. Chandler, Egg jelly layers of Xenopus laevis are unique in ultrastructure and sugar distribution. *Molecular reproduction and development* **44**, 212-220 (1996).

185. M. F. Medina, C. A. Crespo, I. Ramos, S. N. Fernandez, Role of cations as components of jelly coats in Bufo arenarum fertilization. *Zygote (Cambridge, England)* **18**, 69-80 (2010).

186. A. S. Ginzburg, Cortical reaction in axolotl eggs. *The Soviet journal of developmental biology* **2**, 515-518 (1971).

187. K. Machaca, Increased sensitivity and clustering of elementary Ca2+ release events during oocyte maturation. *Developmental biology* **275**, 170-182 (2004).

188. S. E. Webb, A. L. Miller, Ca(2+) signaling during activation and fertilization in the eggs of teleost fish. *Cell calcium* **53**, 24-31 (2013).

189. R. E. Wyrick, T. Nishihara, J. L. Hedrick, Agglutination of jelly coat and cortical granule components and the block to polyspermy in the amphibian Xenopus laevis. *Proceedings of the National Academy of Sciences of the United States of America* **71**, 2067-2071 (1974).

190. G. Freeman, The role of oocyte maturation in the ontogeny of the fertilization site in the hydrozoan Hydractinia echinata. *Roux's archives of developmental biology : the official organ of the EDBO* **196**, 83-92 (1987).

191. K. Kerns, M. Zigo, E. Z. Drobnis, M. Sutovsky, P. Sutovsky, Zinc ion flux during mammalian sperm capacitation. *Nature communications* **9**, 2061 (2018).

192. J. Qiao *et al.*, GPR39 is region-specifically expressed in mouse oviduct correlating with the Zn(2+) distribution. *Theriogenology* **88**, 98-105 (2017).

193. A. Hachem *et al.*, PLCzeta is the physiological trigger of the Ca2+ oscillations that induce embryogenesis in mammals but offspring can be conceived in its absence. *Development (Cambridge, England)*, (2017).

194. K. Nozawa, Y. Satouh, T. Fujimoto, A. Oji, M. Ikawa, Sperm-borne phospholipase C zeta-1 ensures monospermic fertilization in mice. *Scientific reports* **8**, 1315 (2018).

195. C. M. Saunders *et al.*, PLC zeta: a sperm-specific trigger of Ca(2+) oscillations in eggs and embryo development. *Development (Cambridge, England)* **129**, 3533-3544 (2002).

196. K. Coward *et al.*, Identification and functional analysis of an ovarian form of the egg activation factor phospholipase C zeta (PLCzeta) in pufferfish. *Molecular reproduction and development* **78**, 48-56 (2011).

197. M. Ito *et al.*, Difference in Ca2+ oscillation-inducing activity and nuclear translocation ability of PLCZ1, an egg-activating sperm factor candidate, between mouse, rat, human, and medaka fish. *Biology of reproduction* **78**, 1081-1090 (2008).

198. U. Hellsten *et al.*, The genome of the Western clawed frog Xenopus tropicalis. *Science (New York, N.Y.)* **328**, 633-636 (2010).

199. P. R. Turner, L. A. Jaffe, A. Fein, Regulation of cortical vesicle exocytosis in sea urchin eggs by inositol 1,4,5-trisphosphate and GTP-binding protein. *The Journal of cell biology* **102**, 70-76 (1986).

200. W. M. Kuhtreiber, I. Gillot, C. Sardet, L. F. Jaffe, Net calcium and acid release at fertilization in eggs of sea urchins and ascidians. *Cell calcium* **14**, 73-86 (1993).

201. J. Zhao, B. A. Bertoglio, K. R. Gee, A. R. Kay, The zinc indicator FluoZin-3 is not perturbed significantly by physiological levels of calcium or magnesium. *Cell calcium* **44**, 422-426 (2008).

202. W. D. Mosher, J. Jones, Use of contraception in the United States: 1982-2008. *Vital and health statistics. Series 23, Data from the National Survey of Family Growth*, 1-44 (2010).

203. A. Chandra, G. M. Martinez, W. D. Mosher, J. C. Abma, J. Jones, Fertility, family planning, and reproductive health of U.S. women: data from the 2002 National Survey of Family Growth. *Vital and health statistics. Series 23, Data from the National Survey of Family Growth*, 1-160 (2005).